INFORMATION TO USERS

This manuscript has been reproduced from the microfilm master. UMI films the text directly from the original or copy submitted. Thus, some thesis and dissertation copies are in typewriter face, while others may be from any type of computer printer.

The quality of this reproduction is dependent upon the quality of the copy submitted. Broken or indistinct print, colored or poor quality illustrations and photographs, print bleedthrough, substandard margins, and improper alignment can adversely affect reproduction.

In the unlikely event that the author did not send UMI a complete manuscript and there are missing pages, these will be noted. Also, if unauthorized copyright material had to be removed, a note will indicate the deletion.

Oversize materials (e.g., maps, drawings, charts) are reproduced by sectioning the original, beginning at the upper left-hand corner and continuing from left to right in equal sections with small overlaps.

Photographs included in the original manuscript have been reproduced xerographically in this copy. Higher quality 6" x 9" black and white photographic prints are available for any photographs or illustrations appearing in this copy for an additional charge. Contact UMI directly to order.

Bell & Howell Information and Learning
300 North Zeeb Road, Ann Arbor, MI 48106-1346 USA

UMI®
800-521-0600

DISSERTATION

INDIRECT DETERMINATION OF THE RATE OF IRON UPTAKE INTO *E. COLI* RIBONUCLEOTIDE REDUCTASE R2 BY COMPETITION WITH FERROZINE

Submitted by

Noelle J. Umback

Department of Chemistry

In partial fulfillment of the requirements

For the Degree of Doctor of Philosophy

Colorado State University

Fort Collins, Colorado

Spring 2000

COLORADO STATE UNIVERSITY

March 31, 2000

WE HEREBY RECOMMEND THAT THE DISSERTATION PREPARED UNDER OUR SUPERVISION BY NOELLE J. UMBACK ENTITLED INDIRECT DETERMINATION OF THE RATE OF IRON UPTAKE INTO *E. COLI* RIBONUCLEOTIDE REDUCTASE R2 BY COMPETITION WITH FERROZINE BE ACCEPTED AS FULFILLING IN PART REQUIREMENTS FOR THE DEGREE OF DOCTOR OF PHILOSOPHY.

Committee on Graduate Work

Adviser

Department Head

ABSTRACT OF DISSERTATION

INDIRECT DETERMINATION OF THE RATE OF IRON UPTAKE INTO *E. COLI* RIBONUCLEOTIDE REDUCTASE R2 BY COMPETITION WITH FERROZINE

The rate of iron(II) uptake by apo R2 ribonucleotide reductase from *E. coli* has been determined. A ferrozine–based competition method for indirectly observing this rate was devised. Ferrozine, an iron(II)–specific ligand, complexes iron from solution at rates competitive with apo R2's iron uptake rate, enabling competition experiments to succeed.

The ferrozine–iron complexation reaction (formation of $Fe^{II}Fz_3$) was characterized in HEPES buffer at 5.0 °C. The reaction order in ferrozine was found to decrease significantly below third at ferrozine concentrations greater than 800 μM, approaching first at high (≥ 5 mM) ferrozine concentrations. This phenomenon is predicted by the complete derived rate law.

The rate of uptake of the first equivalent of ferrous iron into R2 (k_{apo}) has been measured as $1.3(2) \times 10^6$ $M^{-1}s^{-1}$. This step of the reconstitution mechanism appears to occur *before* the conformational change step, which thus has the same rate constant (8–10 s^{-1}) as the formation of the first observed intermediate in the reconstitution mechanism. Attempts to determine the rate constant for uptake of the second iron equivalent into R2 (k_{apoFe}) were only marginally successful, as the reaction conditions employed precluded

an accurate measurement. A mechanistic scheme which includes the iron and oxygen uptake steps and the proposed conformational change is offered.

Noelle Joreen Umback
Chemistry Department
Colorado State University
Fort Collins, CO 80523
Spring 2000

ACKNOWLEDGMENTS

While many persons have been instrumental in the scientific aspects of my graduate career, there are also many others without whom this dissertation may not have come about. These are the friends and family members who, although many of them will claim not to understand any of what is written in these pages, have encouraged and supported me over the years. Education has always been important in our family (there are other post–graduate degrees[i,ii] and scientific publications[iii,iv] in the family) and now I add my first contribution to the Umback bibliography.

Thank you to my parents and the rest of my family for everything, from having "the imp" correct their attempted improvisations to "I think I can, I think I can"[v] during story–reading time, to early lessons in thermodynamics: "Close the door, you're letting the heat out!" Also to my network of friends from the Dakotas, California, Colorado and

---

[i] Umback, C. R. "Effects of Wind on Falling Drops" M. S. Thesis, South Dakota State University, Dec. 1965.

[ii] Umback, E. M. "The Application of Occupational Therapy in the Rehabilitation of Patients Who Have Had Strokes: A Survey Examining Treatment Methods in the Midwestern States of Indiana, Illinois, Michigan, and Wisconsin" M. S. Thesis, University of South Dakota, April 1997.

[iii] Umback, C. R.; Lembke, W. D. "Effect of wind on falling water drops" *Trans. Am. Soc. Ag. Eng.* **1966,** *9,* 805-808.

[iv] Umback, E. M. " Life After A Stroke: What Counselors Need to Know to Help Survivors and Their Families" *The Dakota Counselor* **1997,** *4,* 21–23.

[v] Piper, W. *The Little Engine That Could*; Platt & Munk: New York, 1930.

New York; you helped keep me sane and let me feel as if I had a semblance of "a life" away from the laboratory, and gave me the luxury of not always thinking about science.

There are two early mentors who stand out in my mind as getting me into chemistry. Richard Mattes during freshman physical science class kindled a strong enough flame to help me survive senior chemistry and ultimately go on to major in chemistry in college, despite the best efforts of his successor in the position. Professor Ron Utecht at SDSU took me into his lab as a freshman who knew science only from books and lab exercises, and taught me how to be a researcher. Along the way he fostered my appreciation for not only hemiacetals but also Hemi 'Cudas.

Of course Jack, thanks for the opportunity to work on an interesting project, and for keeping me around all these years. It's not every group that teaches you not just chemistry, but also how to pack entire labs for moves down the hall and across the country. Who'd have thought I'd like New York? Thanks are also due to the Norton group members past and present, especially Kurt Kramarz, who helped me get started with R2 (and also prepared the stopped–flow diagrams), Frank Rix (who made insightful suggestions regarding the competition experiments), and Philipp Stößel.

Marty Bollinger and Brenda Ley at Penn State have been a pleasure to collaborate with (both on the phone and in person); the time I spent purifying protein there was intense but enjoyable. Their provision of the last few vials of protein was invaluable and allowed me to finish my last few experiments.

"I knew I could, I knew I could."

To Brother

TABLE OF CONTENTS

LIST OF TABLES

LIST OF FIGURES

ABBREVIATIONS

apo, apoR2	the metal–free, radical–free form of R2
apoFe	monoferrous R2
$apoFe_2$	diferrous R2 (reduced R2)
Asp	aspartic acid, aspartate
BSA	bovine serum albumin
Cys	cysteine, cysteinyl
D	aspartic acid, aspartate
DNA	deoxyribonucleic acid
DOPA	dihydroxyphenylalanine
E	glutamic acid, glutamate
E. coli	*Escherichia coli* bacteria
EDTA	ethylenediaminetetraacetic acid
ENDOR	electron nuclear double resonance spectroscopy
EPR	electron paramagnetic resonance spectroscopy
EXAFS	extended X-ray absorption, fine structure
F	phenylalanine
Fz, FZ	ferrozine

HEPES	4–(2–hydroxyethyl)–1–piperazineethanesulfonic acid
His	histidine
I	ionic strength
kD	kiloDaltons; one Dalton = g/mol; used with proteins
L	generic ligand on a transition metal
met, metR2	R2 in which the tyrosyl radical has been reduced
MK	MacKinetics
MMOH	methane monooxygenase hydroxylase (from *M. capsulatus* Bath)
MV	methyl viologen
PMSF	phenylmethylsulfonylfluoride
R1	ribonucleotide reductase R1 subunit (*E. coli* unless specified)
R2	ribonucleotide reductase R2 subunit (*E. coli* unless specified)
RFQ	rapid freeze quench
RNR	ribonucleotide reductase
SDS–PAGE	sodium dodecyl sulfate polyacrylamide gel electrophoresis
Tris	tris(hydroxymethyl)aminomethane
Trp	tryptophan, tryptophanyl
Tyr	tyrosine, tyrosyl
W	tryptophan, tryptophanyl
wt R2	wild type R2 (no mutations)
Y	tyrosine, tyrosyl

CHAPTER I. INTRODUCTION.

A. Historical background of ribonucleotide reductases.

General background. Ribonucleotide reductases (RNRs) are responsible for catalyzing the conversion of nucleotides to deoxyribonucleotides, an essential step of DNA synthesis.[1,2,3,4,5,6,7] All three known classes of RNRs feature the presence of a stabilized radical within the protein, although Nature uses widely different methods to accomplish this reduction. Class Ia RNRs[8,9,10,11] such as those from *E. coli* and

---

[1] Wallar, B. J.; Lipscomb, J. D. Dioxygen Activation by Enzymes Containing Binuclear Non–Heme Iron Clusters. *Chem. Rev.* **1996,** *96,* 2625–2657.

[2] Sjöberg, B.–M. Ribonucleotide Reductases–A Group of Enzymes with Different Metallosites and a Similar Reaction Mechanism. In *Metal Sites in Proteins and Models*; Hill, H. A. O.; Sadler, P. J.; Thomson, A. J., Eds.; Structure and Bonding Series 88; Springer–Verlag: Berlin, 1997; pp 139–173.

[3] Fontecave, M. Ribonucleotide reductases and radical reactions. *Cell. Mol. Life Sci.* **1998,** *54,* 684–695.

[4] Stubbe, J.; van der Donk, W. A. Protein Radicals in Enzyme Catalysis. *Chem. Rev.* **1998,** *98,* 705–762.

[5] Buckel, W.; Golding, B. T. Radical species in the catalytic pathways of enzymes from anaerobes. *FEMS Microbiol. Rev.* **1999,** *22,* 523–541.

[6] Sawers, G. Biochemistry, physiology and molecular biology of glycyl radical enzymes. *FEMS Microbiol. Rev.* **1999,** *22,* 543–551.

[7] Solomon, E. I.; Brunold, T. C.; Davis, M. I.; Kemsley, J. N.; Lee, S.–K.; Lehnert, N.; Neese, F.; Skulan, A. J.; Yang, Y.–S.; Zhou, J. Geometric and Electronic Structure/Function Correlations in Non–Heme Iron Enzymes. *Chem. Rev.* **2000,** *100,* 235–349.

[8] Thelander, L.; Gräslund, A. Ribonucleotide Reductase in Mammalian Systems. In *Metal Ions in Biological Systems* 30; Sigel, H. and Sigel, A., Eds.; Marcel Dekker: New York, 1994, pp. 109–129.

[9] Gräslund, A.; Backlund, B.-M.; Behravan, G.; Lycksell, P.-O.; Nyholm, S.; Sen, S. The Iron/Tyrosyl Radical Site of Ribonucleotide Reductase. In *Structural Biology: The State of the Art;* Sarma, R. H. and Sarma, M. H., Eds.; Adenine Press: Schenectady, NY, 1994; pp 77–82.

mammalian sources are composed of a pair of homodimeric subunits, α2 and β2, known as R1 and R2 (Figure 1.1). The larger, R1, contains the substrate–binding site and redox–active cysteines. The R2 subunit contains a μ–oxo–diiron(III) cluster (hence the inorganic interest) with a tyrosyl radical in an adjacent pocket, where the unpaired electron resides

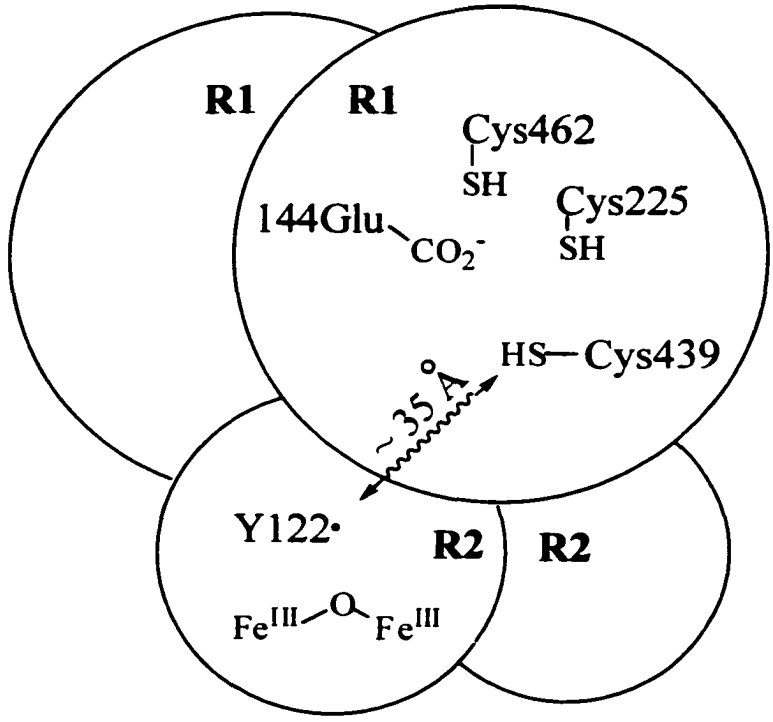

Figure 1.1. Schematic of ribonucleotide reductase, a dimer of dimers. For clarity, only one set of active sites is shown.

---

[10] Mulliez, E.; Fontecave, M. Structure and Reactivity of the Metal Centers of Ribonucleotide Reductases. *Chem. Ber./Recueil* **1997**, *130*, 317–321.

[11] Stubbe, J.; Riggs-Gelasco, P. Harnessing free radicals: formation and function of the tyrosyl radical in ribonucleotide reductase. *Trends Biochem. Sci.* **1998**, *23*, 438–443.

until its presence is required at R1's active site during enzymatic turnover. This has caused R2's tyrosyl radical to be compared to a "pilot light."[12] The currently accepted RNR mechanism[13] is shown in Figure 1.2.

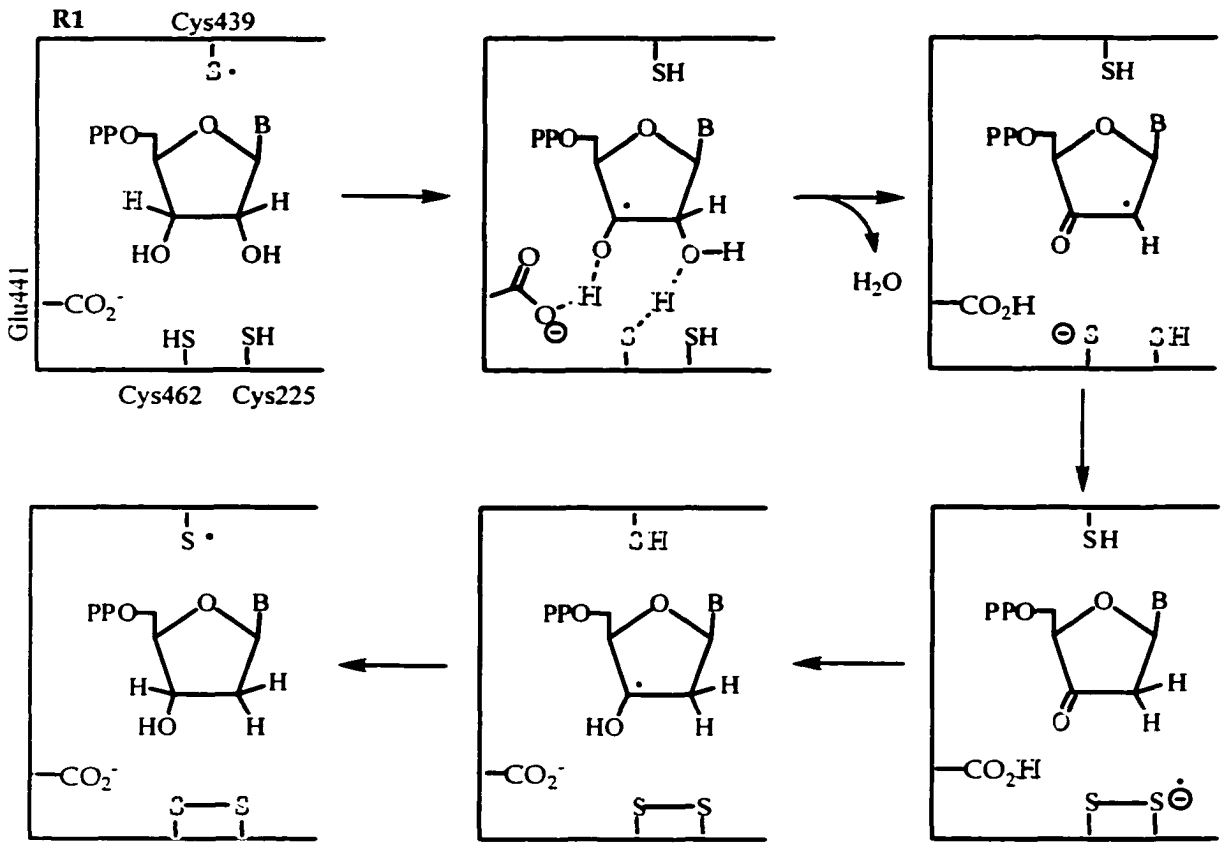

Figure 1.2. The mechanism for reduction of nucleotides by RNR. The actual transformation of the ribose occurs at R1's active site via long–range electron transfer from R2's active site. The hollow letters denote the site of chemical change for a particular step. Figure adapted from Stubbe and van der Donk.[14]

---

[12] Sturgeon, B. E.; Burdi, D.; Chen, S.; Huynh, B.-H.; Edmondson, D. E.; Stubbe, J.; Hoffman, B. M. Reconsideration of X, the Diiron Intermediate Formed during Cofactor Assembly in *E. coli* Ribonucleotide Reductase. *J. Am. Chem. Soc.* **1996,** *118,* 7551–7557.

[13] Mao, S. S.; Holler, T. P.; Yu, G. X.; Bollinger, J. M., Jr.; Booker, S.; Johnston, M. I.; Stubbe, J. A Model for the Role of Multiple Cysteine Residues Involved in Ribonucleotide Reduction: Amazing and Still Confusing. *Biochemistry* **1992,** *31,* 9733–9743.

[14] Stubbe, J.; van der Donk, W. A. Ribonucleotide reductases: radical enzymes with suicidal tendencies. *Chem. Biol.* **1995,** *2,* 793–801.

The enzyme R2 as synthesized is in the apo form and inactive—it lacks both the tyrosyl radical and the metal cluster, and must assemble these components in order to become active R2. In addition, should this tyrosyl radical somehow at a later time be reduced back to tyrosine (to form met R2), the μ-oxo diiron(III) cluster must also be reduced back to the diferrous stage and become oxidized again along with Y122; the reintroduction of molecular oxygen to reduced R2 will trigger this reconstitution of the active site.[15] Both the met and apo forms can be obtained in the laboratory by chemical treatments;[16] the extent of reduction achieved depends on the choice and combination of reagents.

Increased understanding of the assembly and reactivity of the R1–R2 complex may have important public health applications as well; this enzyme is a major target for inhibition in various anticancer, antiviral and antimicrobial therapies. The medical aspects of RNR are extensive and have been reviewed elsewhere.[17,18,19,20,21]

---

[15] Fontecave, M.; Eliasson, R.; Reichard, P. Enzymatic Regulation of the Radical Content of the Small Subunit of *Escherichia coli* Ribonucleotide Reductase Involving Reduction of Its Redox Centers. *J. Biol. Chem.* **1989,** *264,* 9164–9170.

[16] Barlow, T.; Eliasson, R.; Platz, A.; Reichard, P.; Sjöberg, B.-M. Enzymic modification of a tyrosine residue to a stable radical in ribonucleotide reductase. *Proc. Natl. Acad. Sci. USA* **1983,** *80,* 1492–1495.

[17] Cory, J. G.; Sato, A.; Lasater, L. Specific Inhibition of the Subunits of Ribonucleotide Reductase As a New Approach to Combination Chemotherapy. *Adv. Enzyme Reg.* **1980,** *19,* 139–150.

[18] Lien, E. J. Ribonucleotide reductase inhibitors as anticancer and antiviral agents. *Prog. Drug Res.* **1987,** *31,* 101–126.

[19] Nocentini, G. Ribonucleotide reductase inhibitors: new strategies for cancer chemotherapy. *Crit. Rev. Oncol. Hematol.* **1996,** *22,* 89–126.

[20] Szekeres, T.; Fritzer-Szekeres, M.; Elford, H. L. The Enzyme Ribonucleotide Reductase: Target for Antitumor and Anti-HIV Therapy. *Crit. Rev. Clin. Lab. Sci.* **1997,** *34,* 503–528.

Extensive characterization of ribonucleotide reductase R2 in various metallation and oxidation states has been reported by numerous groups since the initial purification of this unique system by Reichard and coworkers in 1969.[22] By that time it was known that aerobic *E. coli*'s R2 contained two equivalents per molecule[23] of non–sulfur, non–heme iron[24] which is necessary for catalytic activity. The same authors recognized functional similarities between this protein and the RNR system of *Lactobacillus leichmannii*[25] (later found to be a class II RNR,[5] which is adenosylcobalamin (also known as vitamin or coenzyme B_{12})–dependent). Another class (III) of ribonucleotide reductases is also known today, which accomplishes the same feats as the other two by means of an iron–sulfur cluster and a glycyl radical.[6,26] Ultimately it appears that all the ribonucleotide reductases generate a thiyl radical which does the actual ribonucleotide reduction.

Crystallographic characterization. Many structural details were clarified with the publication in 1990 of the crystal structure of native R2 (Figure 1.3). It showed

---

[21] Louie, A. Y.; Meade, T. J. Metal Complexes as Enzyme Inhibitors. *Chem. Rev.* **1999,** *99,* 2711–2734.

[22] Brown, N. C.; Canellakis, Z. N.; Lundin, B.; Reichard, P.; Thelander, L. Ribonucleotide Diphosphate Reductase. Purification of the two Subunits, Proteins B1 and B2. *Eur. J. Biochem.* **1969,** *9,* 561–573.

[23] Brown, N. C.; Eliasson, R.; Reichard, P.; Thelander, L. Spectrum and Iron Content of Protein B2 from Ribonucleotide Diphosphate Reductase. *Eur. J. Biochem.* **1969,** *9,* 512–518.

[24] Brown, N. C.; Eliasson, R.; Reichard, P.; Thelander, L. Nonheme Iron as a Cofactor in Ribonucleotide Reductase from *E. coli*. *Biochem. Biophys. Res. Commun.* **1968,** *30,* 522–527.

[25] Biakley, R. L. Ribonucleoside Triphosphate Reductase from *Lactobacillus leichmannii*. *Meth. Enzymol.* **1978,** *51,* 246–259.

[26] Stubbe, J.; van der Donk, W. A. Ribonucleotide reductases: radical enzymes with suicidal tendencies. *Chem. Biol.* **1995,** *2,* 793-801.

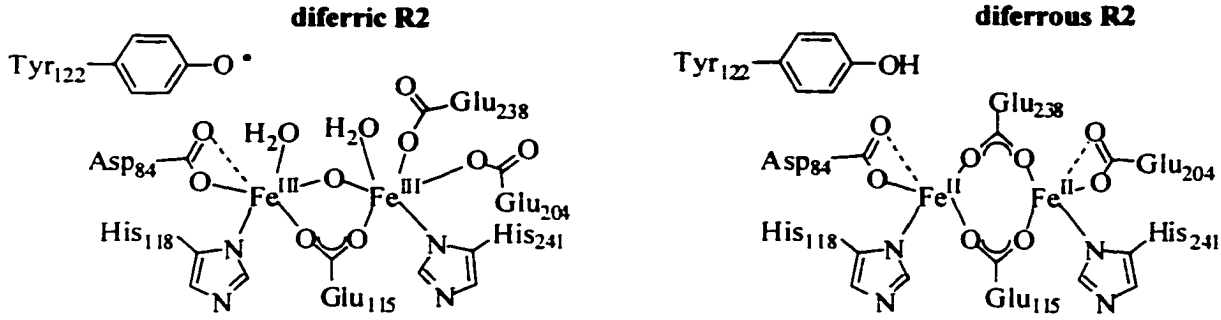

Figure 1.3. The iron coordination spheres of oxidized (diferric) and reduced (diferrous) *E. coli* R2. Note the "carboxylate shift" from the active form (in which there is a water bound to each metal, an oxo bridge, and monodentate Glu238 and Glu204) to the reduced form, where Asp84 remains bidentate and Glu115 remains as a bridging ligand. The oxo bridge and waters are lost, and Glu204 becomes bidentate. Adapted from Eklund, *et al.*, and Logan, *et al.*, respectively; not to scale.

definitively that there are *two* μ-oxo diiron sites in the R2 dimer, each with a separate radical Y122. (Early speculations had included a structure with an oxo bridge between the two subunits, having one iron atom in each, near the surface.[27]) Surprisingly, these clusters were found to be buried 10 Å from the surface of the protein! The tyrosyl radical is 5.3 Å from the closer iron, in a hydrophobic pocket. These facts preclude direct reduction of ribonucleotides by the iron center, and broach the possibility of an electron transfer pathway through conserved residues to the surface and into R1.

Stable tyrosyl radical in the active site. When the iron content of R2 was being quantified, a unique spectroscopic feature was noted, a small sharp peak at 410 nm

[27] Stubbe, J. Ribonucleotide reductases. In *Advances in Enzymology and Related Areas of Molecular Biology;* Meister, A., Ed.; Interscience: New York, 1990; Vol. 63; pp 349-419.

(Figure 1.4). Following treatment with hydroxyurea or hydroxylamine, it disappeared (along with bands at 325 and 360 nm); iron was not removed by either reagent.

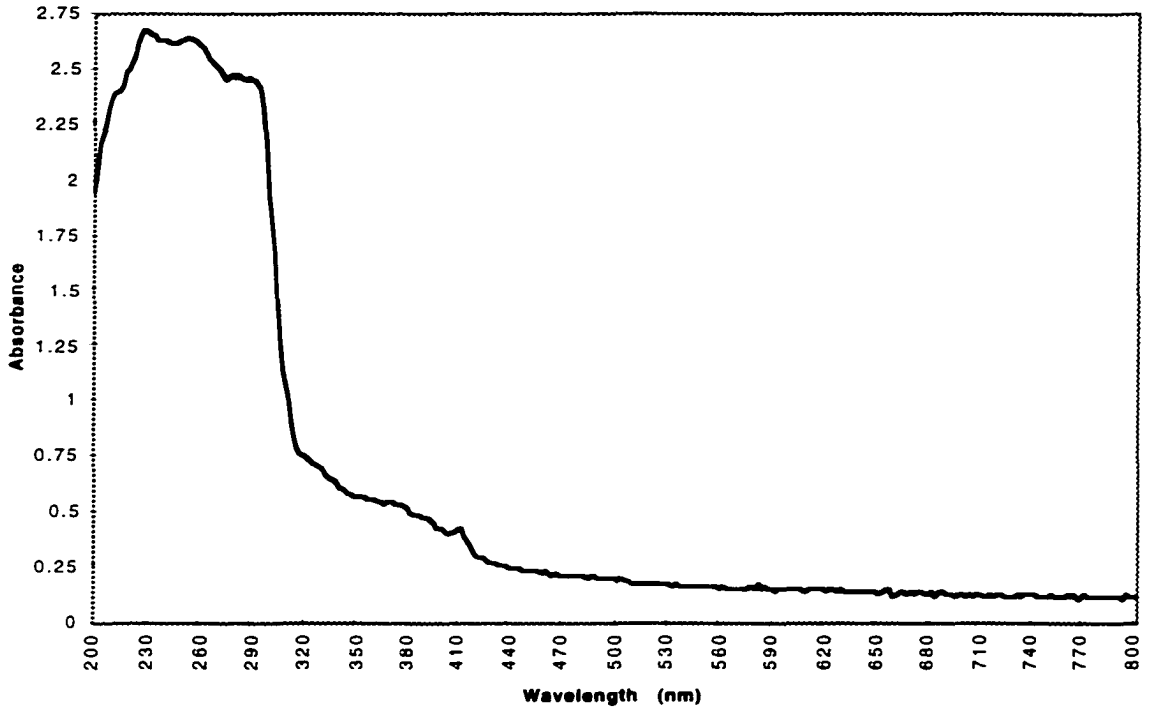

Figure 1.4. Electronic spectrum of active R2 in tris buffer. Important features include the tyrosyl radical (410 nm) and the μ-oxo metal cluster (325, 360 nm). Collected routinely during our work with the enzyme as a measure of concentration and activity.

Subsequent EPR studies demonstrated the presence of a signal at $g = 2.0047$ (Figure 1.5).[28] The spectrum recorded from 14–293 K is a slightly asymmetric doublet with only a weak g anisotropy, and showed "striking similarities" to the spectra of oxy– and methemerythrin. The possibility that the species responsible for the signal was an iron

[28] Ehrenberg, A.; Reichard, P. Electron Spin Resonance of the Iron-containing Protein B2 from Ribonucleotide Reductase. *J. Biol. Chem.* **1972**, *247*, 3485–3488.

complex was considered and discounted in favor of a free radical, possibly a semiquinone or sulfur species.

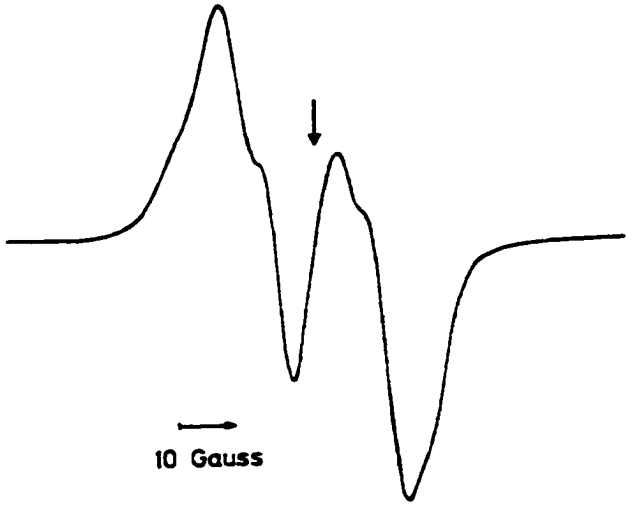

Figure 1.5. EPR spectrum of the tyrosyl radical of ribonucleotide reductase R2. Collected at 9.1 GHz and 88 K, it is centered at $g = 2.0047$ (indicated by the vertical arrow). From Ehrenberg and Reichard. Used with permission.

This stable organic free radical was linked both to the presence of iron in the protein and the 410 nm feature in the electronic spectrum.[29] Finally in 1977 this unknown species was identified by isotopic substitution as a tyrosine residue,[30] although the authors' exact interpretation was somewhat in error. The radical is not on the benzyl

[29] Atkin, C. L.; Thelander, L.; Reichard, P.; Land, G. Iron and Free Radical in Ribonucleotide Reductase: Exchange of Iron and Mössbauer Spectroscopy of the Protein B2 Subunit of the *Escherichia coli* Enzyme. *J. Biol. Chem.* **1973**, *248*, 7464–7472.

[30] Sjöberg, B.-M.; Reichard, P.; Gräslund, A.; Ehrenberg, A. Nature of the Free Radical in Ribonucleotide Reductase from *Escherichia coli*. *J. Biol. Chem.* **1977**, *252*, 536–541.

carbon ($HO–C_6H_4–CH•–$), but is delocalized *into the aromatic ring* from the oxygen of an oxidized tyrosine residue.[31]

An in–depth high–frequency EPR study of the tyrosyl radical in R2 conducted in 1993[32] allowed fine structure to be observed. This was the first such spectrum of a protein radical that exhibited both Zeeman and hyperfine structure, allowing a detailed characterization: Y122• is not ortho–substituted like some other enzymatic radicals; and R2 has approximately 30% more spin density on the phenoxy oxygen than does the neutral tyrosyl radical in photosystem II or irradiated tyrosine crystals. Hydrogen bonding to phenoxy radicals reduces spin density at oxygen, so the results suggest that Y122• in RNR is not hydrogen–bonded.

Further evidence regarding the lack of hydrogen bonding was published in 1999,[33] when a single crystal of *N*-acetyl-L-tyrosine was subjected to γ–irradiation and the resulting radicals studied by various EPR methods. (Hydrogen bonding in proteins can sometimes be confirmed crystallographically when the data are of sufficiently high resolution, which is not always the case for proteins.) Hydrogen bonding alters the π spin density distribution around the ring in tyrosyl radicals, whether the matrix happens to be a single crystal or a biological macromolecule. Phenoxyl radicals that are not

---

[31] Gräslund, A.; Sahlin, M.; Sjöberg, B.-M. The Tyrosyl Free Radical in Ribonucleotide Reductase. *Environ. Health Perspect.* **1985,** *64,* 139–149.

[32] Gerfen, G. J.; Bellew, B. F.; Un, S.; Bollinger, J. M., Jr.; Stubbe, J.; Griffin, R. G.; Singel, D. J. High–Frequency (139.5 GHz) EPR Spectroscopy of the Tyrosyl Radical in *Escherichia coli* Ribonucleotide Reductase. *J. Am. Chem. Soc.* **1993,** *115,* 6420–6421.

hydrogen–bonded, such as the compound *N*-acetyl-L-tyrosine, or the Y122• in R2, typically have *g* tensor components slightly larger than those in hydrogen–bonded systems such as Y_D• and Y_Z• of photosystem II. For instance, the g_x and g_{iso} values for the four tyrosyl radicals are 2.0094 and 2.0055 (*N*-acetyl-L-tyrosine), 2.00868 and 2.00500 (Y122•), 2.00740 and 2.00466 (Y_D•), and 2.00750 and 2.00466 (Y_Z•).

In 1996 Sjöberg and Babcock[34] reported the spin density distribution (as determined using ^{17}O hyperfine coupling EPR and ENDOR). The tyrosine phenol oxygen spin density is 0.29(2), with substantial spin density located at the carbons ortho and para to the phenolic oxygen. This gives the tyrosyl radical an odd-alternant pattern like an isoelectronic benzyl radical. The proton hyperfine couplings in *E. coli* RNR are shown in Table 1.

Table 1. Proton hyperfine couplings of the tyrosyl radical in *E. coli* R2. From Sjöberg and Babcock. Couplings are in MHz, angles ϕ are rotations about the molecular *Z* axis (normal to the phenol ring plane) between the *g* tensor and the hyperfine tensors.

Position	A_X	A_Y	A_Z	A_{iso}	ϕ
ring 3,5	–26.7	–8.4	–19.6	–18.2	25
ring 2,6	+5.0	+7.6	+2.1	+4.9	44
methylene	+61.2	+53.7	+53.7	+56.2	16
methylene	+2.1	–5.0	–4.0	–2.3	–26

[33] Mezzetti, A.; Maniero, A. L.; Brustolon, M.; Giacometti, G.; Brunel, L. C. A Tyrosyl Radical in an Irradiated Single Crystal of *N*-acetyl-L-tyrosine Studied by X-band cw-EPR, High-Frequency EPR, and ENDOR Spectroscopies. *J. Phys. Chem. A* **1999,** *103,* 9636–9643; and references therein.

[34] Hoganson, C. W.; Sahlin, M.; Sjöberg, B.–M.; Babcock, G. T. Electron Magnetic Resonance of the Tyrosyl Radical in Ribonucleotide Reductase from *Escherichia coli*. *J. Am. Chem. Soc.* **1996,** *118,* 4672–4679.

Mutagenesis experiments localized the radical to Y122 in 1986,[35] by showing that the mutant protein R2–Y122F,[36] while enzymatically inactive and lacking an EPR signal and the peak at 410 nm in the UV-vis, formed the same metal center as wt R2 (the form of the protein without any engineered mutations).

The oxo bridge of the diiron site. Resonance Raman studies of the protein R2 in both its active and met forms were published in 1982. It was shown that incubation of R2 in $H_2{}^{18}O$ resulted in the shifting of a 496 cm^{-1} peak (in resonance with the iron–based electronic transition at 370 nm) to 481 cm^{-1}, indicating an iron–oxygen moiety having the ability to exchange with solvent (such as the bridging oxo in oxyhemerythrin). Similar treatment with D_2O, however, failed to identify any isotopic shifts, signifying that the bridge is unprotonated in R2.[37]

Reconstitution of the active site in the presence of $^{16}O_2$ or $^{18}O_2$ was monitored by Resonance Raman.[38] This work was facilitated by two important R2 mutants (Figure 1.6): Y122F, which produces the same iron center as wild type R2 but is more stable to the laser irradiation necessary to collect Raman data; and F208Y, in which F208Y is

---

[35] Larsson, Å.; Sjöberg, B.-M. Identification of the stable free radical tyrosine residue in ribonucleotide reductase. *EMBO J.* **1986,** *5,* 2037–2040.

[36] Standard biochemical notation for site–directed mutations uses the one–letter amino acid abbreviations on either side of the location number. Thus, Y122F R2 is the mutant where the tyrosine at position 122 in the native enzyme has been replaced by phenylalanine.

[37] Sjöberg, B.-M.; Loehr, T. M.; Sanders-Loehr, J. Raman Spectral Evidence for a μ-Oxo Bridge in the Binuclear Iron Center of Ribonucleotide Reductase. *Biochemistry* **1982,** *21,* 96–102.

[38] Ling, J.; Sahlin, M.; Sjöberg, B.-M.; Loehr, T. M.; Sanders-Loehr, J. Dioxygen Is the Source of the μ-Oxo Bridge in Iron Ribonucleotide Reductase. *J. Biol. Chem.* **1994,** *269,* 5595–5601.

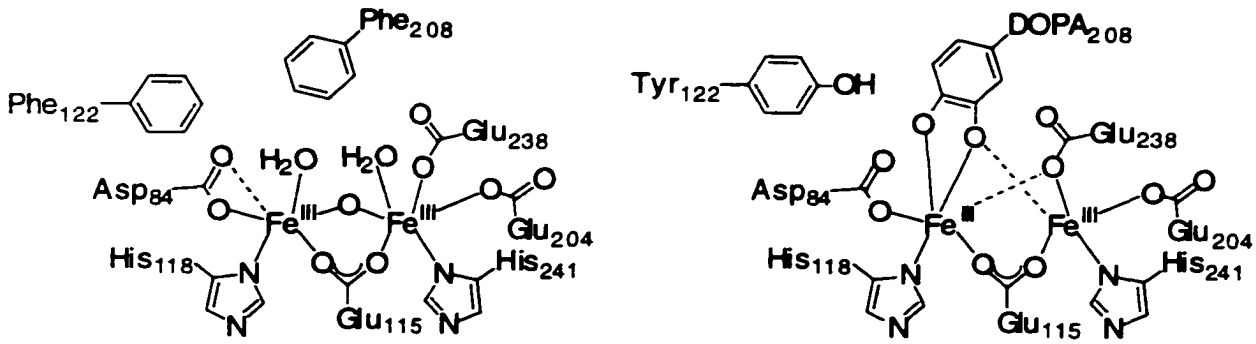

Figure 1.6. The iron sites of two important R2 mutants. Y122F is on the left, and F208Y is on the right; the latter forms DOPA upon reconstitution. Adapted from Tong[39] and Åberg.[40]

hydroxylated (during the reassembly of the active site) to DOPA, which binds to iron(III) as a bidentate ligand and inactivates the protein. After reconstitution of R2–F208Y, numerous characteristic Fe–O/catecholate stretching frequencies were observed in the resonance Raman spectra, and the chelation was subsequently confirmed by crystallography.[41] Vibrational studies of DOPA–208 R2 reconstituted with $^{16}O_2$, $^{18}O_2$ (or $^{16}O_2$ in the presence of $H_2{}^{18}O$) showed quantitative incorporation of the dioxygen label into the oxo bridge, and into the extra hydroxyl of DOPA–208.[38] In 1991 Elgren, *et*

---

[39] Tong, W.; Burdi, D.; Riggs-Gelasco, P.; Chen, S.; Edmondson, D.; Huynh, B. H.; Stubbe, J.; Han, S.; Arvai, A.; Tainer, J. Characterization of Y122F R2 of *Escherichia coli* Ribonucleotide Reductase by Time-Resolved Physical Biochemical Methods and X-ray Crystallography. *Biochemistry* **1998**, *37*, 5840-5848.

[40] Åberg, A.; Ormö, M.; Nordlund, P.; Sjöberg, B.-M. Autocatalytic Generation of Dopa in the Engineered Protein R2 F208Y from *Escherichia coli* Ribonucleotide and Crystal Structure of the Dopa-208 Protein. *Biochemistry* **1993**, *32*, 9845-9850.

[41] Logan, D. T.; deMare, F.; Persson, B. O.; Slaby, A.; Sjöberg, B.-M.; Nordlund, P. Crystal Structures of Two Self-Hydroxylating Ribonucleotide Reductase Protein R2 Mutants: Structural Basis for the Oxygen-Insertion Step of Hydroxylation Reactions Catalyzed by Diiron Proteins. *Biochemistry* **1998**, *37*, 10798–10807.

al. quantified the iron and oxygen necessary for reconstitution of R2; each equivalent of O_2 oxidized 3.1 Fe(II) and 0.8 equivalents of Y122.[42]

B. Mechanism of reconstitution of R2.

The first mechanistic studies by Norton and Stubbe in 1991[43,44] identified and partially characterized the intermediates **U** and **X**. The formation of Y122• (which is also the easiest characteristic to follow spectroscopically; see Figures 1.7 and 1.8 for my own repetitions of this reaction) from apo R2, excess Fe(II) and O_2 proceeds at 1 s^{-1} at 5 °C. The rate constant is independent of [apo], [Fe(II)] and [O_2]. This could be explained by a conformational change, as suggested by Stubbe in 1994.[45]

---

[42] Elgren, T. E.; Lynch, J. B.; Juarez-Garcia, C.; Münck, E.; Sjöberg, B.-M.; Que, L., Jr. Electron Transfer Associated with Oxygen Activation in the B2 Protein of Ribonucleotide Reductase from *Escherichia coli*. *J. Biol. Chem.* **1991,** *266,* 19265–19268.

[43] Bollinger, J. M., Jr.; Edmondson, D. E.; Huynh, B. H.; Filley, J.; Norton, J. R.; Stubbe, J. Mechanism of Assembly of the Tyrosyl Radical—Dinuclear Iron Cluster Cofactor of Ribonucleotide Reductase. *Science* **1991,** *253,* 292–298.

[44] Bollinger, J. M., Jr.; Stubbe, J.; Huynh, B. H.; Edmondson, D. E. Novel Diferric Radical Intermediate Responsible for Tyrosyl Radical Formation in Assembly of the Cofactor of Ribonucleotide Reductase. *J. Am. Chem. Soc.* **1991,** *113,* 6289-6291.

[45] Bollinger, J. M., Jr.; Tong, W. H.; Ravi, N.; Huynh, B. H.; Edmondson, D. E.; Stubbe, J. Mechanism of Assembly of the Tyrosyl Radical—Diiron(III) Cofactor of *E. coli* Ribonucleotide Reductase. 2. Kinetics of The Excess Fe^{2+} Reaction by Optical, EPR, and Mössbauer Spectroscopies. *J. Am. Chem. Soc.* **1994,** *116,* 8015-8023.

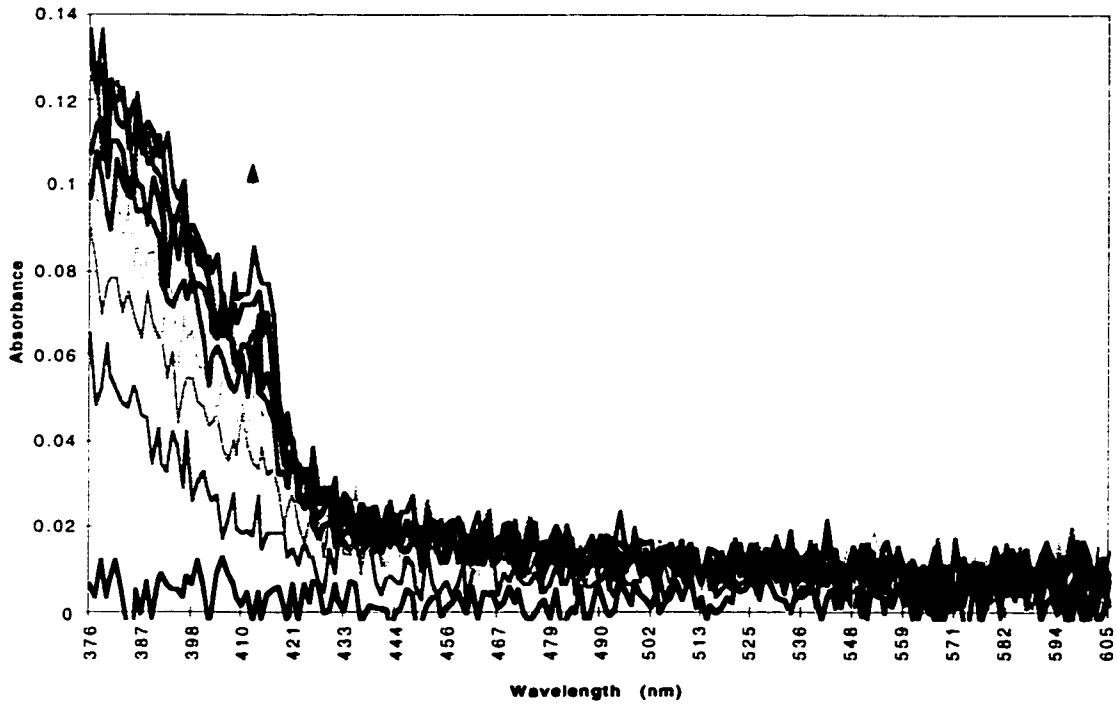

Figure 1.7. Reconstitution of apo R2 by excess ferrous iron and oxygen. Conditions: apo R2, 19.5 μM; ferrous iron, 100 μM; ascorbate, 1.5 mM; HEPES buffer 50 mM, pH 7.6 at 5.0 °C, $I = 0.1$ M. Interval between spectra is approximately 100 ms.

Depending on conditions, the activation of R2 can take either pathway of a bifurcated mechanism: when there is only limited iron(II) available, **U** builds up and is observed; if there is an excess of iron(II) or if ascorbate (a one-electron reducing agent) is present, **X** is observed instead.

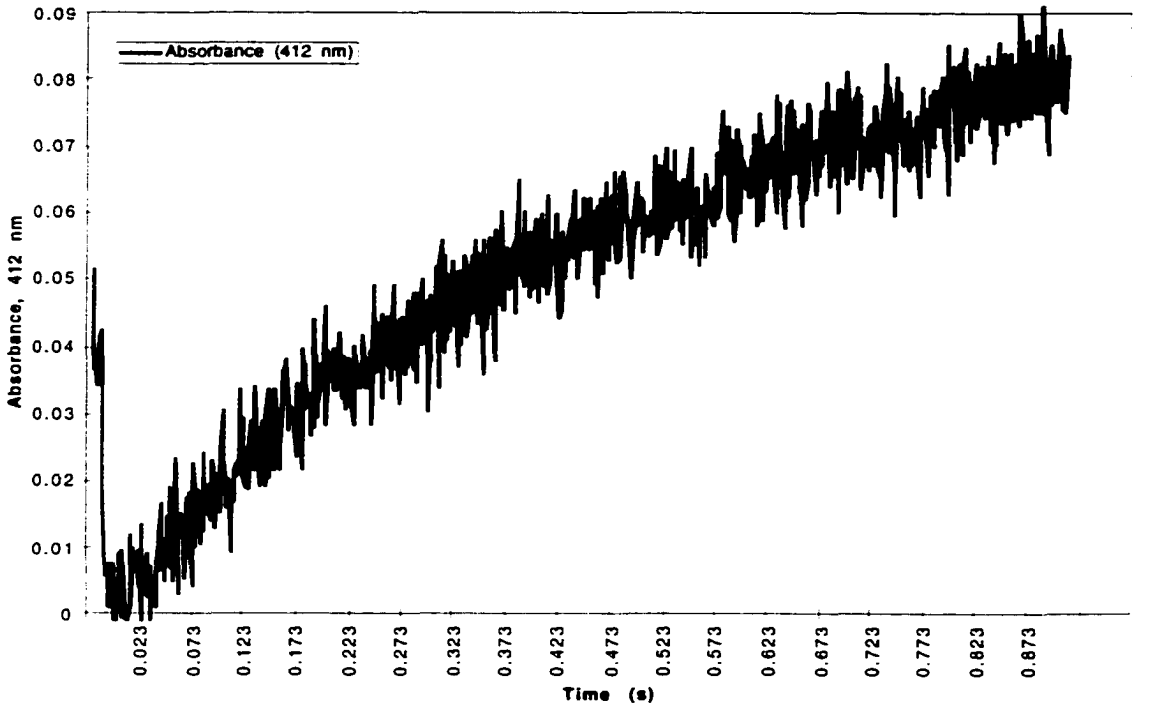

Figure 1.8. Reconstitution of apo R2 with oxygen and excess iron, followed at 410 nm. Single–wavelength trace (412 nm) extracted from the rapid–scanned stopped–flow data of Figure 1.7. This particular reaction was performed at 5.0 °C in 50 mM HEPES (pH 7.6) buffer, with 100 μM Fe(II), 19.5 μM apo, and 1.5 mM ascorbate.

Intermediate U. Intermediate **U** (observed during reconstitutions by limiting amounts of iron(II)) is a species which has a broad absorbance at approximately 560 nm (ε = 1500–4800 M^{-1} cm^{-1}), appearing at the rate of 8 s^{-1} and decaying at 3 s^{-1} with maximal concentration at 0.25 seconds. Because it disappears at approximately the same rate as Y122• is formed, **U** must be an intermediate in the formation of that product. The fact that **U** does not build up in the presence of reductant indicates it is not stable under those conditions and is quickly (> 20 s^{-1}) reduced to the next intermediate. Rapid freeze–

quench (RFQ) Mössbauer and EPR evidence[46] indicated **U** is *not* iron–based (μ–peroxodiiron(III)) as first proposed by Stubbe.[43] Instead, this 560–nm intermediate has been assigned to •**W48H**$^+$, fulfilling the spectroscopic requirements of a carbon–based radical. R2's hydrogen bonding network from Trp48 to Fe_A appears very similar to that between the heme iron and W191 of cytochrome *c* peroxidase.[47] It is Trp48 that breaks the otherwise 2–electron chemistry into two 1–electron steps, dividing the oxidizing equivalents between •**WH**$^+$ and **X**, thus preventing high–valency chemistry (for instance Fe^{IV}–Fe^{IV}, reminiscent of MMOH) at the R2 active site (Figure 1.14).[48]

I was able to reproduce the stopped–flow observation of intermediate **U** in our laboratory. The raw data (Figure 1.9) as collected show the same information but are much noisier than the back–calculated spectra (Figure 1.11) of the three species in solution during an A→B→C situation such as this one. A slice perpendicular to the spectral axis can be taken at a specific wavelength, of absorbance vs. time, to view the rise and fall of the intermediate. Figure 1.10 (from the raw data) illustrates the lifetime of •W48H$^+$ as observed at 561 nm, the λ_{max} of intermediate **U**.

---

[46] Bollinger, J. M., Jr.; Tong, W. H.; Ravi, N.; Huynh, B. H.; Edmondson, D. E.; Stubbe, J. Mechanism of Assembly of the Tyrosyl Radical—Diiron(III) Cofactor of *E. coli* Ribonucleotide Reductase. 3. Kinetics of The Limiting Fe^{2+} Reaction by Optical, EPR, and Mössbauer Spectroscopies. *J. Am. Chem. Soc.* **1994,** *116,* 8024–8032.

[47] Finzel, B. C.; Poulos, T. L.; Kraut, J. Crystal Structure of Yeast Cytochrome *c* Peroxidase Refined at 1.7–Å Resolution. *J. Biol. Chem.* **1984,** *259,* 13027–13036.

[48] Parkin, S. E.; Chen, S.; Ley, B. A.; Mangravite, L.; Edmondson, D. E.; Huynh, B. H.; Bollinger, J. M., Jr. Electron Injection through a Specific Pathway Determines the Outcome of Oxygen Activation at the Diiron Cluster in the F208Y Mutant of Ribonucleotide Reductase Protein R2. *Biochemistry* **1998,** *37,* 1124–1130.

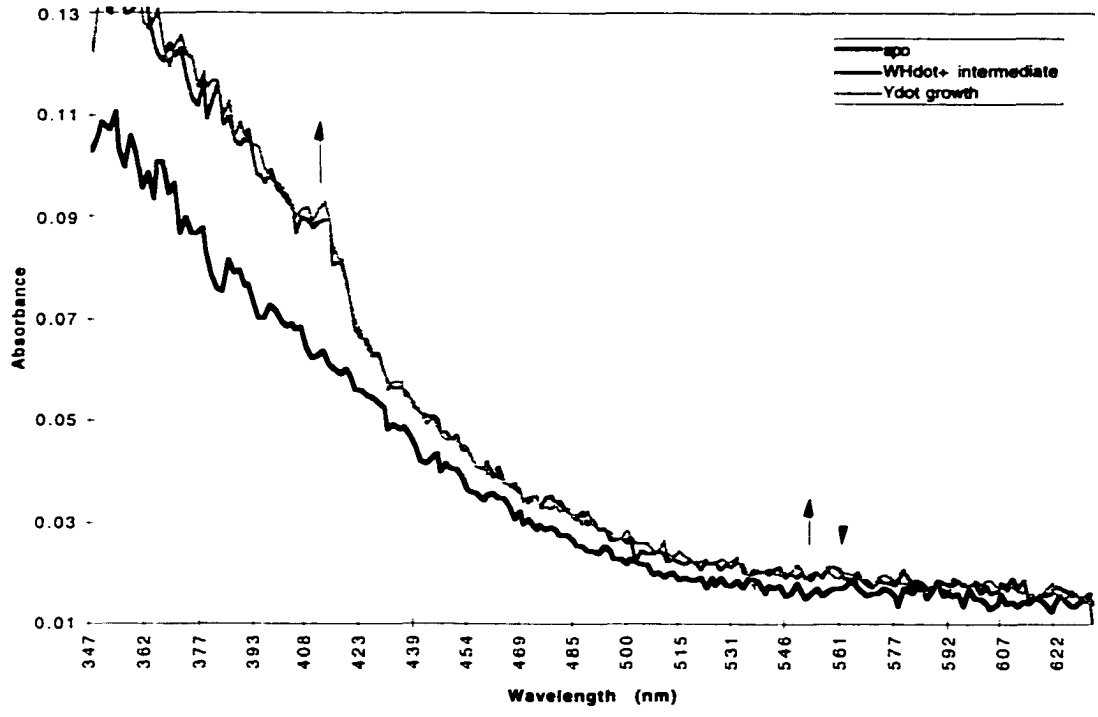

Figure 1.9. Selected stopped–flow spectra of apoR2, •W48H$^+$, and active R2. The transient feature centered at 560 nm is due to •W48H$^+$. The broad absorbance due to the oxo–bridged diiron center (360 nm) forms concomitantly with intermediate **U**, but the sharp 410 nm signature of the tyrosyl radical only appears as the tryptophan radical disappears. Conditions: 21.6 μM apo R2, 44.9 μM ferrous ammonium sulfate, 50 mM Tris buffer (5% v/v glycerol) pH 7.6 at 4.0 °C.

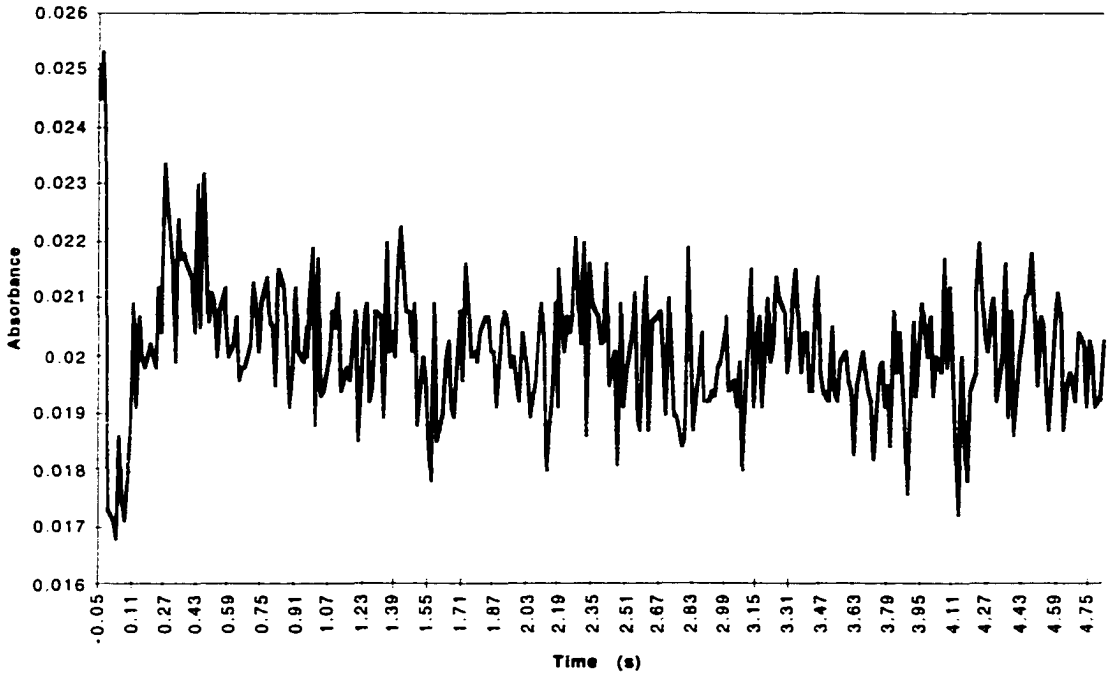

Figure 1.10. Single–wavelength (561 nm) stopped–flow data during the reconstitution of R2 protein under limiting iron conditions. The absorbance is maximal by 250–300 ms, in agreement with Bollinger, *et al.*[43] Conditions: 21.6 μM apo R2, 44.9 μM ferrous ammonium sulfate, 50 mM Tris buffer (5% v/v glycerol) pH 7.6 at 4.0 °C.

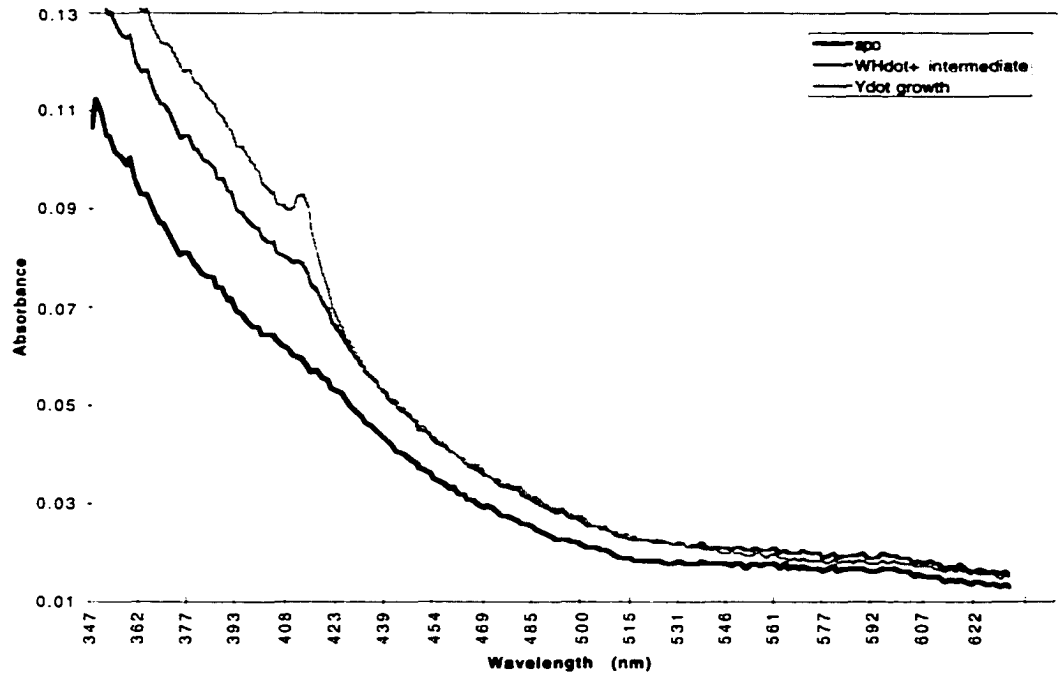

Figure 1.11. Back-calculated individual spectra of apo R2, •W48H$^+$, and Y122•. Apo R2 is mostly featureless over the range shown; •W48H$^+$ has a broad absorbance at 560 nm and some tyrosyl radical already formed; and the small, sharp signature peak of active R2's •Y122 is at 410 nm. Conditions: 21.6 μM apo R2, 44.9 μM ferrous ammonium sulfate, 50 mM Tris buffer (5% v/v glycerol) pH 7.6 at 4.0 °C.

Along with calculating "true" spectra of the three species in solution, the global fitting routine generates plots of the relative populations of the apo, •W48H$^+$ and •Y122 present over the course of the reaction (Figure 1.12). From this we found a maximal concentration of •W48H$^+$ at approximately 300 ms.

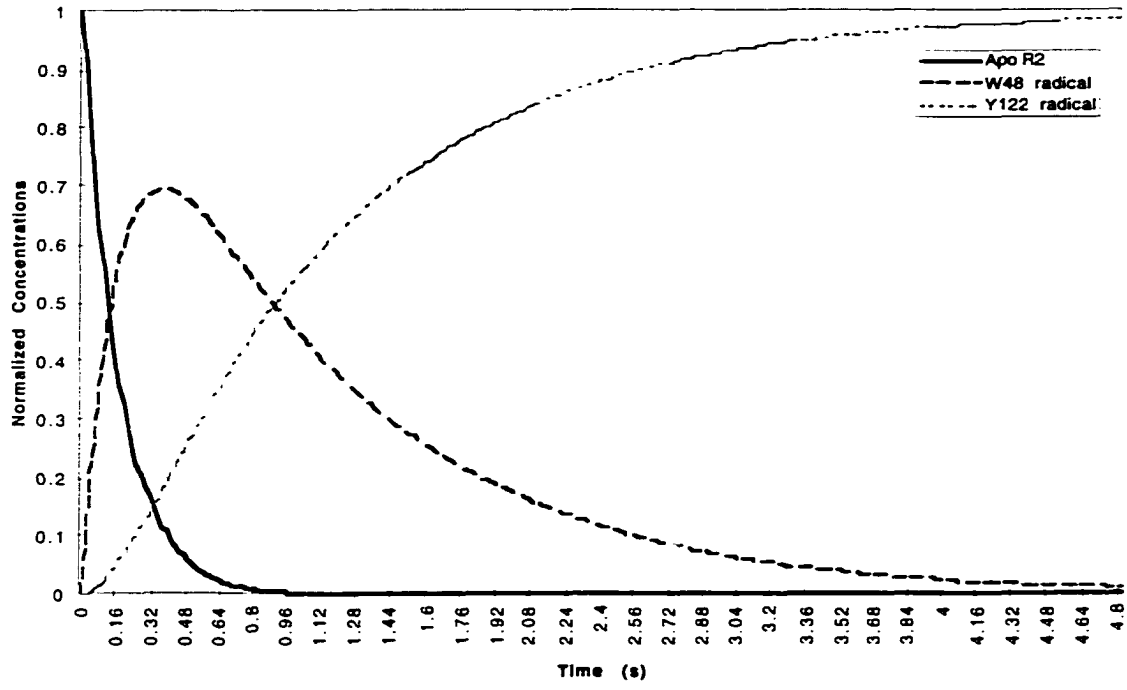

Figure 1.12. Relative populations of apo R2, •W48H+ and •Y122 during reconstitution with limited amounts of iron. Conditions: 21.6 μM apo R2, 44.9 μM ferrous ammonium sulfate, 50 mM Tris buffer (5% v/v glycerol) pH 7.6 at 4.0 °C.

Intermediate X. As determined using RFQ EPR spectroscopy,[43,49] **X** is formed at 8 s^{-1} (in the excess iron mechanism) and decays concomitantly (at 0.7–1.0 s^{-1}) as Y122• and the μ-oxo diferric cluster are formed; its concentration is maximal at 0.33 seconds in wild–type R2. Reconstitution of the R2 mutant Y122F (in which the tyrosine is substituted by the inoxidizable residue phenylalanine, allowing **X** to build up at a yield of one equivalent per subunit) confirms that **X** is indeed a competent intermediate. Significant amounts of it remain after 5 seconds in R2–Y122F; rapid–freeze–quench

[49] Ravi, N.; Bollinger, J. M., Jr.; Huynh, B. H.; Edmondson, D. E.; Stubbe, J. Mechanism of Assembly of the Tyrosyl Radical—Diiron (II) Cofactor of *E. coli* Ribonucleotide Reductase. 1. Mössbauer Characterization of the Diferric Radical Precursor. *J. Am. Chem. Soc.* **1994,** *116,* 8007–8014.

treatment of the mutant enzyme in this state has enabled many EPR and Mössbauer experiments. Such stabilization allowed the breakthrough hypothesis in 1996[12] that **X** is a spin–coupled ferric/ferryl (Fe^{III}–Fe^{IV}) species without an organic radical component. ENDOR studies of this species[50] reported in 1997 determined the nature of the protonated oxygenic ligands of **X**. Extensive work using both H_2O and D_2O buffers enabled the assignment of two oxygenic protons as a terminal water (or a 2–fold disordered hydroxyl) bound to Fe(III). Just as importantly, the possibility of a bridging hydroxo between the two metal atoms was eliminated. Subsequent ^{17}O ENDOR experiments[51] determined that the terminal ligand is indeed water. Thus, **X** can best be represented as a [$(H_2O)Fe^{III}OFe^{IV}$] fragment. Interatomic distances were determined (using RFQ EXAFS[52]) to be quite short (Fe–Fe = 2.5 Å, Fe–O = 1.8 Å) This was observed in both the wild–type and Y122F proteins. In order to achieve such small metal–metal separations, multiple bridges must be present. In contrast, the Fe–Fe distance in diferric R2 is 3.23 Å, and undetectable in diferrous R2 (although it would be expected to be ca. 3.9 Å).

---

[50] Willems, J.-P.; Lee, H.-I.; Burdi, D.; Doan, P. E.; Stubbe, J.; Hoffman, B. M. Identification of the Protonated Oxygenic Ligands of Ribonucleotide Reductase Intermediate X by Q-Band $^{1,2}H$ CW and Pulsed ENDOR. *J. Am. Chem. Soc.* **1997,** *119,* 8916–9824.

[51] Burdi, D.; Willems, J.-P.; Riggs-Gelasco, P.; Antholine, W. E.; Stubbe, J.; Hoffman, B. M. The Core Structure of X Generated in the Assembly of the Diiron Cluster of Ribonucleotide Reductase: $^{17}O_2$ and $H_2{}^{17}O$ ENDOR. *J. Am. Chem. Soc.* **1998,** *120,* 12910–12919.

[52] Riggs-Gelasco, P. J.; Shu, L.; Chen, S.; Burdi, D.; Huynh, B. H.; Que, L., Jr.; Stubbe, J. EXAFS Characterization of the Intermediate X Generated During the Assembly of the *Escherichia coli* Ribonucleotide Reductase R2 Diferric Tyrosyl Radical Cofactor. *J. Am. Chem. Soc.* **1998,** *120,* 849–860.

The originally proposed mechanism of reconstitution of RNR R2 is summarized in Figure 1.13. Numerous studies have since focused on the various intermediates and the rates at which they and the final protein products are formed.[53,54,55]

In many cases, site–directed mutagenesis ("engineering") of one or more amino–acid residues crucial to reconstitution has allowed workers to stabilize intermediates enough to perform both static[51,56,57] and kinetic[39] spectroscopic studies. Use of mutant R2s (in particular Y122F; see Figure 1.5) coupled with X–ray crystallographic studies of the native enzyme in various states of oxidation and metallation including diferric (active),[58,59,60] reduced (diferrous, radical–free),[61] and apo (metal–free, radical–free)[62] has

---

[53] Tong, W. H.; Chen, S.; Lloyd, S. G.; Edmondson, D. E.; Huynh, B. H.; Stubbe, J. Mechanism of Assembly of the Diferric Cluster—Tyrosyl Radical Cofactor of *Escherichia coli* Ribonucleotide Reductase from the Diferrous Form of the R2 Subunit. *J. Am. Chem. Soc.* **1996,** *118,* 2107–2108.

[54] Moenne-Loccoz, P.; Baldwin, J.; Ley, B. A.; Loehr, T. M.; Bollinger, J. M., Jr. O_2 Activation by Non-Heme Diiron Proteins: Identification of a Symmetric μ-1,2-Peroxide in a Mutant of Ribonucleotide Reductase. *Biochemistry* **1998,** *37,* 14659–14663.

[55] Huynh, B. H.; Bollinger, J. M., Jr.; Edmondson, D. E. Reaction Intermediates in Oxygen Activation Reactions by Enzymes Containing Carboxylate-Bridged Binuclear Iron Clusters. In *Spectroscopic Methods in Bioinorganic Chemistry;* Solomon, E. I., Hodgson, K. O., Eds.; ACS Symposium Series 692; American Chemical Society: Washington, DC, 1998, pp 403–422.

[56] Regnström, K.; Åberg, A.; Ormö, M.; Sahlin, M.; Sjöberg, B.-M. The Conserved Serine 211 Is Essential for Reduction of the Dinuclear Iron Center in Protein R2 of *Escherichia coli* Ribonucleotide Reductase. *J. Biol. Chem.* **1994,** *269,* 6355–6561.

[57] Persson, B. O.; Karlsson, M.; Climent, I.; Ling, J.; Loehr, J. S.; Sahlin, M.; Sjöberg, B.-M. Iron ligand mutants in protein R2 of *Escherichia coli* ribonucleotide reductase: Retention of diiron site, tyrosyl radical and enzymatic activity in mutant proteins lacking an iron-binding chain. *J. Bioinorg. Chem.* **1996,** *1,* 247–256.

[58] Nordlund, P.; Uhlin, U.; Westergren, C.; Joelson, T.; Sjöberg, B.-M.; Eklund, H. New crystal forms of the small subunit of ribonucleotide reductase from *Escherichia coli. FEBS Lett.* **1989,** *258,* 251–254.

[59] Nordlund, P.; Sjöberg, B.-M.; Eklund, H. Three-dimensional structure of the free radical protein of ribonucleotide reductase. *Nature* **1990,** *345,* 593–598.

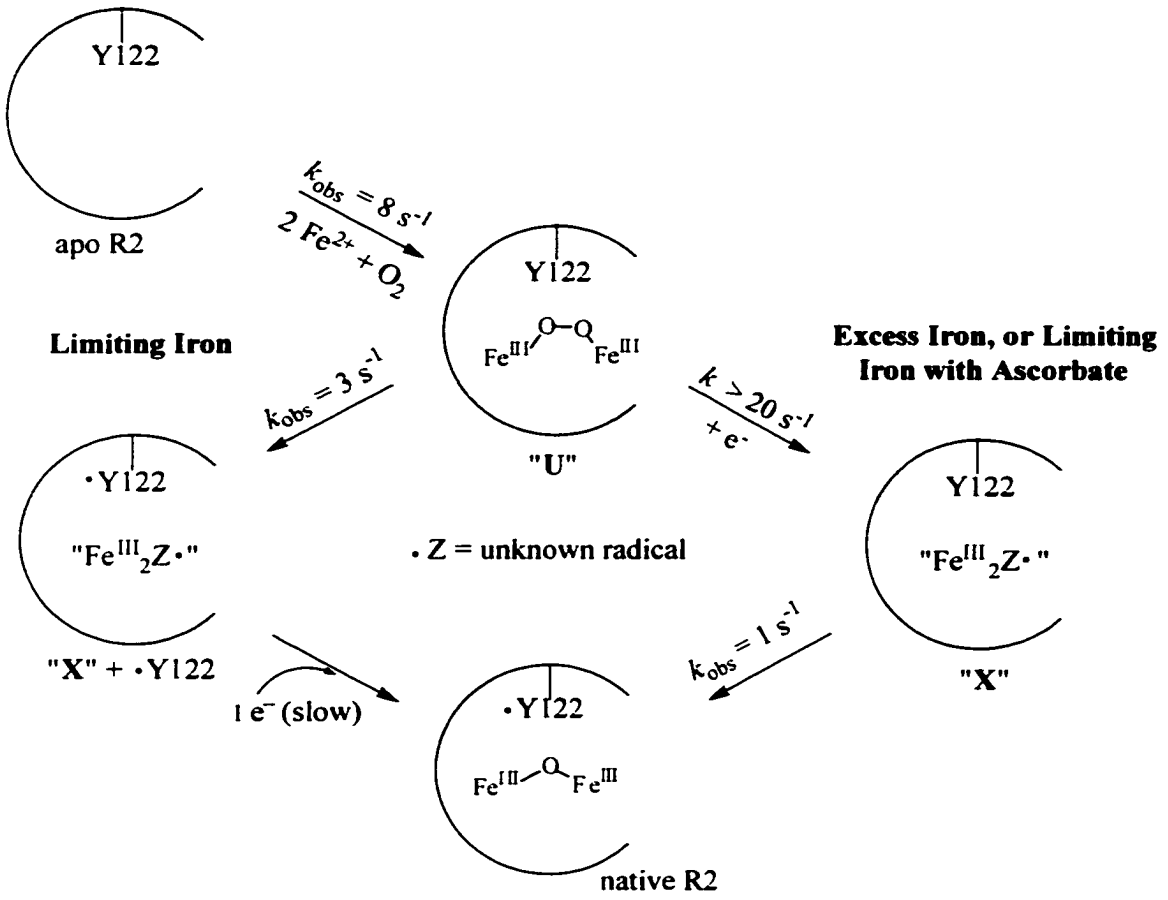

Figure 1.13. The originally–proposed mechanism (1991) of reconstitution of the R2 active site. Adapted from Stubbe, *et al.*[46] Limiting iron is 2.2 equivalents; excess iron is at least 5 equivalents. Subsequent work has further refined this scheme.

helped to define the probable electron transfer paths, both for activation of the radical center and for the catalytic turnover of substrate. The reduced (diferrous) form (Figure

---

[60] Nordlund, P.; Eklund, H. Structure and Function of the *Escherichia coli* Ribonucleotide Reductase Protein R2. *J. Mol. Biol.* **1993,** *232,* 123–164.

[61] Logan, D. T.; Su, X.-D.; Åberg, A.; Regnström, K.; Hajdu, J.; Eklund, H.; Nordlund, P. Crystal structure of reduced protein R2 of ribonucleotide reductase: the structural basis for oxygen activation at a dinuclear iron site. *Structure* **1996,** *4,* 1053–1064.

[62] Åberg, A.; Nordlund, P.; Eklund, H. Unusual clustering of carboxyl side chains in the core of iron-free ribonucleotide reductase. *Nature* **1993,** *345,* 276–278.

1.3) is especially relevant to the present work, as it is an intermediate in reconstitution from both apo and met R2 (diferric but lacking the radical on Y122),[63] as well as being the state reached by reduction of the active diferric form.[15,64,65]

The currently–accepted mechanism for reconstitution of the active site of R2 is shown in Figure 1.14.

It has been suggested that the iron sites of the two halves of the R2 dimer may perform different roles during reconstitution.[66] Active R2 exhibited two different reduction rates (one fast, *F*, per two slow, *S*, sites) during coulometric reductive titrations of the protein by dithionite and methyl viologen. The results could be interpreted to indicate via the microscopic reversibility principle that even in active R2, one of every three iron sites is in the met form (with a μ-oxo diiron(III) cluster, but no tyrosyl radical). It was suggested that this one is sacrificed to provide the extra electrons needed to complete the assembly of the other two, serving as the "slow external $Fe^{2+} \rightarrow Fe^{3+}$" step

---

[63] Covès, J.; Laulhère, J.-P.; Fontecave, M. The role of exogenous iron in the activation of ribonucleotide reductase from *Escherichia coli*. *J. Biol. Inorg. Chem.* **1997**, *2*, 418–426.

[64] Covès, J.; Delon, B.; Climent, I.; Sjöberg, B.-M.; Fontecave, M. Enzymic and chemical reduction of the iron center of the *Escherichia coli* ribonucleotide reductase protein R2: The role of the C-terminus. *Eur. J. Biochem.* **1995**, *233*, 357–363.

[65] Sahlin, M.; Gräslund, A.; Petersson, L.; Ehrenberg, A.; Sjöberg, B.-M. Reduced Forms of the Iron-Containing Small Subunit of Ribonucleotide Reductase from *Escherichia coli*. *Biochemistry* **1989**, *28*, 2618–2625.

[66] Miller, M. A.; Gobena, F. T.; Kauffmann, K.; Münck, E.; Que, L., Jr.; Stankovich, M. T. Differing Roles for the Diiron Clusters of Ribonucleotide Reductase from Aerobically Grown *Escherichia coli* in the Generation of the Y122 Radical. *J. Am. Chem. Soc.* **1999**, *121*, 1096–1097.

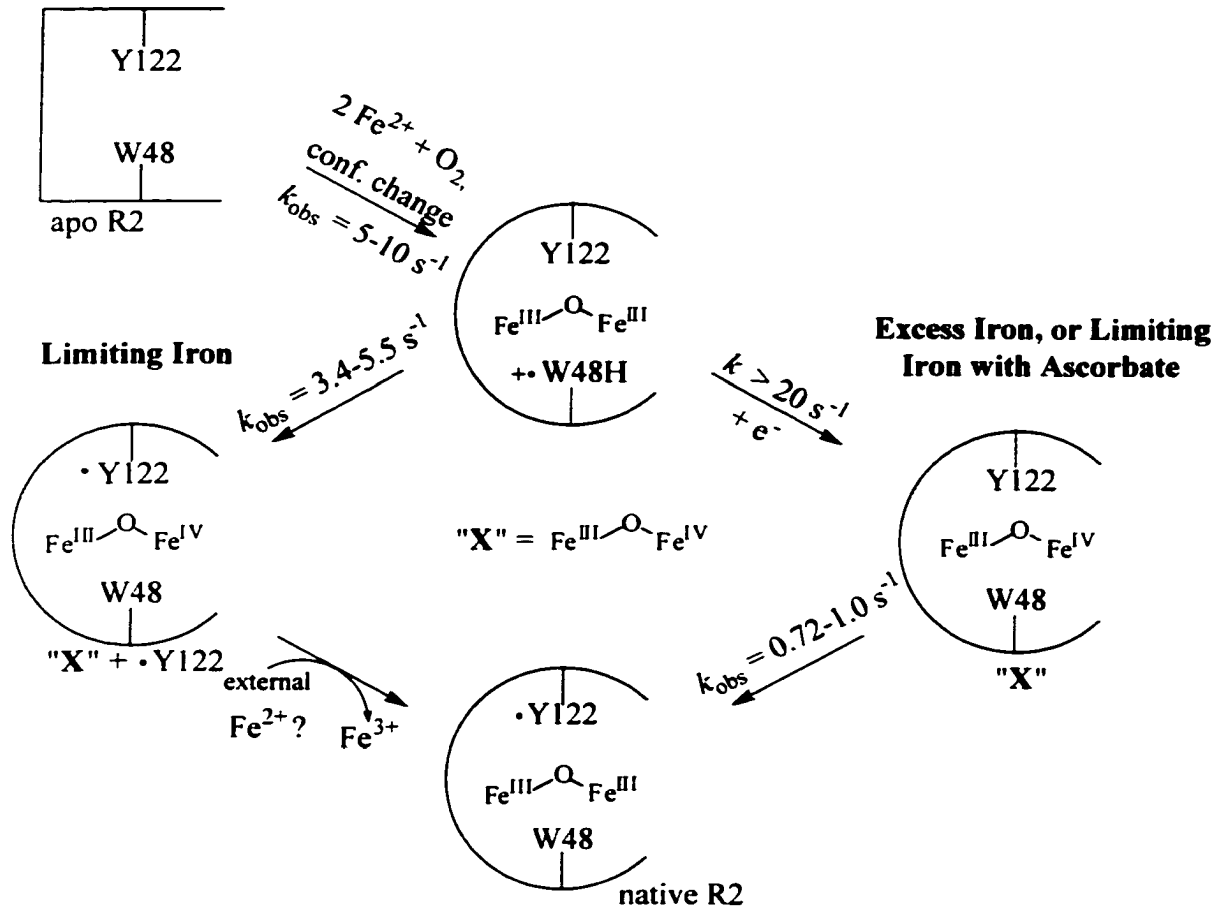

Figure 1.14. The currently accepted mechanism of the reconstitution of R2. The major modifications have been in the identification of **X** and the measurement of the rate of oxygen uptake. Summarized from Stubbe, *et al.*[12,46,53]

in the reconstitution (Figures 1.13, 1.14). Those authors proposed that the overall stoichiometry of reconstitution should therefore be modified as follows.

$$2\,S_{red} + 1\,F_{red} + 2\,O_2 \rightarrow 2\,[Y122\bullet, Fe^{III}\text{–}O\text{–}Fe^{III}] +$$

$$[Y122, Fe^{III}\text{–}O\text{–}Fe^{III}] + 2\,OH^- \qquad \textbf{Eq 1}$$

This proposal *could be* correct—there *are* a wide range of reported reconstitution stoichiometries in the literature.[42,43,67,68]

Electron–transfer path for reconstitution and catalytic turnover. The electron–transfer pathway between the R1 and R2 active sites has been the subject of much interest in recent years.[69,70,71,72,73] Using crystallographic data, the pathway of hydrogen–bonded amino acid side chains has been proposed to be R2's Tyr122, Asp84, His118, Asp237, Trp48 and Tyr356; R1's Tyr730, Tyr731 and Cys439.[74] Several site–directed mutagenesis studies have demonstrated that substitution of any one of a number

---

[67] Ochiai, E.–I.; Mann, G. J.; Gräslund, A.; Thelander, L. Tyrosyl free-radical formation in the small subunit of mouse ribonucleotide reductase. *J. Biol. Chem.* **1990,** *265,* 15758–15761.

[68] Silva, K. E.; Elgren, T. E.; Que, L., Jr.; Stankovich, M. T. Electron Transfer Properties of the R2 Protein of Ribonucleotide Reductase from *Escherichia coli. Biochemistry* **1995,** *34,* 14093–14103.

[69] Uhlin, U.; Eklund, H. Structure of ribonucleotide reductase protein R1. *Nature* **1994,** *370,* 533–539.

[70] Ekberg, M.; Pötsch, S.; Sandin, E.; Thunnissen, M.; Nordlund, P.; Sahlin, M.; Sjöberg, B.-M. Preserved Catalytic Activity in an Engineered Ribonucleotide Reductase R2 Protein with a Nonphysiological Radical Transfer Pathway: The Importance of Hydrogen Bond Connections Between the Participating Residues. *J. Biol. Chem.* **1995,** *270.* 6570–6576.

[71] Siegbahn, P. E. M.; Blomberg, M. R. A.; Crabtree, R. H. Hydrogen transfer in the presence of amino acid radicals. *Theor. Chem. Acc.* **1997,** *97,* 289–300.

[72] Siegbahn, P. E. M.; Eriksson, L.; Himo, F.; Pavlov, M. Hydrogen Atom Transfer in Ribonucleotide Reductase (RNR). *J. Phys. Chem. B* **1998,** *102,* 10622–10629.

[73] Mohr, M.; Zipse, H. C–H Bond Activation In Ribonucleotide Reductases–Do Short, Strong Hydrogen Bonds Play a Role? *Chem. Eur. J.* **1999,** *5,* 3046–3054.

[74] Ekberg, M.; Sahlin, M.; Eriksson, M.; Sjöberg, B.-M. Two Conserved Tyrosine Residues in Protein R1 Participate in an Intermolecular Electron Transfer in Ribonucleotide Reductase. *J. Biol. Chem.* **1996,** *271,* 20655–20659.

of the above residues can inactivate the protein.[35,75,76,77] Of particular interest recently has been Trp48, in both laboratory[78] and theoretical circles,[79] due to its apparent participation in not only the RNR mechanism of action on ribonucleotides, but also in the injection of the electron into the R2 active site during reconstitution. Burdi, *et al.*[80] used an *N*-hydroxypyridine-2-thione tryptophan derivative as a source of •TrpH$^+$ for comparison with intermediates observed in R2. The radical was initially generated as •Trp (pK_a = 4.5) with λ_{max} = 510 nm (ε=1800 M^{-1} cm^{-1}). Upon protonation by trifluoroacetic acid, •TrpH$^+$ was observed (λ_{max} = 560 nm), helping to confirm the assignment of the 560 nm temporal feature during R2 reconstitution.

---

[75] Åberg, A.; Hahne, S.; Karlsson, M.; Larsson, Å.; Ormö, M.; Åhgren, A.; Sjöberg, B.-M. Evidence for Two Different Classes of Redox-active Cysteines in Ribonucleotide Reductase of *Escherichia coli*. *J. Biol. Chem.* **1989**, *264*, 12249–12252.

[76] Climent, I.; Sjöberg, B.-M.; Huang, C. Y. Site-Directed Mutagenesis and Deletion of the Carboxyl Terminus of *Escherichia coli* Ribonucleotide Reductase Protein R2. Effects on Catalytic Activity and Subunit Interaction. *Biochemistry* **1992**, *31*, 4801–4807.

[77] Persson, B. O.; Karlsson, M.; Climent, I.; Ling, J.; Loehr, J. S.; Sahlin, M.; Sjöberg, B.-M. Iron ligand mutants in protein R2 of *Escherichia coli* ribonucleotide reductase: Retention of diiron site, tyrosyl radical and enzymatic activity in mutant proteins lacking an iron-binding chain. *J. Biol. Inorg. Chem.* **1996**, *1*, 247–256.

[78] Sahlin, M.; Lassmann, G.; Pötsch, S.; Slaby, A.; Sjöberg, B.-M.; Gräslund, A. Tryptophan Radicals Formed by Iron/Oxygen Reaction with *Escherichia coli* Ribonucleotide Reductase Protein R2 Mutant Y122F. *J. Biol. Chem.* **1994**, *269*, 11699–11702.

[79] Himo, F.; Eriksson, L. A. Theoretical Study of Model Tryptophan Radicals and Radical Cations: Comparison with Experimental Data of DNA Photolyase, Cytochrome *c* Peroxidase, and Ribonucleotide Reductase. *J. Phys. Chem. B* **1997**, *101*, 9811–9819.

[80] Burdi, D.; Aveline, B. M.; Wood, P. D.; Stubbe, J.; Redmond, R. W. Generation of a Tryptophan Radical in High Quantum Yield from a Novel Amino Acid Analog Using Near-UV/Visible Light. *J. Am. Chem. Soc.* **1997**, *119*, 6457–6460.

C. Statement of problem: remaining issues in the reconstitution mechanism.

While much of the mechanism of assembly of the active site in R2 is known, it is not yet completely characterized. When ferrous iron is added to apo R2 in the presence of oxygen, one or more intermediates *must* exist before the generation of intermediate **X**,[50,51,52] the first characterizable species, currently described as a doubly–bridged Fe^{III}–Fe^{IV} species. This presumption is supported by spectroscopically characterized organometallic models.[81,82] A crystallographic study has recently appeared in which N_3^- was found to bind to the metal center of R2 potentially characteristic of dioxygen binding in R2.[83] Azide binds in an η^1–terminal manner to the iron further from Y122, and induces a novel type of carboxylate shift in which E238 becomes μ–(η^1,η^2). A potential mechanism for the oxygen activation steps offered by the same authors features a carboxylate shift, a bridging peroxo intermediate **P**, and **X**, the Fe^{III}–Fe^{IV} species with an oxo and two carboxylate bridges (Figure 1.15).

Where might a protein conformational change occur, in the R2 reconstitution pathway? As discussed on p 14, the fact that the rate of reconstitution

---

[81] Dong, Y.; Zang, Y.; Shu, L.; Wilkinson, E. C.; Que, L., Jr.; Kauffmann, K.; Münck, E. Models for Nonheme Diiron Enzymes. Assembly of a High-Valent $Fe_2(\mu\text{-}O)_2$ Core from Its Peroxo Precursor. *J. Am. Chem. Soc.* **1997**, *119*, 12683–12684.

[82] Zheng, H.; Zang, Y.; Dong, Y.; Young, V. G., Jr.; Que, L., Jr. Complexes with $Fe^{III}_2(\mu\text{-}O)(\mu\text{-}OH)$, $Fe^{III}_2(\mu\text{-}O)_2$, and $Fe^{III}_3(\mu_2\text{-}O)_3$] Cores: Structures, Spectroscopy, and Core Interconversions. *J. Am. Chem. Soc.* **1999**, *121*, 2226–2235.

[83] Andersson, M. E.; Högbom, M.; Rinaldo-Matthis, A.; Andersson, K. K.; Sjöberg, B.-M.; Nordlund, P. The Crystal Structure of an Azide Complex of the Diferrous R2 Subunit of Ribonucleotide Reductase Displays a Novel Carboxylate Shift with Important Mechanistic Implications for Diiron-Catalyzed Oxygen Activation. *J. Am. Chem. Soc.* **1999**, *121*, 2346–2352.

of R2 from apoprotein, Fe^{2+}, and O_2 is independent of the concentrations of Fe^{2+} and of O_2 implies that the rate-detemining step does not involve either or these reagents. Stubbe has suggested that a conformational change must occur in the apoprotein before the Fe^{2+} is incorporated.[53] She has also shown that apoprotein preloaded with Fe^{2+} (diferrous R2) reacts with oxygen (Eq 5) an order of magnitude faster (60–80 s^{-1}) than apoprotein freshly mixed with Fe^{2+}, so the rate-determining step must occur *before* the *last* Fe^{2+} is

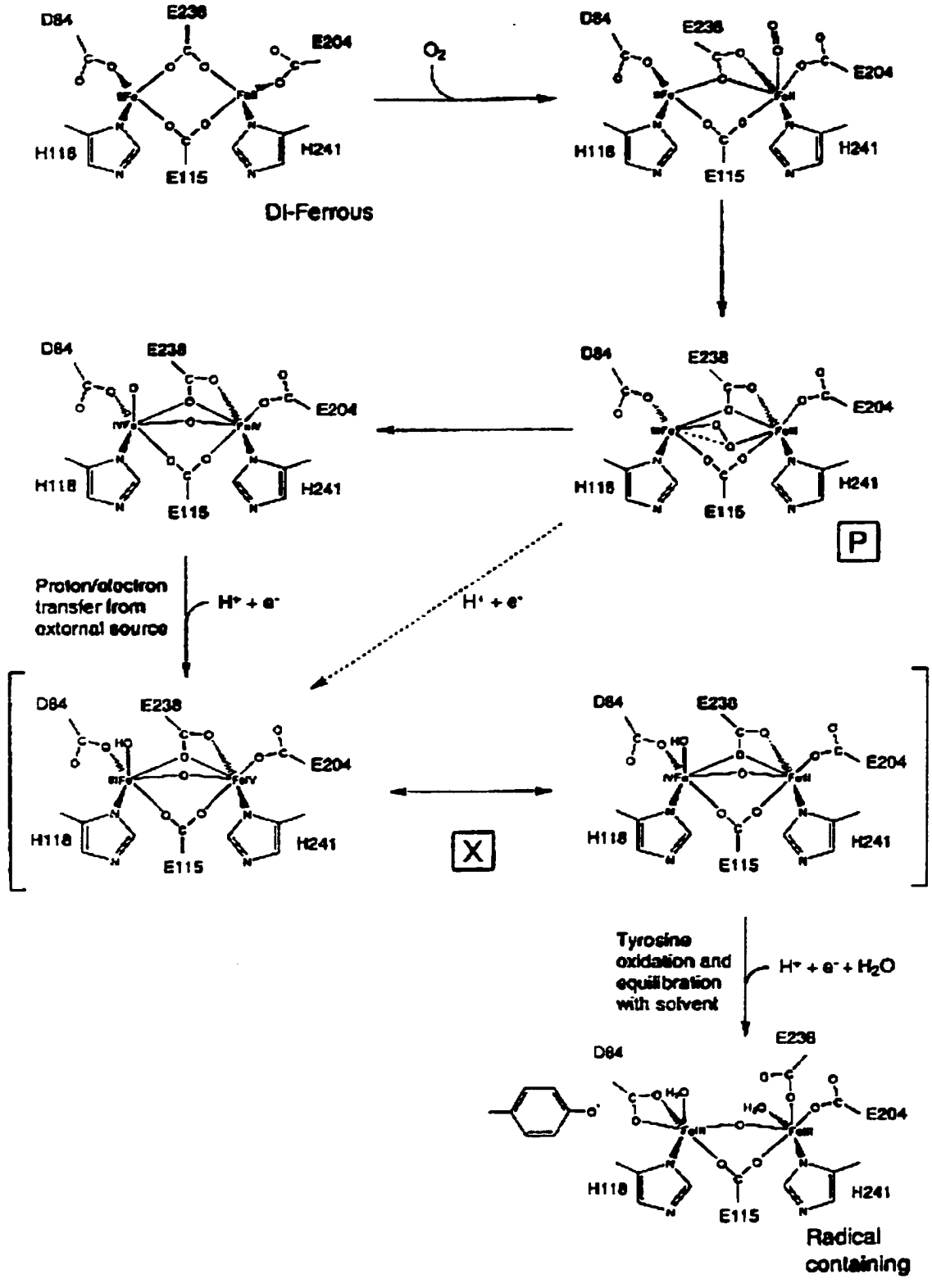

Figure 1.15. A proposed detailed mechanism of dioxygen activation in R2. From Nordlund, et al.

incorporated, and she has remarked that "The kinetics suggest that formation of the diferrous–R2 complex from apo is slow." However, neither of the above results excludes a rate-determining conformational change that occurs (Eq 3) *between* Eq 2 and Eq 4.[84]

$$\text{apo} + \text{Fe}^{\text{II}} \xrightarrow{k_{\text{apo}}} \text{apoFe} \qquad \textbf{Eq 2}$$

$$\text{apoFe} \xrightarrow{k_{\text{conf}}} \text{apoFe}^{*};\ k_{\text{conf}}\ \textit{may be}\ \text{the overall rate constant } 5\text{–}10\ \text{s}^{-1} \qquad \textbf{Eq 3}$$

$$\text{apoFe}^{*} + \text{Fe}^{\text{II}} \xrightarrow{k_{\text{apoFe}}} \text{apoFe}_2\ k_{\text{apoFe}} = \text{fast} \qquad \textbf{Eq 4}$$

$$\text{apoFe}_2 \xrightarrow{\text{O}_2} \text{active R2};\ k_{\text{O}_2} = 60\text{–}80\ \text{s}^{-1} \qquad \textbf{Eq 5}$$

This hypothesis creates the need to determine the kinetics of Fe^{2+} uptake by the R2 apoprotein. The rate of the first Fe^{2+} uptake will be independent of Fe^{2+} if it is preceded by a rate-determining conformational change, and first order in Fe^{2+} if it occurs by the mechanism of Eqs 2–4.

Unfortunately, Fe^{2+} at micromolar concentrations is spectroscopically invisible (except in Mössbauer, by which kinetics are cumbersome). During reconstitution of R2 from its apoprotein, there are no spectral changes in the UV–visible spectrum.

---

[84] This hypothesis has been presented at a meeting: Umback, N. J.; Norton, J. R., *Abstracts of Papers*, 216th National Meeting of the American Chemical Society, Boston, MA; American Chemical Society: Washington, DC, 1998; INOR 422.

Method to be employed. We have devised a ferrozine–based competition method for indirectly determining the rate of Fe^{2+} uptake by the apoprotein, by letting it compete with a spectroscopically observable reaction such as Fe^{2+} uptake by ferrozine. Both the Bollinger and Norton groups have found that ferrozine and the various forms of R2 are fully compatible, and other published work confirms that the ligand has no effect on the protein once it has reached the diferric state.[63] This is not surprising, as the iron in R2 is buried deep within the protein (approximately10 Å from the surface)[85] in a redox state which ferrozine ignores (i. e., ferric). Similar ligands have been used as metal loss indicators in other R2 studies without influencing the metal center.[86]

D. The ferrozine ligand.

Background. Ferrozine[87,88] (Figure 1.16) has found wide application, including

---

[85] Nordlund, P.; Sjöberg, B.-M.; Eklund, H. Three-dimensional structure of the free radical protein of ribonucleotide reductase. *Nature*, **1990**, *345*, 593–598.

[86] Pötsch, S.; Sahlin, M.; Langelier, Y.; Gräslund, A.; Lassmann, G. Reduction of the tyrosyl radical and the iron center in protein R2 of ribonucleotide reductase from mouse, herpes simplex virus and *E. coli* by *p*-alkoxyphenols. *FEBS Lett.* **1995**, *374*, 95–99.

[87] Stookey, L. L. FerroZine—A New Spectophotometric Reagent for Iron. *Anal. Chem.* **1970**, *42*, 779–781.

[88] Gibbs, C. R. Characterization and Application of FerroZine Iron Reagent as a Ferrous Iron Indicator. *Anal. Chem.* **1976**, *48*, 1197–1201.

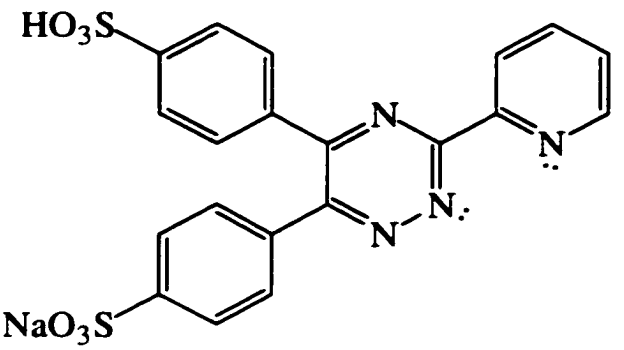

Figure 1.16. Ferrozine. This ligand forms a tris–chelate complex specifically with ferrous iron.

biological,[89,90,91] medical,[92,93,94,95] forensic,[96,97] food,[98,99,100] analytical,[101,102,103,104,105,106,107] and environmental[87,108,109,110,111,112,113,114] disciplines, as an iron(II)–specific chelating

---

[89] Davis, M. D.; Kaufman, S.; Milstien, S. A modified ferrozine method for the measurement of enzyme-bound iron. *J. Biochem. Biophys. Methods* **1986,** *13,* 39–45.

[90] Fish, W. W. Rapid Colorimetric Micromethod for the Quantitation of Complexed Iron in Biological Samples. *Meth. Enzymol.* **1988,** *158,* 357–364.

[91] Boyer, R. F.; McArthur, J. S.; Cary, T. M. Plant Phenolics as Reductants for Ferritin Iron Release. *Phytochemistry* **1990,** *29,* 3717–3719.

[92] Derman, D. P.; Green, A.; Bothwell, T. H.; Graham, B.; McNamara, L.; MacPhail, A. P.; Baynes, R. D. A systematic evaluation of bathophenanthroline, ferrozine and ferene in an ICSH-based method for the measurement of serum iron. *Ann. Clin. Biochem.* **1989,** *26,* 144–147.

[93] Paller, M. S.; Hedlund, B. E.; Patten, M. Extracellular Iron Chelators Protect Kidney Cells from Hypoxia/Reoxygenation. *Free Rad. Biol. Med.* **1994,** *17,* 597–603.

[94] Li, H.; Byrnes, R. W. Association of Redox-Active Iron Bound to High Molecular Weight Structures in Nuclei with Inhibition of Cell Growth by H_2O_2. *Free Radic. Biol. Med.* **1999,** *26,* 49–60.

[95] Remblier, C.; Jolimay, N.; Wahl, A.; Pariat, A.; Huguet, F. Extracellular dopamine and catabolites in rat striatum during lactic acid perfusion as determined by in vivo micordialysis. *Brain Research* **1998,** *804,* 224–230.

[96] Goldman, G. L.; Thornton, J. I. A New Trace Ferrous Metal Detection Reagent. *J. Forensic Sci.* **1976,** *21,* 625–628.

[97] Lee, C.-w. The Detection of Iron Traces on Hands by Ferrozine Sprays: A Report on the Sensitivity and Interference of the Method and Recommended Procedure in Forensic Science Investigation. *J. Forensic Sci.* **1986,** *31,* 920–930.

[98] American Society of Brewing Chemists. Iron in Beer by Ferrozine Method. *J. Am. Soc. Brew. Chem.* **1992,** *50,* 145–146.

[99] Carpenter, C. E.; Clark, E. Evaluation of Methods Used in Meat Iron Analysis and Iron Content of Raw and Cooked Meats. *J. Agric. Food Chem.* **1995,** *43,* 1824–1827.

[100] Perricone, N.; Nagy, K.; Horváth, F.; Dajkó, G.; Uray, I.; Zs.–Nagy, I. The Hydroxyl Free Radical Reactions of Ascorbyl Palmitate as Measured in Various *in Vitro* Models. *Biochem. Biophys. Res. Commun.* **1999,** *262,* 661–665.

[101] Kellen, G. J.; Jaselskis, B. Spectrophotometric Determination of Micro Amounts of Arsenic. *Anal. Chem.* **1976,** *48,* 1538–1540.

[102] Harris, T. D.; Mitchell, J. W. Sub-Part-per-Billion Iron Determination by Laser Intracavity Absorption Spectrometry. *Anal. Chem.* **1980,** *52,* 1706–1708.

[103] Bet-Pera, F.; Srivastava, A. K.; Jaselskis, B. Spectrophotometric Determination of Iron(II) Ferrozine Complex for the Indirect Determination of Phosphate. *Anal. Chem.* **1981,** *53,* 861–864.

[104] Baumann, E. W. Colorimetric Determination of Iron(II) and Iron(III) in Glass. *Analyst,* **1992,** *117,* 913–916.

[105] Molina-Díaz, A.; Ortega-Carmona, I.; Pascual-Peguera, M. I. Indirect spectrophotometric determination of ascorbic acid with ferrozine by flow-injection analysis. *Talanta* **1998,** *47,* 531–536.

[106] Zatar, N. A.; Abu–Zuhri, A. Z.; Abu–Shaweesh, A. A. Spectrophotometric determination of some aromatic amines. *Talanta* **1998,** *47,* 883–890.

[107] Shi, Y.; Seliskar, C. J.; Heineman, W. R. Dual-analyte spectroscopic sensing in sol–gel derived polyelectrolyte–silica composite thin films. *Talanta* **1998,** *47,* 1071–1076.

[108] Langford, C. H.; Wong, S. M.; Underdown, A. W. The interaction of a soil fulvic acid with precipitating hydrous ferric oxide at pH = 6. *Can. J. Chem.* **1981,** *59,* 181–186.

[109] Phillips, E. J. P.; Lovley, D. R. Determination of Iron(III) and Iron(II) in Oxalate Extracts of Sediment. *Soil Sci. Soc. Am. J.* **1987,** *51,* 938–941.

[110] O'Sullivan, D. W.; Hanson, A. K.; Miller, W. L.; Kester, D. R. Measurement of Fe(II) in surface water of the equatorial Pacific. *Limnol. Oceanogr.* **1991,** *36,* 1727–1741.

[111] Yi, Z.; Zhuang, G.; Brown, P. R.; Duce, R. A. High-Performance Liquid Chromatographic Method for the Determination of Ultratrace Amounts of Iron(II) in Aerosols, Rainwater, and Seawater. *Anal. Chem.* **1992,** *64,* 2826–2830.

[112] Blain, S.; Tréguer, P. Iron(II) and Iron(III) determination in sea water at the nanomolar level with selective on-line preconcentration and spectrophotometric determination. *Anal. Chim. Acta* **1995,** *308,* 425–432.

[113] O'Sullivan, D. W.; Hanson, A. K., Jr.; Kester, D. R. The Distribution and Redox Chemistry of Iron in the Pettaquamscutt Estuary. *Estuar. Coast. Shelf Sci.* **1997,** *45,* 769–788.

agent. Its main advantages[115] include this specificity, as well as solubility in water and relatively easy synthesis (hence lower costs) compared to related ligands. The well–characterized, visually (deep magenta) and spectroscopically detectable (tris(ferrozine)Fe^{II} complex ($\varepsilon_{562\ nm}$ = 27,900 $M^{-1}cm^{-1}$)[87] also has a much higher extinction coefficient than the analogous ligands 1,10-phenanthroline ($\varepsilon_{510\ nm}$ = 11,100 $M^{-1}cm^{-1}$), 2,2'-bipyridine ($\varepsilon_{522\ nm}$ = 8,650 $M^{-1}cm^{-1}$) and 2,2':6',2"-terpyridine (ε_{552} = 11,500 $M^{-1}cm^{-1}$).[116]

Kinetic studies on iron(II) chelation by ferrozine. The kinetics of the ferrozine–iron chelation reaction have been studied in aqueous phthalate buffers.[117] In 1984 Thompsen and Mottola, using 800 μM ferrozine, 8 μM ferrous sulfate, an ionic strength of 0.1 M (adjusted with $NaClO_4$) and a pH range of 2.8–5.5, reported an average ferrozine reaction order of 2.95 and a forward rate constant of 3.08(3) × 10^{11} $M^{-3}s^{-1}$ at 20 °C. The activation energy E_a = 9.87(0.17) kJ/mol. They therefore concluded that the reaction was first order in iron(II) and third order in ferrozine (fourth order overall) (Eq 9)

---

[114] To, T. B.; Nordstrom, D. K.; Cunningham, K. M.; Ball, J. W.; McCleskey, R. B. New Method for the Direct Determination of Dissolved Fe(III) Concentration in Acid Mine Waters. *Environ. Sci. Technol.* **1999**, *33*, 807–813.

[115] Cowart, R. E.; Singleton, F. L.; Hind, J. S. A Comparison of Bathophenanthrolinedisulfonic Acid and Ferrozine as Chelators of Iron(II) in Reduction Reactions. *Anal. Biochem.* **1993**, *211*, 151–155.

[116] Schildt, A. A. *Analytical Applications of 1,10-Phenanthroline and Related Compounds*; Pergamon: New York, 1969; p 36.

[117] Thompsen, J. C.; Mottola, H. A. Kinetics of the Complexation of Iron(II) with Ferrozine. *Anal. Chem.* **1984**, *56*, 755–757.

and proposed a mechanism consisting of three chelation steps shown in Eqs 6–8. (It is worth noting that Eq 9 will be correct only if both the K_1 and K_2 equilibria lie to the left!)

$$Fe^{II} + Fz \overset{K_1}{\rightleftharpoons} FeFz \qquad \textbf{Eq 6}$$

$$FeFz + Fz \overset{K_2}{\rightleftharpoons} FeFz_2 \qquad \textbf{Eq 7}$$

$$FeFz_2 + Fz \xrightarrow{k_3} FeFz_3 \qquad \textbf{Eq 8}$$

$$\frac{d[FeFz_3]}{dt} = k_{obs}[Fe(II)][Fz]^3 \qquad \textbf{Eq 9}$$

$$k_{obs} = K_1 K_2 k_3 \qquad \textbf{Eq 10}$$

Independently in 1992 another group studied the kinetics of the ferrozine–iron(II) reaction in seawaters.[118] Mottola was not cited: "No kinetic studies have been reported on the complexation of Fe(II) by FZ before this work." At pH 6.0–8.4, salinity 0–36‰, 5 mM bicarbonate buffer and concentrations of 28–80 μM ferrozine and 0.16–1.25 μM ferrous ammonium sulfate, the reaction order in ferrozine over a temperature range of 15–32 °C was found to be 2.91(4), which the authors felt was close enough to three not to

[118] Lin, J.; Kester, D. R. The kinetics of Fe(II) complexation by Ferrozine in seawater. *Marine Chem.* **1992**, *38*, 283–301.

investigate further. Under these conditions (with ferrozine concentration an order of magnitude lower and iron(II) concentration (at most) one–fiftieth of Mottola's; this is two orders of magnitude lower than some of the higher concentrations used in our studies) it was found that the average rate constant was about 1.2×10^{13} M^{-3} min^{-1} (2.0×10^{11} M^{-3} s^{-1}), and that this was independent of the initial (although extremely low, compared to levels of interest to us) concentration of ferrozine used. The energy of activation was 15.2(6) kJ/mol. Considering the differences in pH, ionic strength and temperature between these two studies, the agreement is remarkable.

The kinetics of decomposition of the $FeFz_3$ complex has been studied at high ($\geq$ 0.3 M) ionic strength, acid concentration (17–333 mM) and temperature (35 °C).[119] Like similar tris(chelate)Fe^{II} complexes, the rate of metal aquation was first order ($\leq 2 \times 10^{-4}$ s^{-1}, depending on the specific conditions—that is, slow!), and nearly pH–independent. Similar decomposition rates were found in 0.33 M hydroxide. Thompsen and Mottola[117] determined a rate constant of $4.25(4) \times 10^{-5}$ s^{-1} when the $Fe^{II}Fz_3$ complex was reacted with 0.10 M hydrochloric acid (apparently at room temperature); and Lin and Kester[118] characterized the dissociation of the complex as having a rate constant of $2.16(2) \times 10^{-3}$ min^{-1} ($0.1296(12) \times 10^{-1}$ s^{-1}) at 36‰ salinity, pH 8.1 and 24 °C. Under milder conditions (including those employed for the competition experiments described in this dissertation) the complex is stable indefinitely.

---

[119] Gardner, E. R.; Mekhail, F. M.; Burgess, J.; Rankin, J. M. Kinetics of Aquation of the Complex Tris[3-(2-pyridyl)-5,6-bis(4-phenylsulphonato)-1,2,4-triazine]iron(II) and its Reactions with Hydroxide, Cyanide, and Peroxodisulphate Ions. *J. Chem. Soc. Dalton Trans.* **1973,** 1340–1344.

Kinetics to be expected for iron uptake by ferrozine. If we assume the first two equilibria are rapidly maintained (Eqs 7, 8, 10 and 11), the rate–determining step will be binding of the third ferrozine ligand (Eq 13). The mathematical derivation of the mechanism is given as Eqs 11–27.

$$Fe^{II} + L \overset{K_1}{\rightleftharpoons} FeL \qquad \textbf{Eq 11}$$

$$FeL + L \overset{K_2}{\rightleftharpoons} FeL_2 \qquad \textbf{Eq 12}$$

$$FeL_2 + L \xrightarrow{k_3} FeL_3 \qquad \textbf{Eq 13}$$

$$K_1 = \frac{[FeL]}{[Fe][L]} \equiv [Fe] = \frac{[FeL]}{K_1[L]} \qquad \textbf{Eq 14}$$

$$K_2 = \frac{[FeL_2]}{[FeL][L]} \equiv [FeL] = \frac{[FeL_2]}{K_2[L]} \qquad \textbf{Eq 15}$$

In order for the overall reaction to be third order in ferrozine (Eq 16), the equilibria of the first two chelation steps must lie entirely to the left (i.e., as free ferrous ion and free ferrozine). This is the case for the studies performed at 80 and even 800 μM ferrozine (Lin and Kester, and Thompsen and Mottola, respectively).

$$k_{obs} = K_1 K_2 k_3 [L]^3 \qquad \textbf{Eq 16}$$

At higher ferrozine concentrations, an appreciable fraction of the total iron, T, (Eq 17) will be FeL and FeL_2 after mixing.

$$T = [Fe] + [FeL] + [FeL_2] \qquad \textbf{Eq 17}$$

Substitution of Eqs 14 and 15 in Eq 17 gives (Eqs 18–20) the equilibrium expression for $[FeL_2]$ in Eqs 21–23. Consideration of Eqs 13 and 24 leads to the complete rate law in Eq 25.

$$T = \frac{[FeL]}{K_1[L]} + \frac{[FeL_2]}{K_2[L]} + [FeL_2] \qquad \textbf{Eq 18}$$

$$T = \frac{[FeL_2]}{K_1 K_2 [L]^2} + \frac{[FeL_2]}{K_2[L]} + [FeL_2] \qquad \textbf{Eq 19}$$

$$T = [FeL_2]\left\{\frac{1}{K_1 K_2 [L]^2} + \frac{1}{K_2[L]} + 1\right\} \qquad \textbf{Eq 20}$$

$$[FeL_2] = \frac{T}{\left(\frac{1}{K_1 K_2 [L]^2} + \frac{1}{K_2[L]} + 1\right)} \qquad \textbf{Eq 21}$$

$$[FeL_2] = \frac{T}{\left(\frac{1 + K_1[L] + K_1K_2[L]^2}{K_1K_2[L]^2}\right)} \qquad \textbf{Eq 22}$$

$$[FeL_2] = \frac{TK_1K_2[L]^2}{1 + K_1[L] + K_1K_2[L]^2} \qquad \textbf{Eq 23}$$

$$\frac{d[FeL_3]}{dt} = \text{rate} = k_3[FeL_2][L] \qquad \textbf{Eq 24}$$

$$\frac{d[FeL_3]}{dt} = \text{rate} = \frac{K_1K_2k_3[L]^3T}{1 + K_1[L] + K_1K_2[L]^2} \qquad \textbf{Eq 25}$$

Presumably the limits for reaction order in ferrozine are 3.0, as expected from the stoichiometry at low ferrozine concentrations, and 1.0, required of true pseudo–first–order conditions, at high ferrozine concentrations.

$$\text{As } \lim_{[L]\to\infty}, \text{ rate} \to k_3T[L] \text{ (the reaction is first order in [L])} \qquad \textbf{Eq 26}$$

$$\text{As } \lim_{[L]\to 0}, \text{ rate} \to K_1K_2k_3T[L]^3 \text{ (the reaction is third order in [L])} \qquad \textbf{Eq 27}$$

CHAPTER II. EXPERIMENTAL.

A. Materials.

The *E. coli* ribonucleotide reductase R2 for most experiments was produced in the overproducing strain BL21DE3 (Novagen) containing the plasmid pR2wt–HindIII, and isolated in the apo form as previously reported.[54] This strain and procedure produce a higher yield of pure R2 than the use of the overproducing strain N6405/pSPS2 and an isolation procedure[120] which yields the active form of R2 (from which apo R2 can be produced via reduction and chelation steps). Once purified both proteins react similarly.[121]

Bovine serum albumin (Cohn V fractionate powder) [9048–46–8]; ferrous ammonium sulfate hexahydrate [7783–85–9], ferrozine (3-(2-pyridyl)-5,6-diphenyl-1,2,4-triazine-p,p′-disulfonic acid, monosodium salt (hydrate)) [28048–33–1], HEPES (4–(2–hydroxyethyl)–1–piperazineethanesulfonic acid, monosodium salt hydrate) [7365–45–9], methyl viologen (1,1′-dimethyl-4,4′-bipyridinium dichloride) [1910–42–5], sodium ascorbate [134–03–2], sodium hydrosulfite [7775–14–6] Tris

---

[120] Bollinger, J. M., Jr. On the Chemical Mechanism of Assembly of the Tyrosyl Radical-Dinuclear Iron Cluster Cofactor of *E. coli* Ribonucleotide Reductase. Ph. D. Thesis, Massachusetts Institute of Technology, Cambridge, MA, 1993.

[121] Bollinger, J. M., Jr. Personal communication.

(tris(hydroxymethyl)aminomethane) [77–86–1], and Tris–HCl (tris(hydroxymethyl)aminomethane hydrochloride) [1185–53–1] were purchased from Sigma–Aldrich and used as received. Column media (G–25 Sephadex, DEAE Biogel, and QAE Sephadex) were purchased from Sigma or Bio–Rad. Water used for solutions was Type I reagent grade water (Barnstead/Thermolyne Model D4751).

B. Instrumentation.

An SF–40 Canterbury Stopped–Flow (Hi–Tech Scientific) thermostatted to 5.0 ± 0.1 °C, with an RSM–1000 rapid–scanning device (On–Line Instrument Systems; OLIS) and software, was used to collect rapid kinetic data between 400 and 600 nm (Figures 2.1–2.3). Parameter settings for the RSM were as follows: scans were collected in dual beam mode, 1000 scans/second, with a stopped–flow delay of 20 ms and sampling time of 4 μs. The monochromator grating was 400 lines with a blaze wavelength of 500 nm. The speed of the 16–slit scanning disk was 62.50 Hz with the step motor set at 4.0 steps/nm. Data were collected over the range of approximately 390–610 nm.

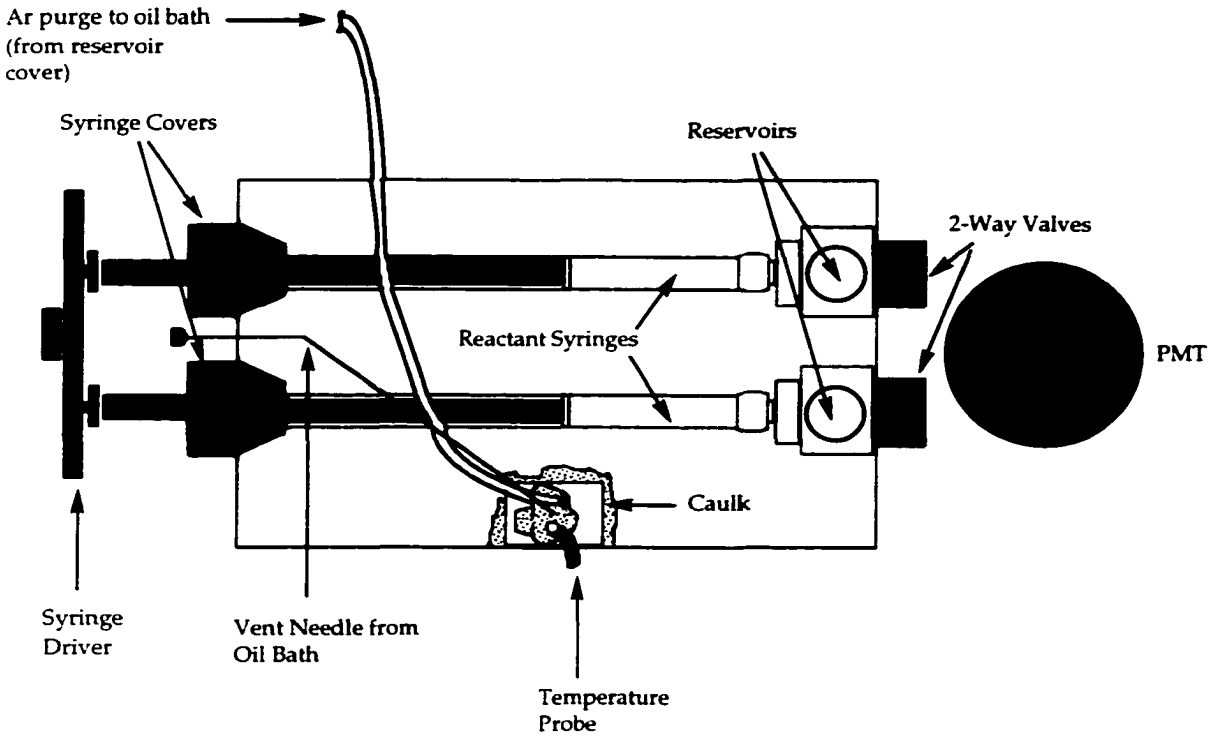

Figure 2.1. Overhead view of the syringe chamber on the SF–41 Canterbury stopped–flow. The syringes are enclosed in an anaerobic–capable chamber having a clear, gasket–sealed lid. Samples can be syringed through silicon rubber septa into the reservoirs, drawn into the reactant syringes, and thence into the reagent lines toward the mixing chamber (Figure 2.2). When the reaction of interest does not require the exclusion of air, the argon purge and chamber lid are omitted.

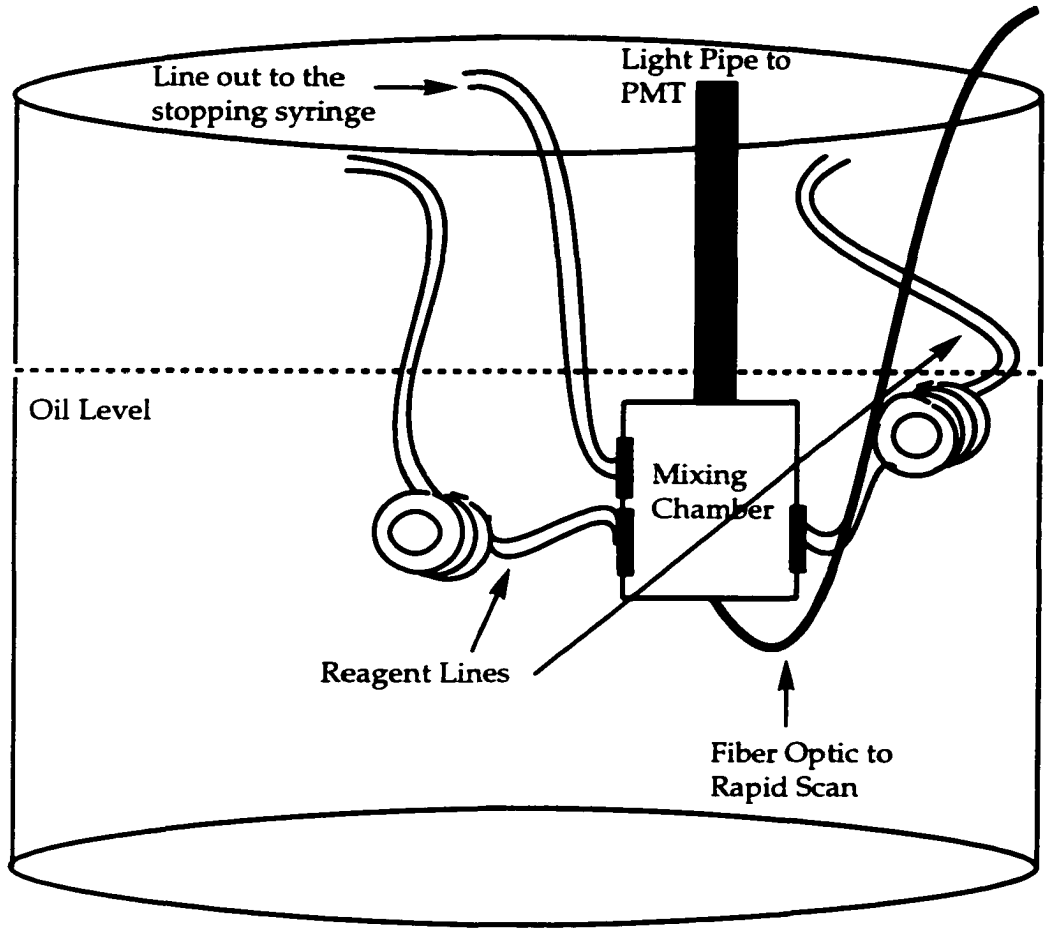

Figure 2.2. Side view of the reagent lines and mixing chamber of the stopped flow. The mixing chamber is also the observation cell (10 mm path length); the silicone oil bath that surrounds the reaction chamber and reagent lines is temperature–controlled (Figure 2.3). The light from the OLIS–RSM is delivered to the reaction via fiberoptic cable. A silicon light guide transmits the light (less that absorbed by the solution) from the mixing and observation cell back to the photomultiplier tube on top of the instrument.

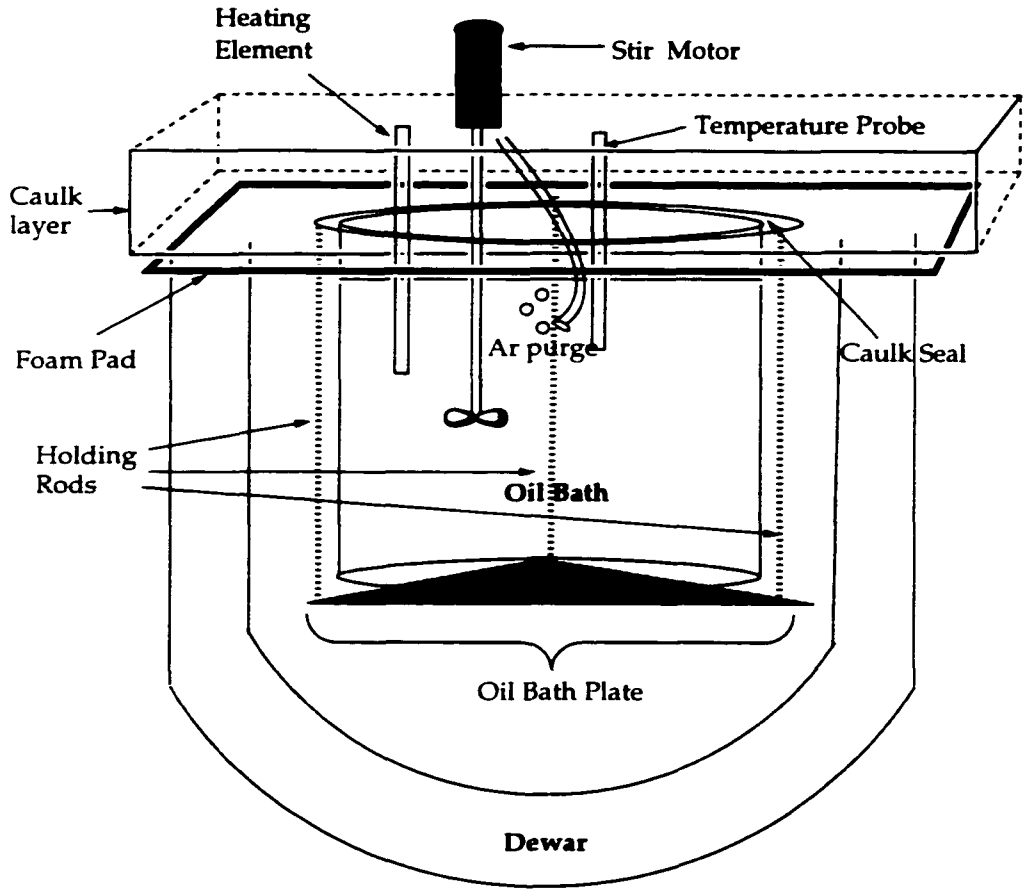

Figure 2.3. The temperature and atmosphere control mechanisms of the stopped–flow apparatus. Thermostatting is accomplished via a thermocouple, heater and evaporating liquid nitrogen (from a Dewar enclosing the entire oil bath). The oil bath is sealed to the foam rubber on the underside of the top of the apparatus housing using silicone sealant (labeled "caulk" in the diagrams) and anaerobic integrity confirmed by a thermal conductivity gas-leak detector.

Static UV–visible spectra and slower kinetics were obtained on a Hewlett–Packard (HP) 8453 instrument equipped with Peltier temperature control. The pH of solutions was measured with an Orion Research digital Ionalyzer/501 equipped with an Ag/AgCl 91 series electrode. Centrifuge rotors used in the isolation procedures were chilled to 4 °C prior to use. Denaturing polyacrylamide gel electrophoresis (SDS–PAGE) by the method

of Laemmli[122] (for verification of purity) was performed using a Hoefer SE 600 vertical slab unit at 25–30 mA constant current, with standards ranging from 14.4–200 kD (Bio–Rad). The gels were stained with Coomassie Brilliant Blue R-250, then destained first with an aqueous 50% methanol, 10% acetic acid solution, followed by a 5% methanol, 7% acetic acid solution, and heat–dried either onto filter paper or between cellophane sheets under vacuum with a Bio–Rad gel dryer.

C. Software.

OLIS' RSM program was used to collect and manipulate rate data, as well as to fit simple first order situations such as the excess and limited iron reconstitution experiments, and the initial competition experiments using BSA and ferrozine. HP's kinetics package was used to collect and fit the data for the long time–scale observation of stopped flow reaction mixtures. Both stopped–flow and UV-vis data could be exported in ASCII format to various other programs; data for use in MacKinetics files was formatted in Excel (Microsoft) and pasted into text files (Microsoft Word). Graphs were generated and curve fitting was accomplished using KaleidaGraph (Synergy Software), Cricket Graph (Computer Associates International), Mathcad 8 Professional Academic (MathSoft) or Excel. Activation parameters for the ferrozine reaction in HEPES and Tris buffers, and extrapolations to 5 °C for the phthalate system, were calculated with KinPar 5.0 (a Norton group routine which uses nonlinear regression fitting to the Eyring equation

[122] Laemmli, U. K. Cleavage of Structural Proteins during the Assembly of the Head of Bacteriophage T4.

and a covariance analysis[123]). Kinetic fits for complex situations such as the competition reactions and the Fz–BSA controls were fit iteratively using MacKinetics (developed by Walter S. Leipold III, formerly of E. I. du Pont de Nemours, Inc.).

D. Biochemical methods.

NOTE: All concentrations involved in stopped–flow reactions are given here as the pre–mixing value; they are diluted by 50% in the mixing chamber to the concentrations listed in the text and figure captions.

Buffer preparation. HEPES buffer was made up as 100 mM from the free acid form. The solution was chilled to 5.0 °C then titrated to the desired pH using NaOH. A pH of 7.6 was standard for all the protein experiments; pH–dependence studies of the ferrozine reaction with no protein were performed between pH 6.8–8.2 in Tris or HEPES. The Tris buffers were made in a similar manner starting from a mixture of Tris and Tris-HCl for approximately the correct pH, glycerol was added to 5% v/v, then titrated at 5 °C with NaOH or HCl as necessary. Fresh stock solutions of PMSF (phenylmethylsulfonyl fluoride) and *o*-phenanthroline to add to the Tris buffer were made as needed for protein isolation and purification. PMSF was 250 mM in absolute ethanol, and *o*-phenanthroline was 100 mM in 0.1 N HCl.

Nature **1970,** *227,* 680–685.

[123] Jordan, R. F.; Norton, J. R. Kinetic and Thermodynamic Acidity of Hydrido Transition–Metal Complexes. 1. Periodic Trends in Group 6 Complexes and Substituent Effects in Osmium Complexes. *J. Am. Chem. Soc.* **1982,** *104,* 1255–1263.

Direct purification of ribonucleotide reductase apo R2 (procedure from Bollinger laboratory at Penn State). This procedure was used for isolation of the protein from the BL21DE3 (Novagen) strain containing the plasmid pR2wt–HindIII. All steps were carried out either under refrigeration or on ice. Tris buffer (450 mL) containing 1 μL/mL PMSF[124] (PMSF is an inhibitor[125,126,127,128] of the cellular protease enzymes which otherwise would degrade the protein) and 10 μL/mL *o*-phenanthroline was used to suspend 90 g of *E. coli* cells (grown with *o*-phenanthroline in the medium to chelate any free iron) containing overexpressed R2. This salmon–colored suspension was passed once through a chilled French pressure cell at 1000 psig, and another 1 μL/mL PMSF added to the lysate. The resulting solution was centrifuged at 12000 rpm for 10 minutes to remove cellular debris and the pellet discarded. Streptomycin sulfate (6% w/v, in Tris) was added slowly, to 20% of the original volume of the supernatant to precipitate the ribosomes, and then the solution was recentrifuged at 12000 rpm for 10 minutes. The pellet was once again discarded, and ammonium sulfate was added to 60% saturation in

---

[124] Sjöberg, B.–M.; Hahne, S.; Karlsson, M.; Jörnvall, H.; Göranssihn M.; Uhlin. B. E. Overproduction and Purification of the B2 Subunit of Ribonucleotide Reductase from *Escherichia coli*. *J. Biol. Chem.* **1986,** *261,* 5658–5662.

[125] Fahrney, D. E.; Gold, A. M. Sulfonyl Fluorides as Inhibitors of Esterases. I. Rates of Reaction with Acetylcholinesterase, α–Chymotrypsin, and Trypsin. *J. Am. Chem. Soc.* **1963,** *85,* 997–1000.

[126] Turini, P.; Kurooka, S.; Steer, M.; Corbascio, A. N.; Singer, T. P. The Action of Phenylmethylsulfonyl Fluoride on Human Acetylcholinesterase, Chymotrypsin and Trypsin. *J. Pharmacol. Exp. Ther.* **1969,** *167,* 98–104.

[127] James, G. T. Inactivation of the Protease Inhibitor Phenylmethylsulfonyl Fluoride in Buffers. *Anal. Biochem.* **1978,** *86,* 574–579.

[128] Moss, D. E.; Fahrney, D. Kinetic Analysis of Differences in Brain Acetylcholinesterase from Fish or Mammalian Sources. *Biochem. Pharmacol.* **1978,** *27,* 2693–2698.

the supernatant, with stirring over about an hour, to precipitate the R2. This solution was centrifuged (15000 rpm for 10 minutes) and the pellet collected. The precipitated R2 was gently resuspended in 90 mL Tris containing PMSF and *o*-phenanthroline as before. The orange–red protein solution was dialyzed vs. 6 L of Tris buffer for 4 hours. The desalted apo R2 was diluted by ≥ 50 % with Tris and PMSF, and loaded onto a G–25 column equilibrated in Tris buffer. Once the protein eluted (with Tris) from the G–25 column, the apoprotein–containing fractions, free of iron and exhibiting the pale yellow–green of apo R2, were pooled and loaded onto a DEAE Biogel–A column; it was rinsed with one column volume of Tris, then with 1–2 column volumes of Tris with 110 mM NaCl, before elution with 140 mM NaCl in Tris. Fractions with $A_{280} \geq 0.2$ were pooled, diluted by 50% with buffer, then loaded onto a Q–Sepharose Fast–Flow column. The column was rinsed with 0.5 column volumes of Tris buffer followed by 1.6 column volumes of Tris containing 225 mM NaCl, and the apo R2 was eluted with 300 mM NaCl Tris. Fractions containing R2 were pooled and concentrated to about 30 mL in an Amicon stirring cell (PM-30 filter) driven by N_2 pressure. The concentrated solution was dialyzed vs. 1 L 100 mM HEPES (pH 7.6 at 4 °C) for 4 hours to remove the salt and put the protein into the buffer system desired for kinetics. The dialysate was centrifuged at 12000 rpm for 10 minutes to remove particulate matter, then the resulting pure protein was divided into aliquots in Eppendorf tubes, flash frozen with liquid nitrogen, and stored at –80 °C. Total yield (as calculated using the dropline method) was ≈ 3 g of apo R2. The dropline method correlates the amount of active R2 to the absorbance due to Y122•. Bollinger[120] determined the extinction coefficient of the peak at 410 nm (based on the

difference between the observed absorbance at 410 and a calculated $A_{410,drop}$ which lies on the straight line drawn between the sides of the peak at 410 as if it were not present) as 1850 M^{-1} cm^{-1} (Eqs 28–31). This concept is illustrated in Figure 2.4.

$$m = \frac{A_{416} - A_{406}}{416 - 406} \qquad \textbf{Eq 28}$$

$$A_{410,drop} = m(416 - 410) - A_{416} \qquad \textbf{Eq 29}$$

$$\Delta A_{410} = A_{410} - A_{410,drop} \qquad \textbf{Eq 30}$$

$$\Delta A_{410} = \varepsilon_{410,drop} bC;\ \varepsilon_{410.drop} = 1850\ M^{-1}cm^{-1};\ b\ (pathlength) = 1\ cm \qquad \textbf{Eq 31}$$

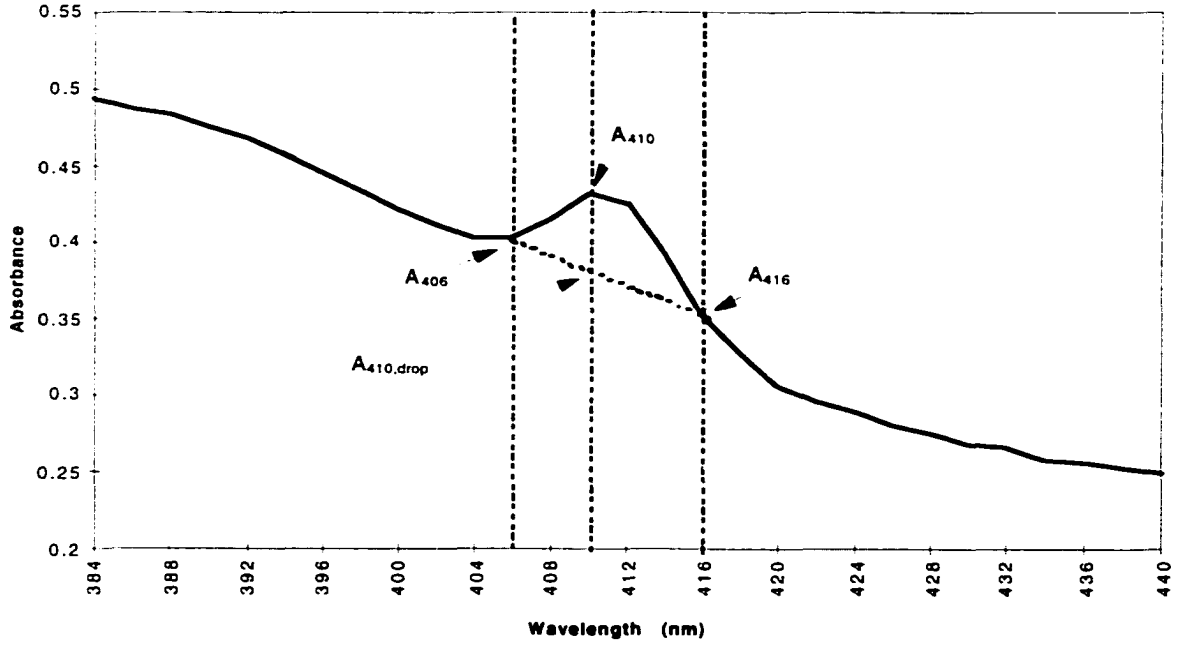

Figure 2.4. Absorbance values needed to perform an $A_{410,dropline}$ calculation by Bollinger's method.

Purification of ribonucleotide reductase R2 (active form), and removal of iron to make apo R2 (Stubbe laboratory, MIT, and original Norton group procedure). This method was used to isolate the protein from the N6405/pSPS2 strain of *Escherichia coli*. All steps were carried out either under refrigeration or on ice. Tris buffer (400 mL) containing 1 μL/mL PMSF was used to suspend 100 g of cell paste containing overexpressed R2. Just prior to French pressing, 5 mL of freshly–made 50 mM aqueous ferrous ammonium sulfate and 100 mM sodium ascorbate was added to the suspension. The cells were put through a French press at 700–1000 psig twice to ensure complete cracking. The extract was centrifuged at 9000 rpm for 40 minutes. The pellet was discarded; the supernatant was collected and 106 mL of 5% (w/v) streptomycin sulfate in Tris buffer was added over 15 minutes, then the resulting solution stirred for another 15 minutes. The liquid was centrifuged again, at 9000 rpm for 25 minutes, and the pellet discarded. Ammonium sulfate was slowly added to 60% saturation (39 g/100 mL); then stirred for 15 minutes more to precipitate the protein. Centrifugation at 9000 rpm for 25–30 minutes deposited a pellet of the brown crude R2 from the clear straw-colored solution. The protein was redissolved in 100 mL Tris containing 1 μL/mL PMSF (Tris/PMSF) and loaded onto a G–25 column. Elution with the same Tris/PMSF buffer separated the protein solution into two bands, a brown one followed by a yellow one. The fractions containing the brown band were pooled and checked by UV-visible spectroscopy to confirm the presence of R2 from the signature peak at 410 nm. The partially–purified protein was diluted to 50% with Tris/PMSF buffer and loaded onto a DEAE column. This column was washed with 1 L Tris/PMSF until the only A_{280}

observed in fractions was due to the PMSF. The protein was then eluted using 130 mM NaCl in Tris/PMSF, and green and brown bands were observed. The fractions from the green band, which contained significant absorbances both at 280 and 410 nm, were pooled and diluted by 50% with Tris/PMSF buffer. This solution was loaded onto a QAE column and rinsed with Tris/PMSF, then 225 mM NaCl in Tris/PMSF. The R2 was eluted from the column using 300 mM NaCl in Tris and the protein–containing fractions (as confirmed by UV-vis analysis) pooled. Centriprep–10 or –30 concentrators (Amicon) were used to reduce the volume from 400 mL to 150 mL. The R2 was then dialyzed vs. 2 L Tris for 4 hours to remove excess salt, then overnight against Tris (1.5 L) containing 20% w/v glycerol. The pure protein was divided into 1 mL aliquots in Eppendorf tubes, flash–frozen with liquid nitrogen and stored at –80 °C. The total yield with this method was ≈ 2 g. Using several loading concentrations of the purified R2, Laemmli gels were run to assess the level of purification achieved (Figure 2.5).

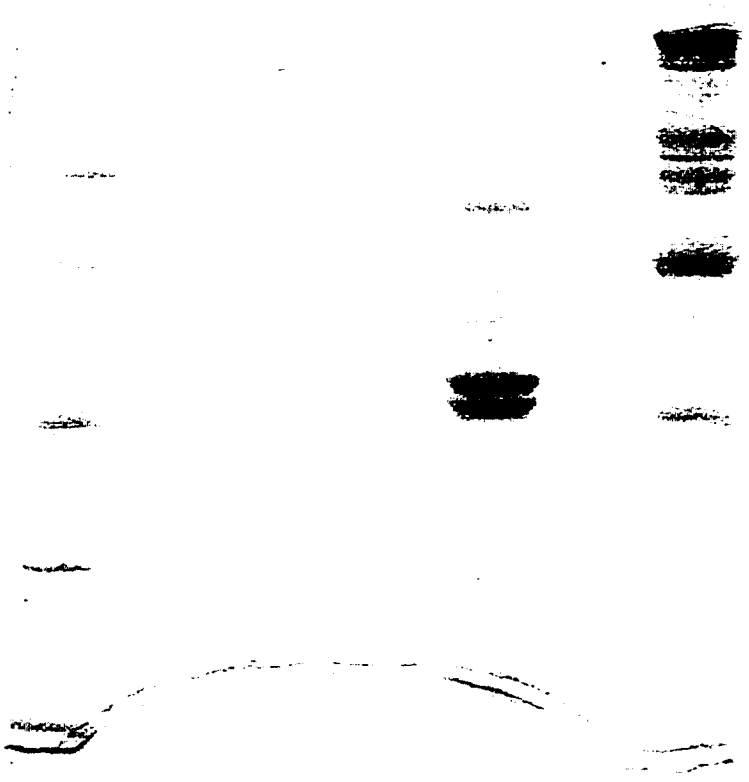

Figure 2.5. Denaturing (SDS–PAGE) gel of ribonucleotide reductase R2. Tracking dye front is at lower edge. Lane 1 = low molecular weight standards; Lane 3 = Purified R2, 1% loading; Lane 5, Purified R2, 10% loading; Lane 7, high molecular weight standards. Lanes 2, 4 and 6 are open. Low molecular weight standards (in kD) include lysozyme (14.4), carbonic anhydrase (31), ovalbumin (45), serum albumin (66.2), and phosphorylase B (97.4). High molecular weight standards include ovalbumin (45), serum albumin (66.2); phosphorylase B (97.4), β-galactosidase (116) and myosin (200). Developed using Coomassie Blue stain.

To convert active R2 into the apo form[16] for iron uptake experiments, 3 mL of active R2 was thawed. Met R2 was formed by reducing the tyrosyl radical with 0.5 g hydroxyurea while stirring for 15 minutes (as confirmed by UV–visible spectroscopy, the sharp peak at 410 nm was gone but the absorbances due to the Fe–O–Fe moiety were still present). The met R2 was sealed in pre-soaked dialysis tubing and dialyzed for 4–5 hours against a freshly–made (bright orange–yellow) aqueous solution of 1 M imidazole

hydrochloride (pH 7.0) with 50 mM 8–hydroxyquinoline–5–sulfonate to reduce and remove the metal center. The protein, a very dark green, was loaded from the dialysis tubing directly onto a G–50 Sephadex column and eluted with Tris buffer. Fractions containing a significant A_{280} (assuming ε_{280} = 120 $mM^{-1}cm^{-1}$)[29] were pooled (as there is no 410 nm peak for apo R2) and concentrated with Centripreps as before. At this point the apo could either be used for experiments or frozen again in liquid nitrogen for storage at –80 °C. The spectral features of active, met and apo R2 are summarized in Figure 2.6.

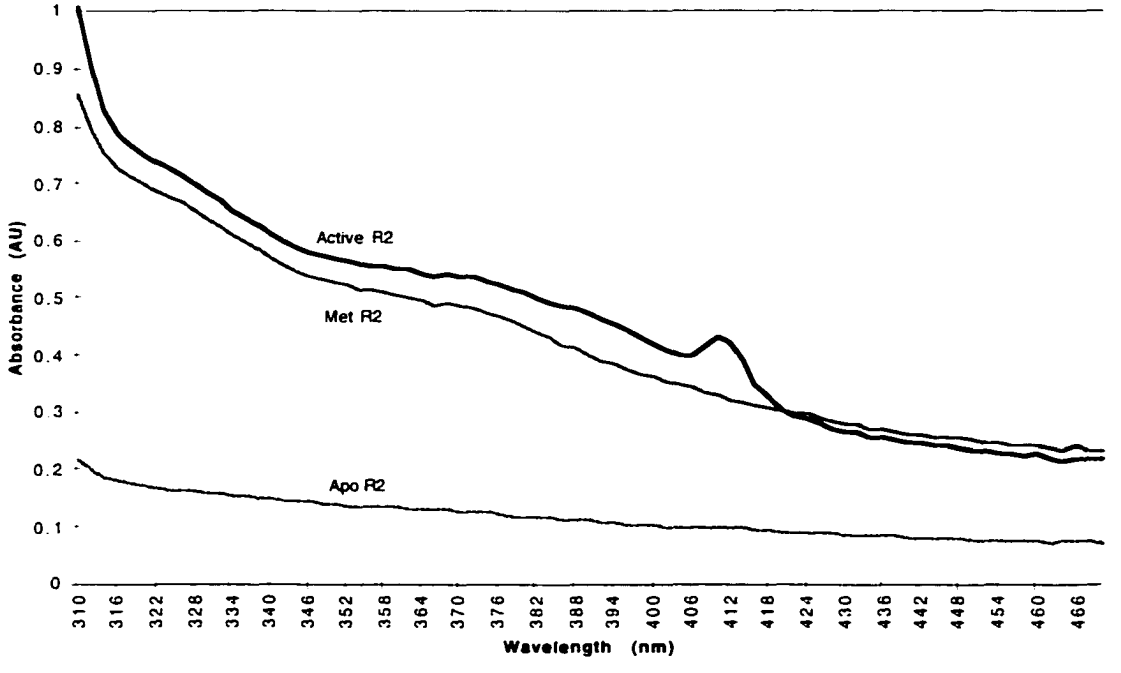

Figure 2.6. Detail UV-vis spectra of the metal cluster and tyrosyl radical of active R2, and changes during apo preparation. Active R2 (21.7 μM) was quantified by the dropline method (Eqs 28–31). The met and apo are at similar concentrations (allowing for changes due to manipulations during the procedure).

E. Conditions employed.

Ferrozine reaction characterization in biological buffers. Conditions for iron uptake by ferrozine in HEPES or Tris were similar to those used for the R2 competition experiments (neglecting ionic strength or viscosity contributions from the protein itself). Ferrozine was dissolved in either 100 mM HEPES or Tris buffer. The iron(II) solutions were freshly made from ferrous ammonium sulfate hexahydrate in 5 mN H_2SO_4, with NaCl added to give a final ionic strength of 0.1 M in the reaction mixture. Unless stated otherwise, all reactions were done in air.

The effect of BSA as a viscogen on the ferrozine reaction. Ferrozine (3.4 mM) was dissolved in HEPES buffer and the resulting solution used as both control solution and as the solvent for the protein of choice. BSA was made up as a stock solution (400 μM) and diluted to produce protein concentrations ranging from 25–350 μM (1.6–26.6 mg/mL). Fresh 60 μM iron(II) solution was made as above. Kinetic data were collected at 5.0 °C. When used as a viscogen, BSA was added to the ferrozine solutions at the same w/v (32–257 μM BSA to 24–198 μM R2) as R2 in the corresponding ferrozine–apo R2 competition reaction.

Competition experiments between apoR2 and ferrozine for Fe(II). Ferrozine (1.4–8.7 mM), apo R2 (24–198 μM), and sodium ascorbate (3 mM) were dissolved in HEPES buffer, and loaded in one reagent syringe. Fresh 60 μM iron (II) solution was made as above, and was placed in the second syringe.

Unless noted, experiments were carried out in air. For anaerobic experiments, standard vacuum–line techniques were employed. During some of the competition experiments, the stopped flow waste stream was collected into a degassed sealed cuvet via a needle–capped piece of tubing and then placed in the UV–visible spectrometer for observation up to an hour, to determine the extent of iron loss from apoFe and/or $apoFe_2$.

Reduction of active R2 by methyl viologen radical, and trapping of iron with ferrozine. Methyl viologen (20 mg) and sodium dithionite (0.5 g) in degassed water (30 mL) under argon afforded methyl viologen cation radical ($\bullet MV^+$) as a deep blue solution.[129] Aliquots of this solution (typically 15 μL; ≤ 1% of the total volume of protein solution) were added via syringe to an anaerobic R2 (9.3–114 μM) solution, either in a Schlenk flask or in the reservoir cups of the stopped flow apparatus to reduce the tyrosyl radical and iron cluster,[65] just moments prior to filling the reactant syringes. In some cases, 4.43–17.7 μM of excess iron(II) was added to the protein solution. The opposite reagent line contained anaerobic ferrozine (800 μM–7.5 mM) solution. The stopped flow apparatus was argon–purged and thermostatted to 4–5 °C.

[129] Trudinger, P. A. On the Absorbancy of Reduced Methyl Viologen. *Anal. Biochem.* **1970,** *36,* 222–225.

CHAPTER III. PRELIMINARY EXPERIMENTS.

A. Initial competition trials.

Preliminary experiments between the two iron–binding systems of RNR R2 and ferrozine conducted to assess the feasibility of measuring the uptake rate of iron into R2 by competition scheme were successful. It was determined that in order to observe a competition, ferrozine must be in higher excess over iron than is protein, even after the 3:1 Fz–Fe ratio is taken into consideration. The concentrations of protein and the organic ligand can be manipulated to create a variety of iron distributions between the two iron–binding species along a continuum from "all iron into protein" (7.3:2.3:1 Fz–Fe–apo), to "all iron into chelate" (≥ 101:2.3:1 Fz–Fe–apo) (Figures 2.7–2.9). In order for detectable amounts of Y122• to form, the concentration of ferrozine must be lowered nearly to a stoichiometric ratio (Figure 3.4 has 7.3:2.3:1 Fz–Fe–apo; or just 3.2 Fz per iron). For ferrozine to trap all the iron in the system when faced with an opposing concentration of just 14.4 μM apo R2, [Fz] would have had to be increased to at least 5 mM, at which point the ferrozine–iron reaction would become too fast (k_{obs} > 200 s^{-1}) to follow by stopped–flow. Good competition, with both apo and ferrozine trapping some iron, was observed at 44.8:2.3:1 Fz–Fe–apo.

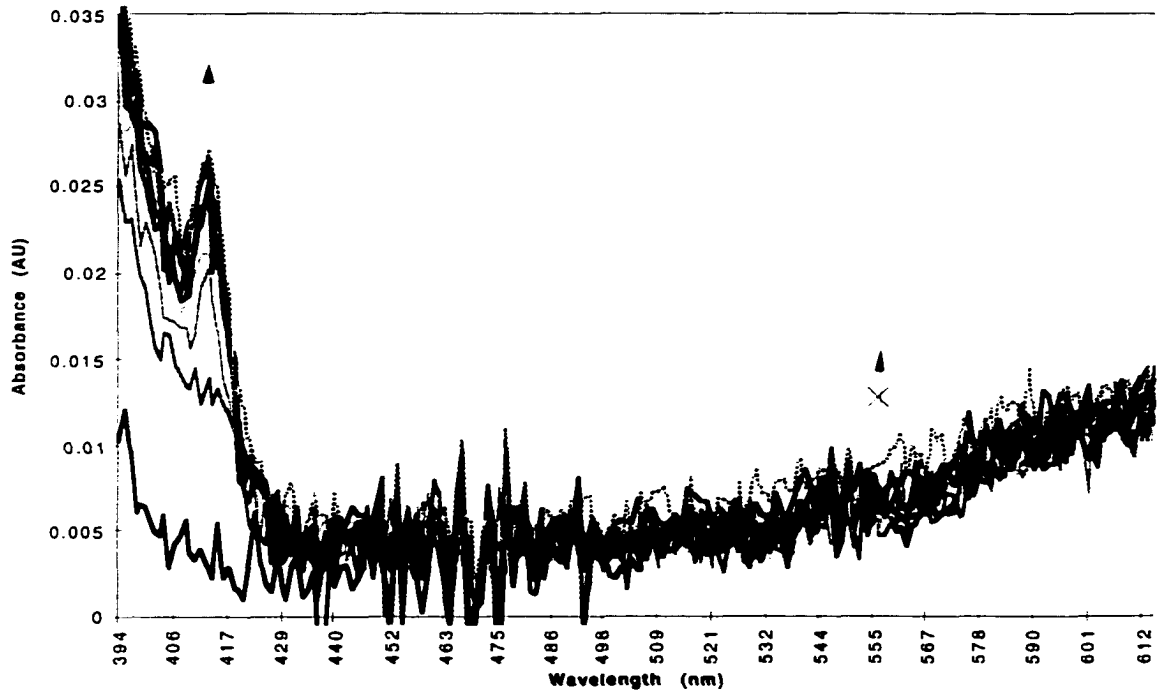

Figure 3.1. Rapid–scanned stopped flow data with all iron taken up by the protein. No $FeFz_3$ (562 nm) is detected, but the signature peak of R2's Y122• is clearly visible. Final (post–mixing) concentrations were 106.5 μM Fz, 33.0 μM Fe(II), 14.4 μM apo R2; 50 mM HEPES buffer, pH 7.6 at 5.0 °C. Ionic strength was not buffered. Spectra shown are approximately 100 ms apart.

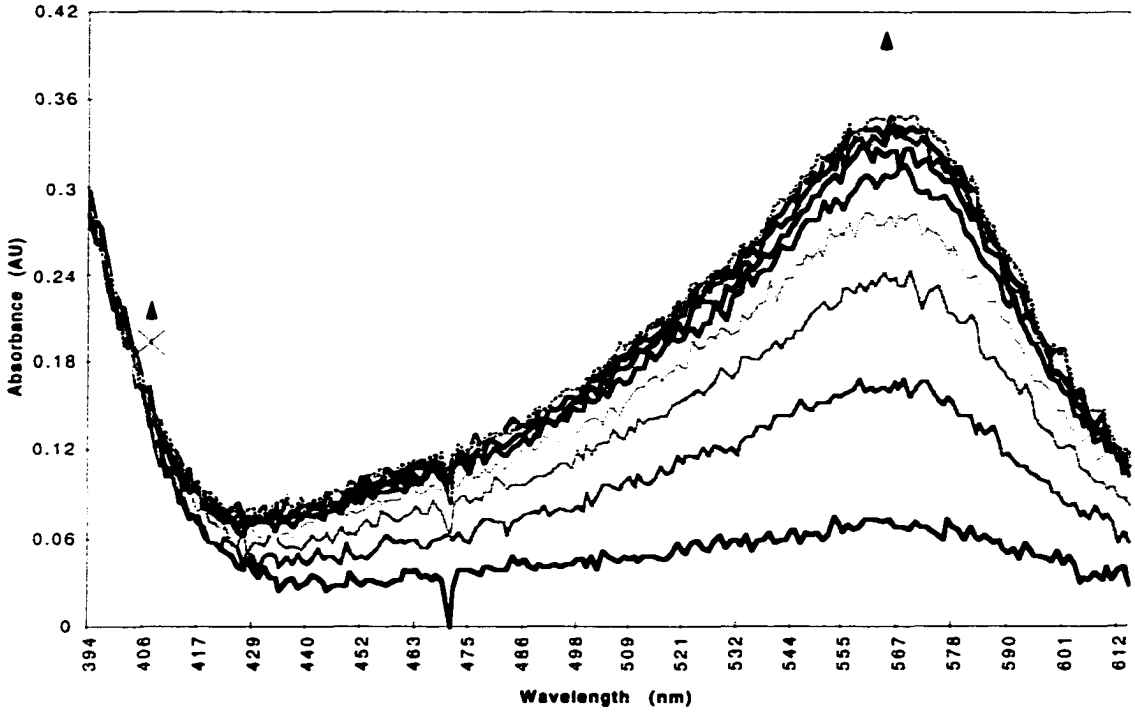

Figure 3.2. Rapid–scanned stopped flow data with all Fe(II) taken up by ferrozine. No Y122• (410 nm) is detected. However, the signature peak of $FeFz_3$ (562 nm) is clearly visible. Final (post–mixing) conditions were 1.452 mM Fz, 33.0 μM Fe(II), 14.4 μM apo R2; 50 mM HEPES buffer, pH 7.6 at 5.0 °C. Ionic strength was not buffered. Spectra shown are approximately 20 ms apart.

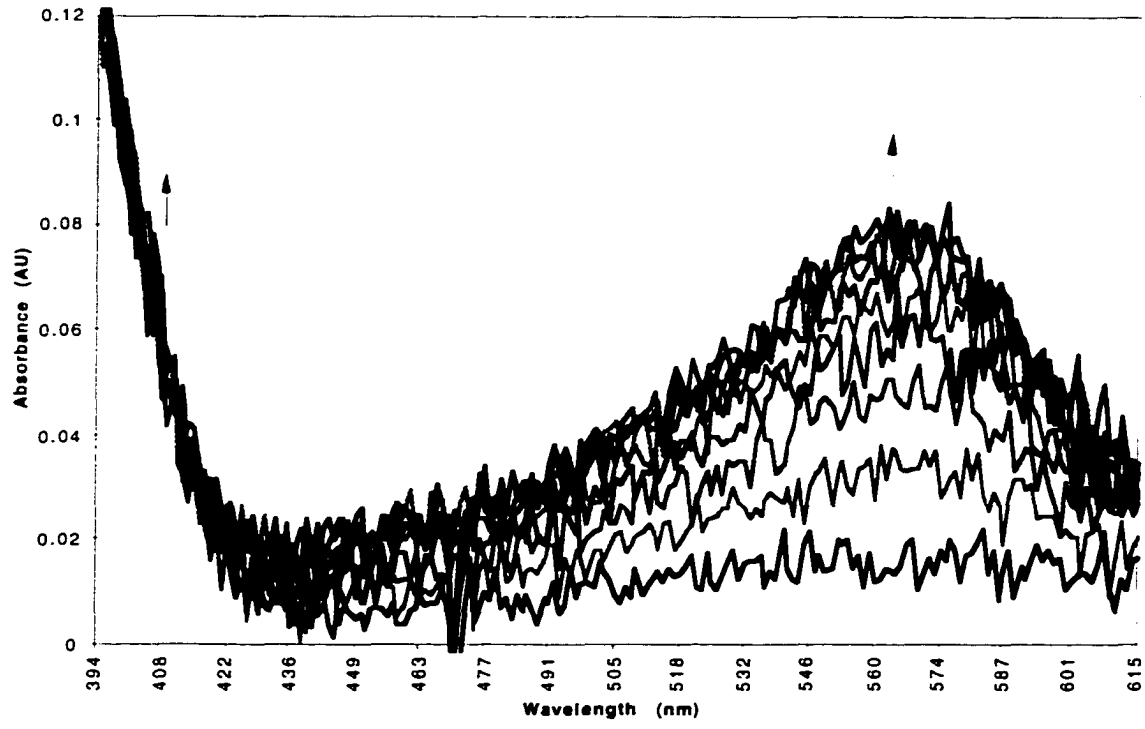

Figure 3.3. Rapid–scanned stopped flow data of a competition situation. Some Fe(II) is taken up by the protein, because the yield of $FeFz_3$ (562 nm), while appreciable, is not quantitative (with respect to iron). There is the faintest hint of a change in absorbance at 410 nm, but not enough to be quantified. Final (post–mixing) conditions 645.5 μM Fz, 33.0 μM Fe(II), 14.4 μM apo R2; 50 mM HEPES buffer, pH 7.6 at 5.0 °C. Ionic strength was not buffered. Spectra shown are approximately 20 ms apart.

For quantitative work, the amount of $FeFz_3$ formed must have a high enough signal–to–noise that its absorbance band centered at 562 nm can be used for kinetic studies. Even if a peak at 410 does not develop, it is also important that the protein still competes for a significant fraction of iron as well. Thus, both extremes are avoided and the two fates for iron are competitive.

Taken as time traces along the 562–nm axis, the three stopped–flow experiments shown in Figures 3.1–3.3 are shown as Figure 3.4. Depending on the amount of iron

trapped by the protein, the absorbances at 562 nm reach different heights. When the protein overwhelms the system and takes all iron from solution, the growth of a peak at 562 nm isn't observed at all (Figure 3.1), and the corresponding time–trace remains along the baseline (Figure 3.4).

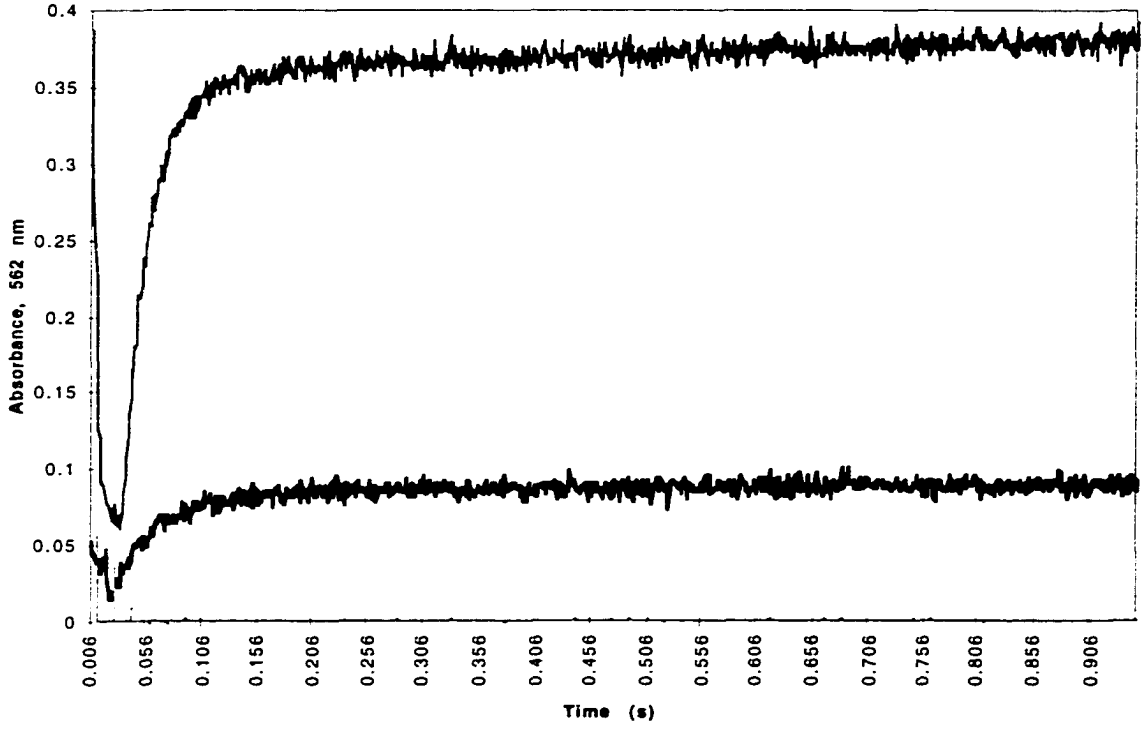

Figure 3.4. Absorbance at 562 nm over the course of three competition reactions. Greater amplitudes imply more iron taken up by ferrozine. The lowest curve runs along the baseline for the entire reaction, and corresponds to the data from Figure 3.1; presumably all iron in this reaction is in the form of either active R2 (as manifest in the growth of the peak at 410 nm) or as monoferrous R2, "apoFe". The middle trace is a slice from Figure 3.3, an intermediate case; and the uppermost curve is from Figure 3.2, where no Y122• was observed to form but ferrozine still hasn't sequestered all the iron; there must be some monoferrous R2, which is invisible.

Because ionic strength is crucial to ferrozine–iron reaction rates, all quantitative competition reactions were performed at an ionic strength of 0.1 M. Multiple molecular charges greatly change ionic strength, and ferrozine is formally – 2. Because ferrozine was

often varied, unadjusted ionic strengths ranged generally between 0.04 and 0.06 M. The addition of sodium chloride to give $I = 0.1$ M ensured this parameter was controlled. Test reconstitutions of apo R2 were performed over the range 0.04–0.10 M and found not to be significantly affected by the extra salt (Figure 3.5).

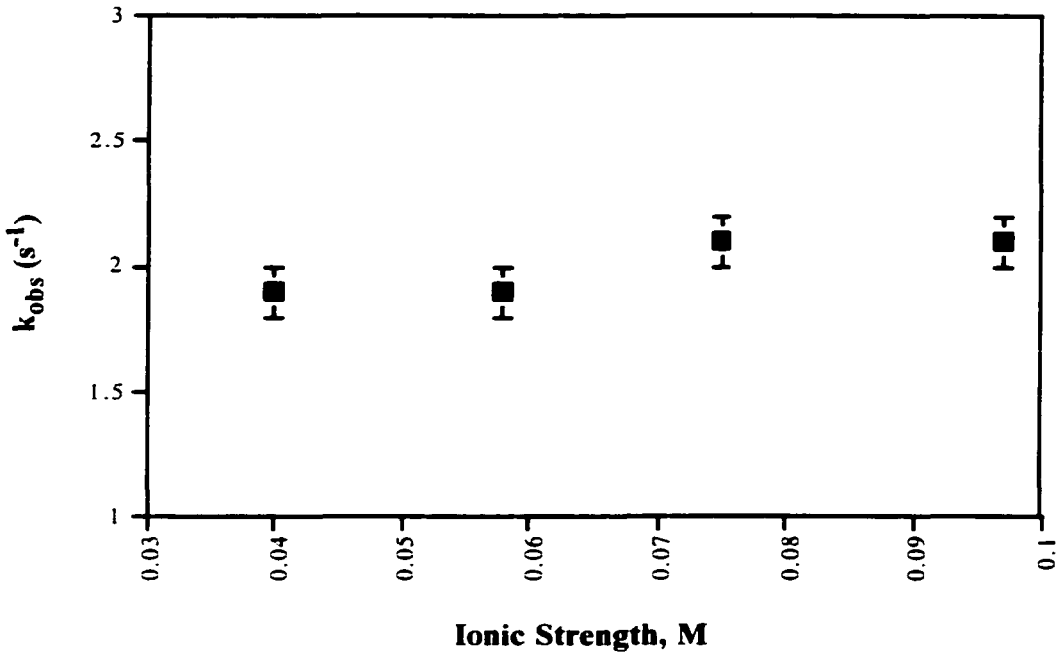

Figure 3.5. Affect of ionic strength variation on the reconstitution reaction. Conditions: 19.5 μM apo, 100 μM Fe(II), 1.5 mM ascorbate, in 50 mM HEPES buffer (pH 7.6 at 5.0 °C). Sodium chloride was added to increase ionic strength beyond that of the original system (0.04 M).

B. Theory.

It can be shown[130] that observation of any one product provides k_{obs} (Eq 33) for a situation where two or more first–order routes exist for consumption of a substrate. When a reactant **A** is converted to three products (Eq 32) the rate of formation of any one of them can be determined using the other two, (Eq 34). The observed rate constant k_{obs} will equal the sum of all three rate constants (k_1–k_3).

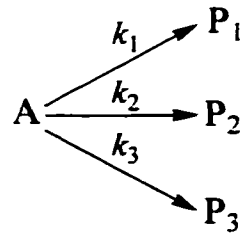

Eq 32

In addition, the ratio of any two rate constants will equal the ratio of the corresponding products.[131]

$$k_{obs} = k_1 + k_2 + k_3 \qquad \textbf{Eq 33}$$

$$\frac{P_1}{P_2} = \frac{k_1}{k_2}, \text{ etc.} \qquad \textbf{Eq 34}$$

---

[130] Bunnett, J. F. In *Investigation of Rates and Mechanisms of Reactions*, 3rd ed.; Lewis, E. S., Ed.; Techniques in Chemistry; John Wiley and Sons: New York, 1974; Vol. 6, Chapter 4.

[131] Espenson, J. H. Reversible and Concurrent Reactions. *Chemical Kinetics and Reaction Mechanisms*, 2nd ed.; McGraw–Hill: New York, 1995; pp 58–59.

If a pathway is not first order, this must be taken into account. Suppose one of the reactions also depends on the concentration of some other reagent X; the expression for that term must be a pseudo–first–order rate constant, $k_X[X]^n$. It is reasonable to assume that the rate of uptake of Fe^{II} by apoprotein is given by Eq 35.

$$\frac{-\,d[Fe^{II}]}{dt} = k_{apo}[apo][Fe^{II}] \qquad \textbf{Eq 35}$$

If [apo] is large and effectively constant, Eq 35 will reduce to a pseudo–first–order rate constant of $k_{apo}[apo]$ for the complexation of FeII by apoprotein. Similarly, if apoFe + Fe → $apoFe_2$ is operative, there will be a term for it as well (Eq 36).

$$\frac{-\,d[Fe^{II}]}{dt} = k_{apo}[apo][Fe^{II}] + k_{apoFe}[apoFe][Fe^{II}] \qquad \textbf{Eq 36}$$

It is not simple to write a pseudo–first–order rate constant for the complexation of Fe^{II} by ferrozine, because the *order* of that reaction will vary with [Fz]. (Recall Eq 25 in the Introduction, with an order of three in ferrozine at low [Fz] and of one in ferrozine at high [Fz]. However, if we keep [Fz] large enough to be effectively constant, we can measure an effective first–order rate constant k_{Fz} that will prevail throughout the reaction.

Therefore, if ferrous ion is being consumed by two second–order processes (first and second iron uptake steps by the protein) and a third effectively first–order process (the ferrozine reaction), to form the three products apoFe, $apoFe_2$ and $FeFz_3$, Eq 33 becomes Eq 37.

$$k_{obs} = k_{Fz} + k_{apo}[apo] + k_{apoFe}[apoFe] \qquad \textbf{Eq 37}$$

C. Complexation of Fe^{II} by ferrozine at concentrations required for the competition experiments. Previous workers (see Introduction) had shown that up to [Fz] ≈ 800 μM the order of the complexation reaction in ferrozine was (nearly) three. We have redetermined the kinetics of the ferrozine reaction in the biological buffer HEPES (described below), and at higher concentrations than previous workers (whose maximum [Fz] = 0.8 mM, a narrow range which fits in the lower–left–most grid box in Figure 3.6). This was necessary because of the ferrozine concentrations required to achieve competition conditions for the main goal of this report. The plot of the observed rate constant vs. ferrozine concentration (Table 2) has a non–third–order profile (Figure 3.6).

Table 2. The rate constants observed during the reaction of ferrozine with iron(II) under conditions necessary for the competition reactions. Illustrated in Figure 3.6. Conditions: 50 mM HEPES, pH 7.6 at 5.0 °C; 30 μM iron(II), I = 0.1 M.

Ferrozine, mM	k_{obs}, s^{-1}
0.0	0.0
0.686	16.1
0.967	33.6
1.38	59.2
1.85	98.9
2.42	138
3.05	182
3.64	218
4.37	249

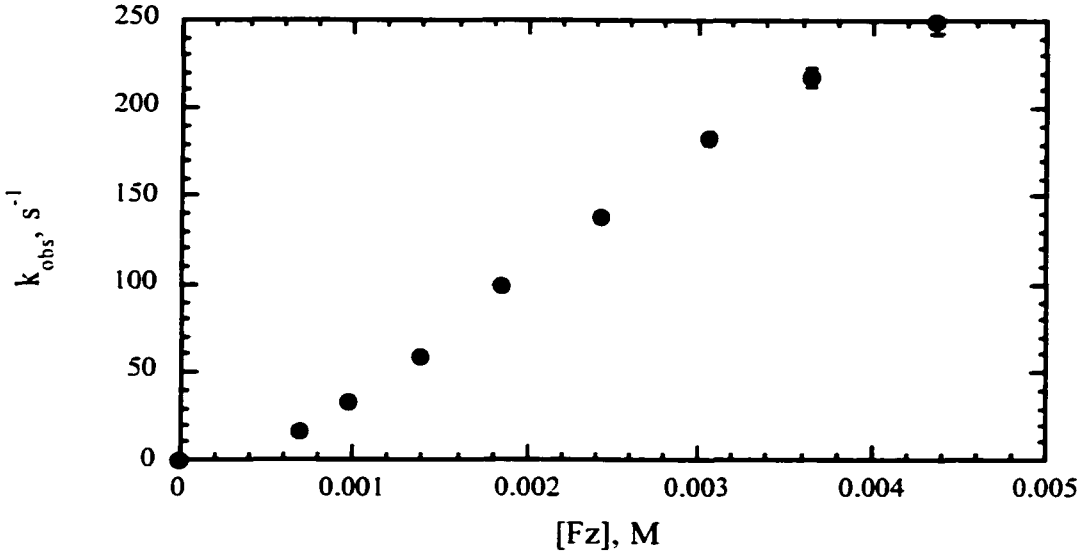

Figure 3.6. Reaction order of ferrozine reaction with iron. This is clearly not a simple third–order chelation reaction under the conditions necessary for competition in later experiments! Data from Table 2. Conditions: 50 mM HEPES, pH 7.6 at 5.0 °C; 30 μM iron(II), I = 0.1 M. This curve was fitted to Eq 40 (see Appendix).

At the [Fz]s in Figure 3.6, the order in ferrozine does indeed decrease as predicted by Eq 25. From orders of 0.715 to 2.157 the average order in ferrozine proves to be 1.48 (Figure 3.7). Increasing ferrozine concentration to even higher levels might induce saturation behavior, stabilizing the order near one, but the upper ranges of the ferrozine concentrations we use already cause rates which push the detection limits of the stopped–flow instrument.

Using the limits of Figure 3.6 and Eqs 26–27, it was possible to predict values for k_3 and the product K_1K_2. At [Fz] = 4.37 mM, in the first–order regime, $k_{obs} = k_3$[Fz]; solving for k_3 gives an initial estimate of 5.8×10^4 $M^{-1}s^{-1}$. At [Fz] = 686 μM, in the

third–order regime, $k_{obs} = K_1K_2k_3[Fz]^3$; using k_3 from above and solving for K_1K_2 gives an initial estimate of 1.32×10^6 M^{-2}. Fitting of the data to a curve (see Appendix) using the calculation package Mathcad resulted in the determation of $k_3 \approx 7.0 \times 10^4$ M^{-1} s^{-1} with K_1K_2 constrained to be 1.32×10^6 M^{-2}.

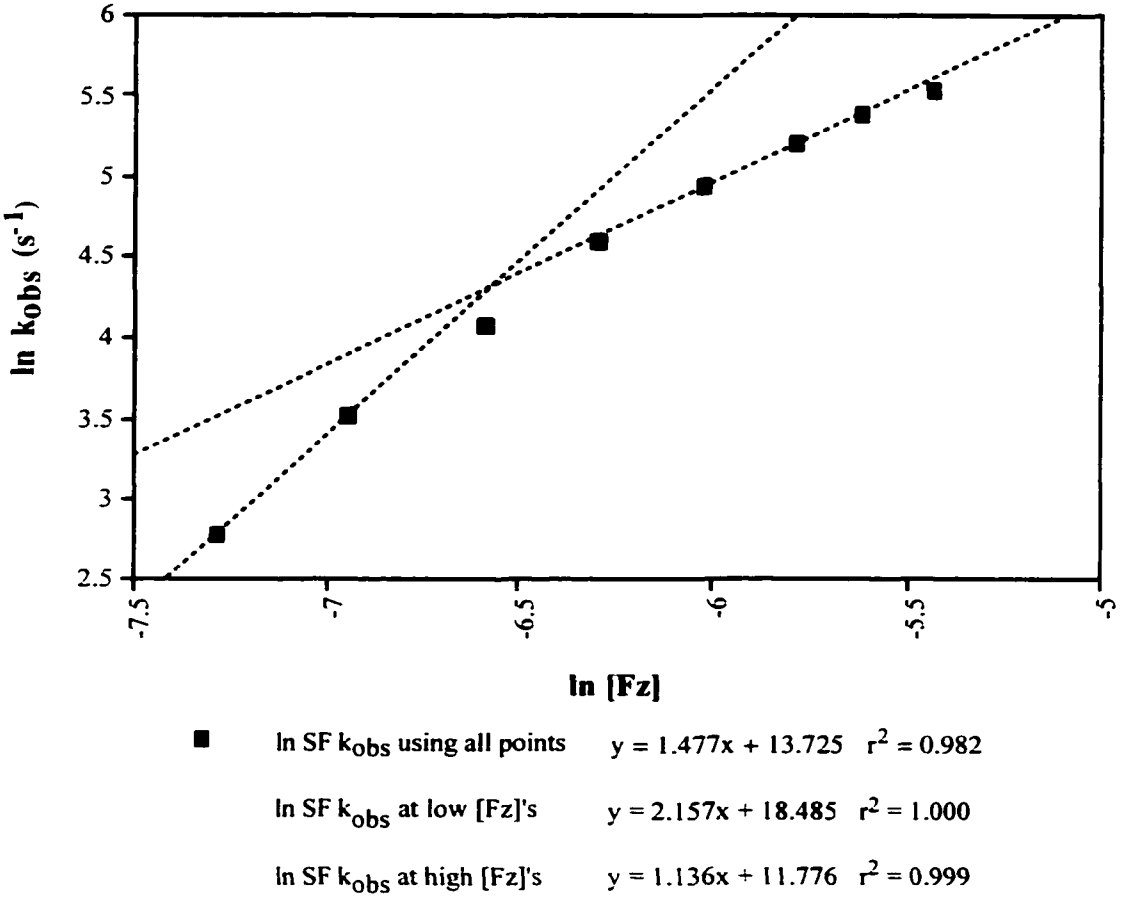

Figure 3.7. Variation in reaction order at ferrozine concentrations of up to 4.5 mM in biological conditions. Final (post–mixing) concentrations were 50 mM HEPES, pH 7.6 at 5.0 °C, ionic strength 0.1 M (by addition of NaCl).

Thus k_{Fz} is defined as a pseudo–first–order rate constant that has been determined during a control reaction at the same conditions and concentrations as a given competition reaction; there is an individualized k_{Fz} for every competition reaction.

Adapting Eq 34 to the situation at hand, taking into account the second–order reaction between apo and ferrous ion, gives Eq 38.

$$\frac{[FeFz_3]}{[apoFe]} = \frac{k_{Fz}}{k_{apo}[apo]} \qquad \textbf{Eq 38}$$

Plots of k_{obs} vs. k_{Fz} should have a slope of k_{apo}[apo]; and [$FeFz_3$]/[apoFe] vs. [Fz]/[apo] should have a slope of $1/k_{apo}$. However, these relationships will hold true only if [Fz] and [apo] are both constant. Our experiments did not meet both these requirements; in combination with the viscosity effects which are discussed at length (*vide infra*) we were forced to use other tactics.

By using a kinetic simulation program (MacKinetics) this analysis can be extended to situations where [apo] and k_{apo}[apo] decrease significantly during the reaction. The practical advantages of this are that pseudo–first–order protein concentrations *are not necessary*, enabling the extraction of meaningful data from practicable experiments (the protein will be fully soluble, and not consumed extravagantly).

To simplify matters, consider two boundary conditions: either $k_{apo} >> k_{apoFe}$ and the protein–related path either converts apo to apoFe until iron is depleted with little to no $apoFe_2$ formed, or $k_{apoFe} >> k_{apo}$ and any apoFe formed is rapidly converted to active R2.

The signature band (410 nm) of the tyrosyl radical in active R2 was detected only during experiments with very low ferrozine concentrations ([Fz] ≈ 3 [Fe^{II}]). The fact that Y122• was not observed at other times, even when little $FeFz_3$ was observed to form, implies that some vital ingredient is missing (probably a second Fe(II) equivalent), preventing the reconstitution from progressing. This suggests the first situation is operative: $k_{apo} >> k_{apoFe}$, and allows us to initially consider only Eq 2 and 5 (and implicitly Eq 3) of the reconstitution scheme. Thus, Eq 37 reduces to Eq 39.

$$k_{obs} = k_{Fz} + k_{apo}[apo] \qquad \textbf{Eq 39}$$

Ideally, true competition experiments should have both reagents (the protein and the ferrozine) in pseudo–first–order excess compared to the iron concentration, but for several reasons, the ferrozine was generally the only species to meet this condition. Running experiments with several hundred micromolar apo simply uses too much of the precious protein, and also thickens the solution to such an extent that reaction rates are severely retarded, due to viscosity effects. These issues were both resolvable. The use of the iterative computer–modeling program MacKinetics removed the necessity of kinetic simplification via pseudo–first–order conditions, allowing parsimony in protein consumption. Adding a dummy protein (BSA) to the reaction mixture as an R2 mimic during control reactions allowed us to deal with viscosity effects. Both issues and their solutions are discussed in more detail later in this document.

D. Competition experiments between apo R2 and ferrozine for Fe(II).

Elimination of possible interfering absorbances. Because the kinetics of the competition reactions were to be followed at 562 nm, any other potentially interfering absorbances from other species in the reaction mixture needed to be ruled out. The transient absorbance due to $\bullet W48H^{+}$ (discussed at length in the Introduction) can be eliminated by the use of sodium ascorbate in solution to direct the reconstitution into the "excess iron" pathway even with the very limiting amounts of iron utilized during the competition reactions. The formation and spectroscopy in solution of iron ascorbate complex were investigated (Figure 3.8). While ferrous ascorbate solution is a deep purple, this complex was found to be spectroscopically quiescent at competition–relevant

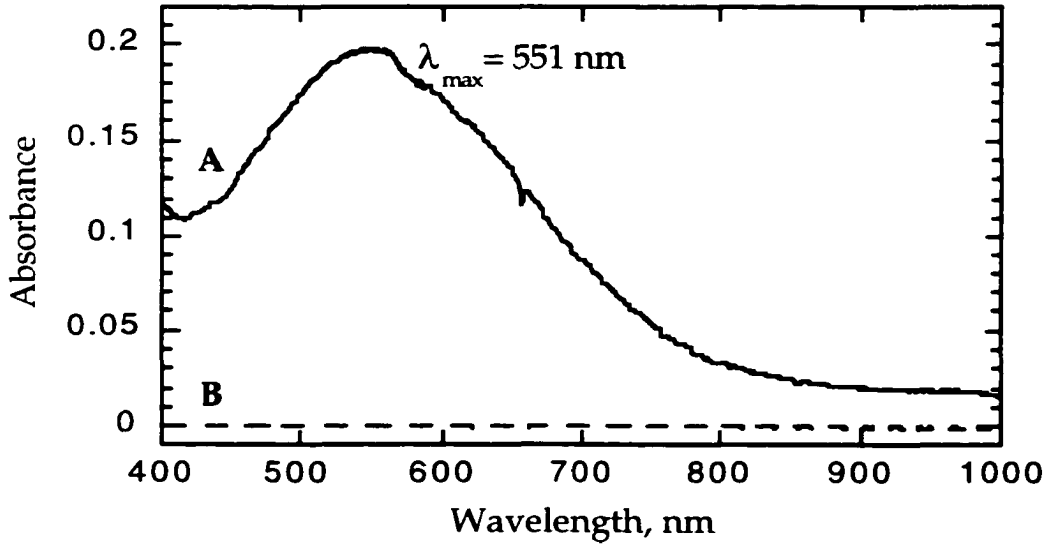

Figure 3.8. Electronic spectrum of ferrous ascorbate. The solution when concentrated is a deep purple, and has a broad absorbance centered at 551 nm (spectrum A). However, at the concentrations used in the competition experiments (30 μM Fe(II) is the limiting reagent), its spectral contribution is negligible (spectrum B).

concentrations, despite having an absorbance maximum similar to the ferrozine–iron complex. In addition, ferrous ascorbate is a labile complex which in normal reconstitutions of R2 has not hindered uptake of iron by the protein, so it should not under competition conditions.

Temperature and pH effects on the ferrozine reaction in the absence of protein. Data have been collected at several temperatures ranging from 5 to 41 °C in the following buffer systems: pH 7.09, 7.66 and 8.10 Tris, and pH 6.81, 7.20, 7.60, and 8.20 HEPES. In these experiments, ferrozine was 1.6 mM, iron(II) 16–32 μM; and ionic strengths were adjusted to ≈ 0.2 M (NaCl). Ascorbate was not added, as its reductant properties (usually added during an apo reconstitution in the "limiting iron" regime as the source of an extra electron) are not needed in the absence of the R2 reconstitution reaction, and it is assumed to be just a spectator in this reaction.

Kinpar 5.0 was employed to calculate activation parameters, using rate constants and temperatures from the stopped flow experiments: the Arrhenius activation energy (E_a), activation entropy ($\Delta S^{\ddagger}$), activation enthalpy ($\Delta H^{\ddagger}$), and activation free energy ($\Delta G^{\ddagger}$). In Tris, E_a, $\Delta S^{\ddagger}$ and $\Delta H^{\ddagger}$ were found to increase with pH, but these values were relatively constant across the pH range in HEPES. $\Delta G^{\ddagger}$'s are quite close for all three buffer systems (Tris, HEPES and phthalate). The pK_a of HEPES is 7.35, and that of Tris is 8.3 (both at 20 °C). The overall rate constant k_{obs} would be the expression (obtained from Eq 25) in Eq 40; the activation parameters for k_{obs} in Table 3 are a function of K_1, K_2

and k_3 and would thus be expected to be quite complex, so the numbers are not especially meaningfui outside this context.

$$k_{obs} = \frac{K_1 K_2 k_3 [L]^3}{1 + K_1[L] + K_1 K_2 [L]^2} \qquad \textbf{Eq 40}$$

Table 3. Activation parameters for the ferrozine reaction under various conditions.

Buffer, pH	E_a, kJ/mol	$\Delta G^{\ddagger}$, 25 °C, kJ/mol	$\Delta G^{\ddagger}$, 5 °C, kJ/mol	$\Delta H^{\ddagger}$, kJ/mol	$\Delta S^{\ddagger}$, J/K-mol
HEPES, 6.81	26(1)	62.76(5)	60.14(8)	24(1)	–131(4)
HEPES, 7.20	26(1)	62.81(4)	60.17(8)	24(1)	–132(4)
HEPES, 7.60	28.0(7)	62.32(3)	59.85(6)	25.6(8)	–123(3)
HEPES, 8.20	28(1)	62.32(6)	59.8(1)	25.3(2)	–124(5)
Tris, 7.09	28(1)	62.51(6)	60.0(1)	26(1)	–123(5)
Tris, 7.66	45(6)	63.1(2)	61.6(4)	42(6)	–69(19)
Tris, 8.10	53(3)	64.1(1)	63.2(2)	50(3)	–46(9)
Phthalate, 5.0[132]	9.9(2)	56.087(5)	52.82(2)	7.4(2)	–163.3(6)

Viscosity effects on the ferrozine reaction. Early in the competition studies, it was observed that as apo R2 concentrations were increased, the rate of reaction actually decreased (while product vs. reactant ratio, and product ratio vs. k_{Fz}, worked more or less as hoped, plots of k_{obs} vs. [apo] had a negative slope–see Figures 3.9–3.11—instead of increasing as expected).

Plots of k_{obs} vs. k_{Fz} should have a slope of k_{apo}[apo] (Figure 3.11); and [$FeFz_3$]/[apoFe] vs. [Fz]/[apo] should have a slope of $1/k_{apo}$ (Figure 3.9). However, these

[132] Mottola, H. A., personal communication.

relationships only hold if [Fz] and [apo] are both constant. Our experiments did not meet both these requirements. It was found that the product vs. reactant ratios did give an estimate (within an order of magnitude of the value ultimately determined) of the rate constant we were seeking, even without the various treatments applied to the reaction system and data (i.e., the standardization of the ferrozine–iron control reactions using BSA, and solving for the rate constants using MacKinetics): the value of k_{apo} as determined using Eq 39 was 4.4×10^6 M^{-1} s^{-1}.

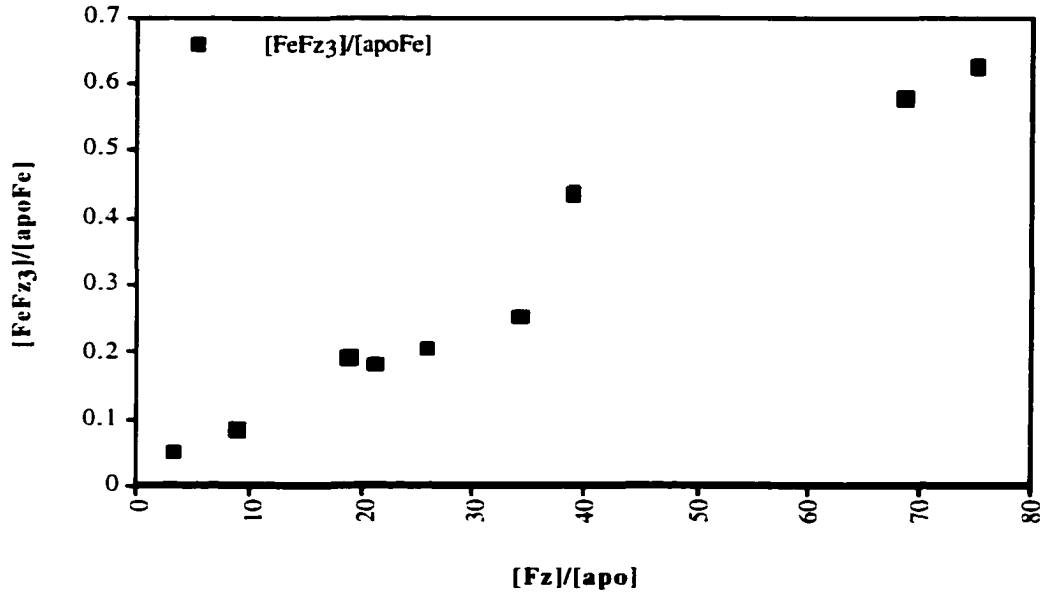

Figure 3.9. Product ratios vs. reactant ratios from early competition trials. The data show linearity over a wide range of reactant ratios, and allow the estimation k_{apo} = 4.4×10^6 M^{-1} s^{-1}.

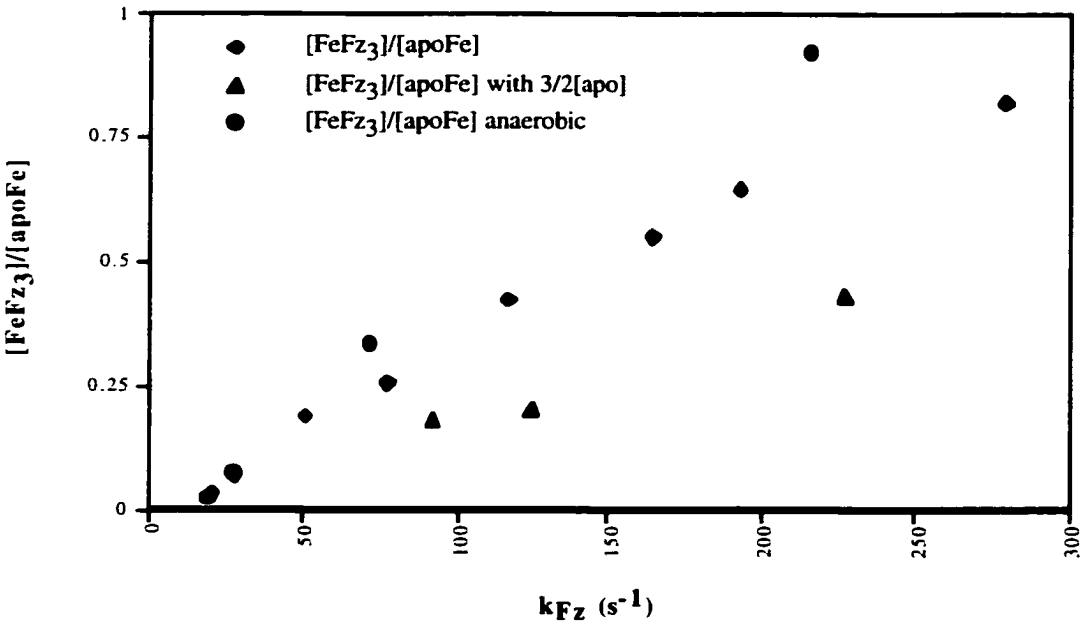

Figure 3.10. The effects of increased [apo] and of O_2 exclusion on product ratios vs. rate constant of ferrozine–free iron reaction. The product ratio vs. k_{Fz} plots are relatively linear and demonstrate that oxygen exclusion (circles) doesn't affect the rate significantly, but increasing the protein concentration (in this case by 50% (triangles)) markedly slows the reaction.

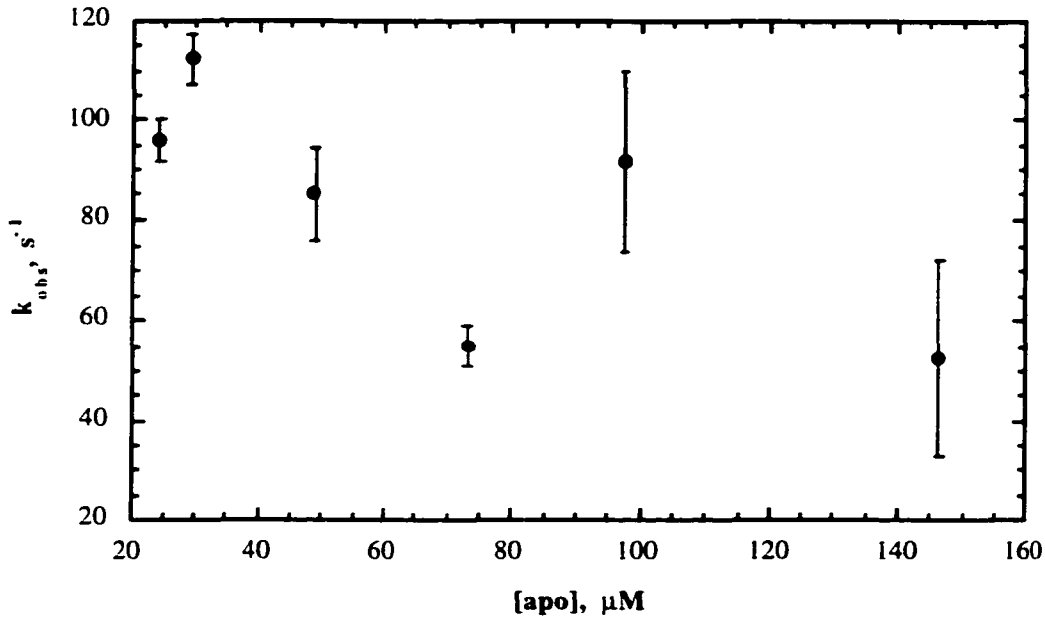

Figure 3.11. Negative slope as an indicator of problems with the competition system. While ferrozine's concentration is held constant and [apo] is varied, the observed rate of total iron uptake k_{obs} decreased rather than increased. There should be a positive slope, but the increasing viscosity counteracts any rate gains.

It was determined that increasing the protein concentration increased the viscosity of the solution to such an extent that the expected concomitant increase of k_{obs} was overpowered. With this in mind we sought methods of dealing with this problem. Three inexpensive and readily available proteins were added to the ferrozine reaction in turn. Both bovine γ-globulin and chicken egg–white lysozyme were tried and discarded due to solubility problems at the concentrations and temperatures required, but bovine serum albumin (BSA) was found to be ideal.

Although several studies of the kinetics of ferrous ion complexation by the water–soluble ligand ferrozine have been reported,[84,117,118] the buffer systems employed were such that the viscosity of the solution is not substantially different than that of pure water. However, as ferrozine gains more kinetic biological applications, generally as a trapping reagent to characterize iron taken up or released by a protein, the tendency of increased solution viscosity to slow down reaction rates will become more important to the community.

Bovine serum albumin was added to the ferrozine solution as a "proteinic viscogen[133]"—a "typical protein"—to mimic the effects of R2 in solution. The general properties of BSA[134] make it ideal for this problem: low cost, high purity, stability over a wide pH range, high solubility even at 5 °C, and a molecular weight of 66.7 kD, close to that of R2 (87 kD).[135] BSA does not bind ferrous iron appreciably without EDTA,[136] citrate[137] or bilirubin[138,139] in solution as well, leading one to suspect that, as is concluded

---

[133] Kyushiki, H.; Ikai, A. The Effect of Solvent Viscosity on the Rate-Determining Step of Fatty Acid Synthetase. *Proteins: Struct., Funct., Genet.* **1990,** *8,* 287–293.

[134] Peters, T., Jr. Serum Albumin. In *Advances in Protein Chemistry*; Anfinsen, C. B.; Edsall, J. T.; Richards, F. M., Eds.; Academic: New York, 1985, Vol. 37, pp 161–245.

[135] Carlson, J.; Fuchs, J. A.; Messing, J. Primary structure of the *Escherichia coli* ribonucleoside diphosphate reductase operon. *Proc. Natl. Acad. Sci. USA* **1984,** *81,* 4294–4297.

[136] Anghileri, L. J. The Binding of Iron to Plasma Proteins–the Effects of Chelating Agents. *Int. J. Clin. Phamacol.* **1968,** *6,* 523–528.

[137] Løvstad, R. A. Interaction of Serum Albumin with the Fe(III)-Citrate Complex. *Int. J. Biochem.* **1993,** *25,* 1015–1017.

[138] Hulea, S. A.; Wasowicz, E.; Kummerow, F. A. Inhibition of metal–catalyzed oxidation of low–density lipoprotein by free and albumin–bound bilirubin. *Biochim. Biophys. Acta* **1995,** *1259,* 29–38.

[139] Loban, A.; Kime, R.; Powers, H. Iron-binding antioxidant potential of plasma albumin. *Clin. Sci.* **1997,** *93,* 445–451.

by Anghileri (in the case of EDTA) that it is actually these other ligands binding the iron. Although serum albumins are known to bind several other inorganic ions (notably Ca^{2+}, Cu^{2+}, Ni^{2+}, Zn^{2+}, Hg^{2+}, Mn^{2+}, Au^{2+}; and Al^{3+}; Co^{2+} and Cd^{2+} weakly) and compounds[140,141] and bioorganic molecules (long–chain fatty acids, various lipids, bile salts, bilirubin, hematin, and the amino acids tryptophan and thyroxine), none of these are part of the R2 experimental design, so they are not of concern to us. No literature references were located regarding the binding of specifically ferrous iron to BSA, but taken in the context of the other, harder cations which can be bound by this protein, it appears there is no predilection in this direction. Published works regarding iron binding by BSA often only look at ferric iron, whether an iron(III) reagent is used or it is generated in situ. Three published examples examined Fenton chemistry during the degradation of lysozyme,[142] albumin,[143] and lipoprotein.[139] Albumin carries a net charge of −18 at pH 7, but if regarded as eighteen single charges (because they are located on various amino acid side chains) instead of as an polyanion, the effect on the ionic strength should be negligible. The molar concentration of BSA contributes less than 0.1% of the

---

[140] Canumalla, A.; Shaw, C. F., III; Wagner, F. E. ^{197}Au Mössbauer Characterization of the Noncovalent Adducts Formed between Serum Albumin and Dicyanoaurate(I), a Gold-Drug Metabolite. *Inorg. Chem.* **1999,** *38,* 3268–3269.

[141] Shaw, C. F., III; Schaeffer, N. A.; Elder, R. C.; Eidsness, M. K.; Trooster, J. M.; Calis, G. H. M. Bovine Serum Albumin–Gold Thiomalate Complex: ^{197}Au Mössbauer, EXAFS and XANES, Electrophoresis, ^{35}S-Radiotracer, and Fluorescent Probe Competition Studies. *J. Am. Chem. Soc.* **1984,** *106,* 3511–3521.

[142] Sellak, H.; Franzini, E.; Hakim, J.; Pasquier, C. Mechanism of Lysozyme Inactivation and Degradation by Iron. *Arch. Biochem. Biophys.* **1992,** *299,* 172–178.

ionic strength; the buffer itself, ferrozine, ferrous ammonium sulfate and sodium chloride are the principal components. Coincidentally, one BSA conformation, the "N form," is even heart–shaped,[144] somewhat like R2.[85]

General conditions for the studies cited above include H_2O_2 and ascorbate in solution along with iron (II or III), BSA and any other proteins in question. The mixtures were allowed to react for several minutes at 25 °C, then assayed. Iron was typically present at many times excess the substrate protein (480 BSA : 32 Fe : 1 lysozyme; 100 Fe : 1 BSA; or 8.5 Fe : 1 BSA). In the last case, the Fe : BSA ratio is reversed, but the 8.5 : 1 is for ferric iron (ferrous was not tested).

Bovine serum albumin was used as the viscogen during the determination of standard k_{Fz}s for each unique [Fz]–[apo R2] combination, at w/v ratios equivalent to that of the R2 in the competitions. The effects of solvent viscosity on rapid reactions can be characterized by this derivative[145] of the Stokes–Einstein equation (Eq 41).

$$k_D = \frac{2RT}{3000\eta} \frac{[(r_A + r_B)^2]}{r_A r_B} \qquad \textbf{Eq 41}$$

---

[143] Ogino, T.; Okada, S. Oxidative damage of bovine serum albumin and other enzyme proteins by iron-chelate complexes. *Biochim. Biophys. Acta* **1995**, *1245*, 359–365.

[144] Carter, D. C.; Ho, J. X. Structure of Serum Albumin. In *Advances in Protein Chemistry*; Anfinsen, C. B.; Edsall, J. T.; Richards, F. M.; Eisenberg, D. S., Eds.; Academic: New York, 1994, Vol. 45, pp 153–203.

[145] Connors, K. A. *Chemical Kinetics: The Study of Reaction Rates in Solution;* VCH: New York, 1990; p 135.

where r_A and r_B are the radii of spherical molecules in a solution with viscosity η in poise (for reactions in water at 25 °C the diffusion–limited second–order rate constant k_D is $\approx 7 \times 10^9$ M^{-1} s^{-1}). With protein in solution, η will increase rapidly, especially at 5 °C—the temperature difference alone accounts for a significant decrease in k_D. This inverse dependence on viscosity was also noted in reactions between small ligands (O_2 and CO) and the heme protein myoglobin,[146] and various catalases and their substrate H_2O_2.[147] The actual size of the molecules providing the viscosity is irrelevant[148] (as originally described by Einstein in 1906)[149] provided the solute molecules are large compared to the solvent; proteins easily meet this requirement.

Kinetic data was collected on the stopped–flow and ultimately fit using MacKinetics (the model is given below). Interestingly, although sometimes two [apo]'s are similar, and the difference between the respective [Fz]'s used is not large, some combinations can lead to *lower* standardized k_{Fz}'s even though [Fz] is higher in the second case than in the first. Matching both [Fz] and [BSA] exactly allowed the direct use of the standard reactions' results instead of necessitating a standard curve.

---

[146] Beece, D.; Eisenstein, L.; Frauenfelder, H.; Good, D.; Marden, M. C.; Reinisch, L.; Reynolds, A. H.; Sorensen, L. B.; Yue, K. T. Solvent Viscosity and Protein Dynamics. *Biochemistry* **1980,** *19,* 5147–5157.

[147] Strother, G. K.; Ackerman, E. Physical Factors Influencing Catalase Rate Constants. *Biochim. Biophys. Acta* **1961,** *47,* 317–326.

[148] Bradbury, J. H.; Viscosity. In *Physical Principles and Techniques of Protein Chemistry, Part B;* Leach, S. J., Ed.; Molecular Biology Series; Academic: New York, 1970; pp 99–145.

[149] Einstein, A. Eine neue Bestimmung der Moleküledimensionen. *Ann. Physik* **1906,** *4s19,* 289–306.

For the initial BSA experiments, the kinetic traces were extracted from rapid–scanned spectra at 562 nm (λ_{max} of $FeFz_3$) and fit as simple one–exponential product growths. Figure 3.12 illustrates these time traces over the first one hundred milliseconds following mixing. The final absorbances all converge to the same endpoint (not shown) at the end of the reaction.

Rates from these reactions were significantly slowed in the presence of even small protein concentrations (Figure 3.13).

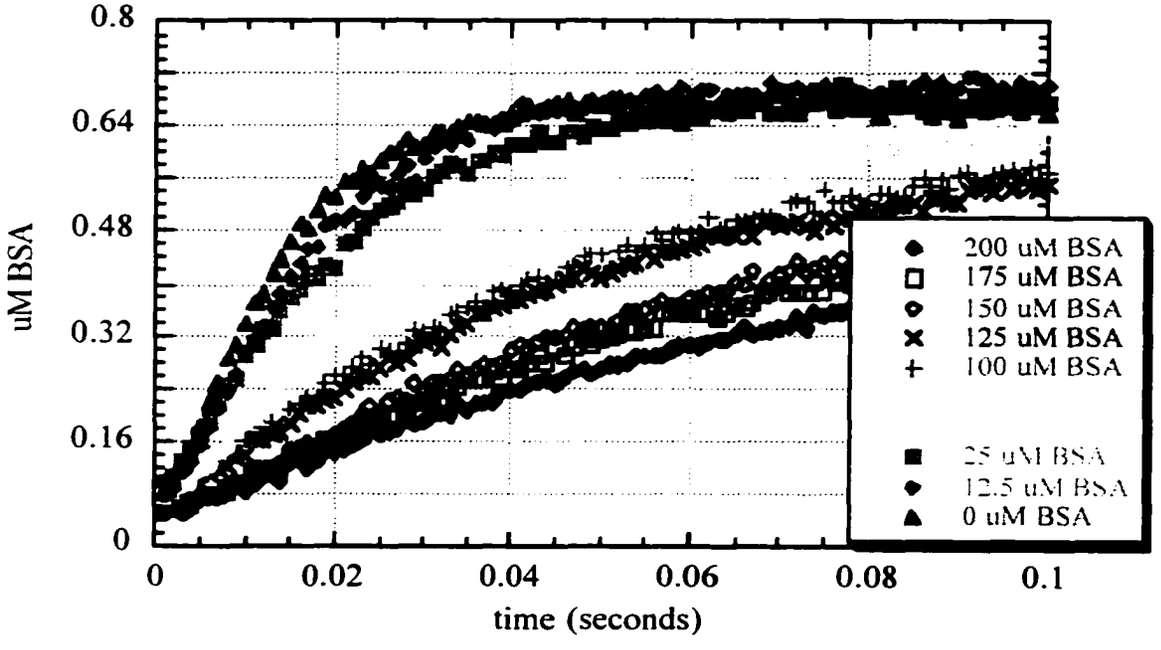

Figure 3.12. The effect of viscosity from added BSA on the ferrozine + Fe(II) reaction. Conditions after mixing in the stopped–flow: I = 0.1 M (NaCl), 5.0 °C, pH 7.6 HEPES 50 mM; Fz = 1.7 mM; Fe(II) = 30 μM; BSA 0–200 μM. The relationship between reaction time and added protein (bovine serum albumin) for the ferrozine reaction. Ferrozine and Fe(II) are both constant. Final absorbances all converge to near–quantitative yields of $FeFz_3$ at the end of each curve (Figure 3.13).

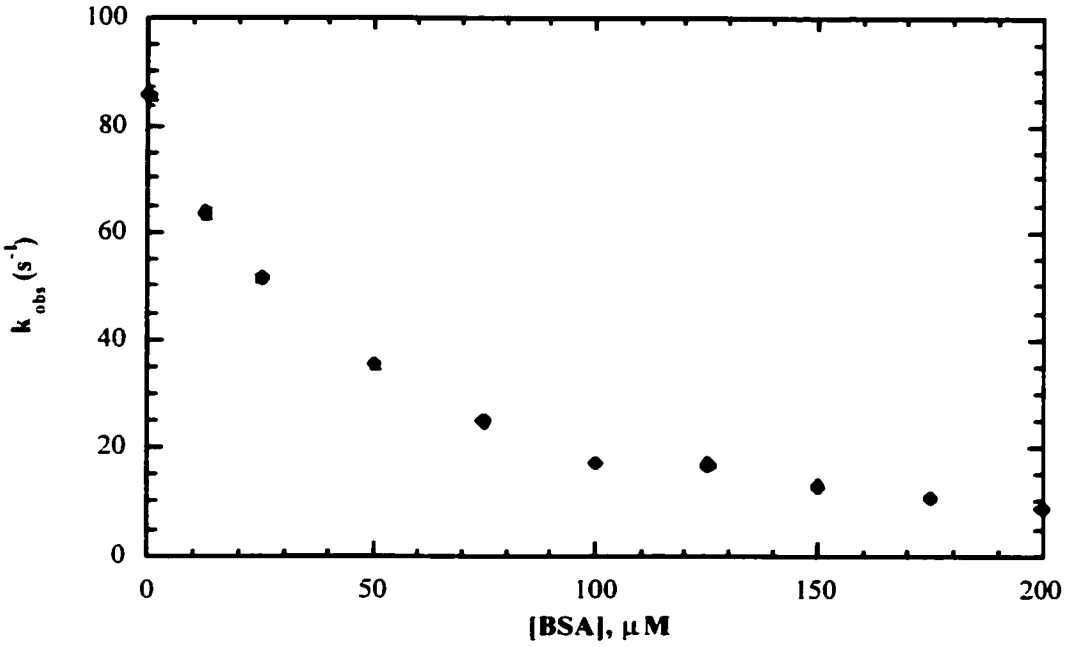

Figure 3.13. Observed rate constants for the ferrozine + Fe(II) reaction with BSA present. Post–mixing conditions *I*= 0.1 M (NaCl), 5.0 °C, pH 7.6 HEPES 50 mM; Fz = 1.7 mM; Fe(II) = 30 μM; BSA = 0–200 μM.

Because the only variable in the BSA–ferrozine experiments is the amount of protein in solution, the changes in the observed rate of Fe(II) complexation by the ligand ferrozine must be due to the presence of BSA; it is apparently a not–so–innocent bystander. The 400 μM stock BSA solution was noticeably more viscous than protein–free HEPES/ferrozine solution.

Protein viscosity has significant effects on the rate of complexation reactions in going from pure water to buffered protein solutions. Standardized ferrozine reaction rates

can be obtained which quantitatively take into account these effects during the R2 vs. ferrozine competition experiments.

In contrast to the BSA–iron studies cited earlier, conditions during our control reactions for the competition experiments have never included peroxide or ascorbate, take place at 5 °C, and BSA > Fe only by a factor of 10 or less. In addition, most of our reactions are complete within one second, as opposed to ten minutes.

Most convincing (and relevant) is our set of control experiments. The rate of the ferrozine reaction with iron(II) is inversely related to increased viscosity due to added protein (Figure 3.13). All the final $FeFz_3$ absorbances converged to nearly quantitative yields (Figure 3.14). There is a small decrease in the amount of $FeFz_3$ formed as more BSA is added to the solution, but the overall change is small. Experiments run at very high [BSA], for instance 200 μM, only lose 1–2 μM (3–6%) of the total Fe(II) in solution (presumably bound by BSA, as suggested by literature). This was compensated for in MacKinetics by decreasing initial [Fe] by 1–2 μM, and is justified by the observed formation of the corresponding amount of only 31 μM $FeFz_3$. The few percent of iron lost is still scarcely more than typical observed scatter in ferrozine standard reactions performed regardless of the presence of BSA.

Figure 3.14 illustrates the slight decrease in yield of $FeFz_3$ (normalized to the yield at 0 % BSA) as [BSA] increases (ferrozine concentration is constant). The results indicate that in conditions relevant to our R2 experiments (in contrast to the published conditions for the various assays performed), with sufficient ferrozine present, BSA is

not a significant factor in the removal of Fe(II) from solution, and is indeed functioning as intended – providing viscosity.

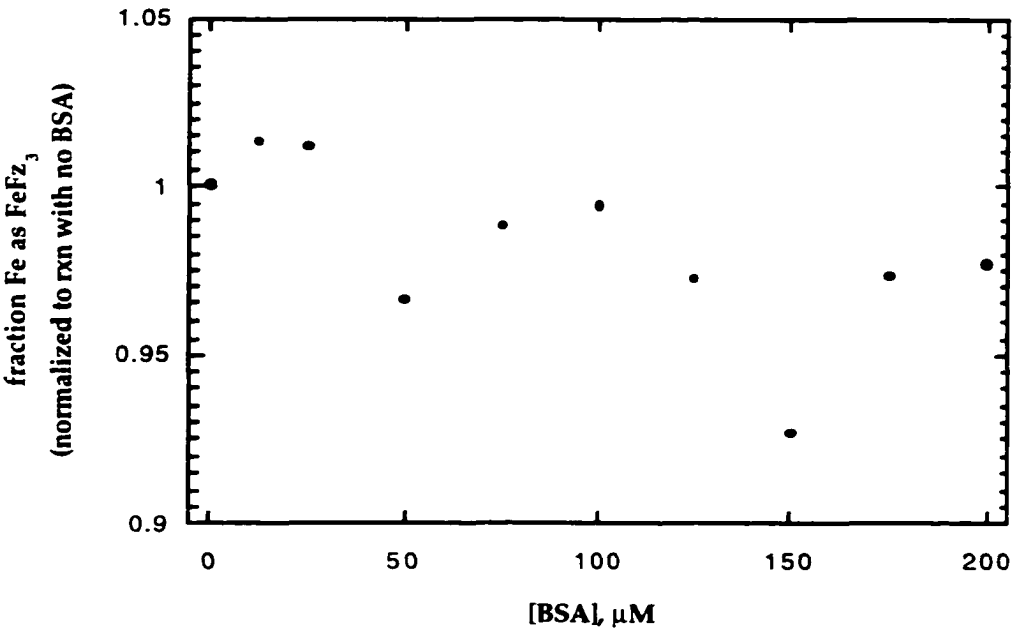

Figure 3.14. Fraction of iron bound by ferrozine as a function of [BSA]. While declining somewhat as [BSA] is increased, the amount of $FeFz_3$ formed during reaction times relevant to the competition experiments is nearly quantitative, especially at 100 μM BSA or less, which is where most of the competition experiments are performed. Conditions (post–mixing): 1.7 mM Fz; 30 μM Fe(II); I = 0.1 M; 50 mM HEPES, pH 7.6 at 5.0 °C; reaction times < 1 second.

CHAPTER IV. THE COMPETITION EXPERIMENTS.

A. Apo R2–ferrozine competitions.

Bovine serum albumin was used to provide viscosity during the determination of standard k_{Fz}'s at all necessary ferrozine concentrations, at w/v ratios equivalent to that of the apo R2 in the competitions (apo and BSA concentrations were matched as mg/mL, not molarity). Kinetic data were collected on the stopped–flow and fit using MacKinetics[150] (the model is shown below). Note (for example, lines 2 and 4 of Table 4) that although sometimes the two apo concentrations are not that different, and the difference between the two [Fz]'s used is not large, the combination can lead to *lower* standardized k_{Fz}'s even though [Fz] is higher in the second case than in the first (see, for example, lines 2 and 4 of Table 4). Matching exactly the BSA and ferrozine concentrations (to within 0.03%) allowed direct use of the standard k_{Fz}'s in the corresponding competition fits, instead of interpolating from a curve.

B. MacKinetics determination of k_{Fz}.

Once stopped-flow data was collected (Figures 4.1 and 4.2), it was exported to

[150] McKinney, R. J.; Weiher, J. F.; Leipold, W. S. III *MacKinetics*, version 0.9.1; E. I. du Pont de Nemours, Inc.: Wilmington, DE 1995.

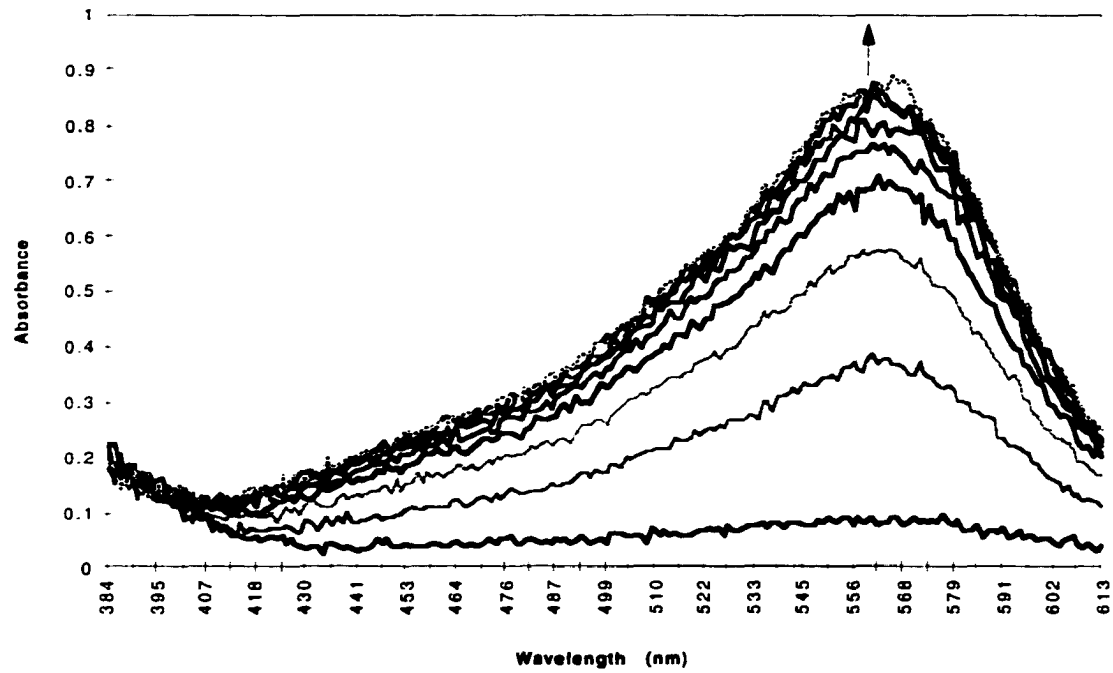

Figure 4.1. Stopped–flow UV-vis spectra of the ferrozine–iron(II) reaction (with BSA present as a viscogen). Collected at even time intervals over 200 ms (approximately 20 ms between spectra shown). For this particular example, [Fz] = 1.319 mM, [Fe] = 30.95 μM, [BSA] = 126.94 μM, I = 0.1 M, in 50 mM HEPES buffer (pH 7.6 at 5.0 °C); post–mixing concentrations.

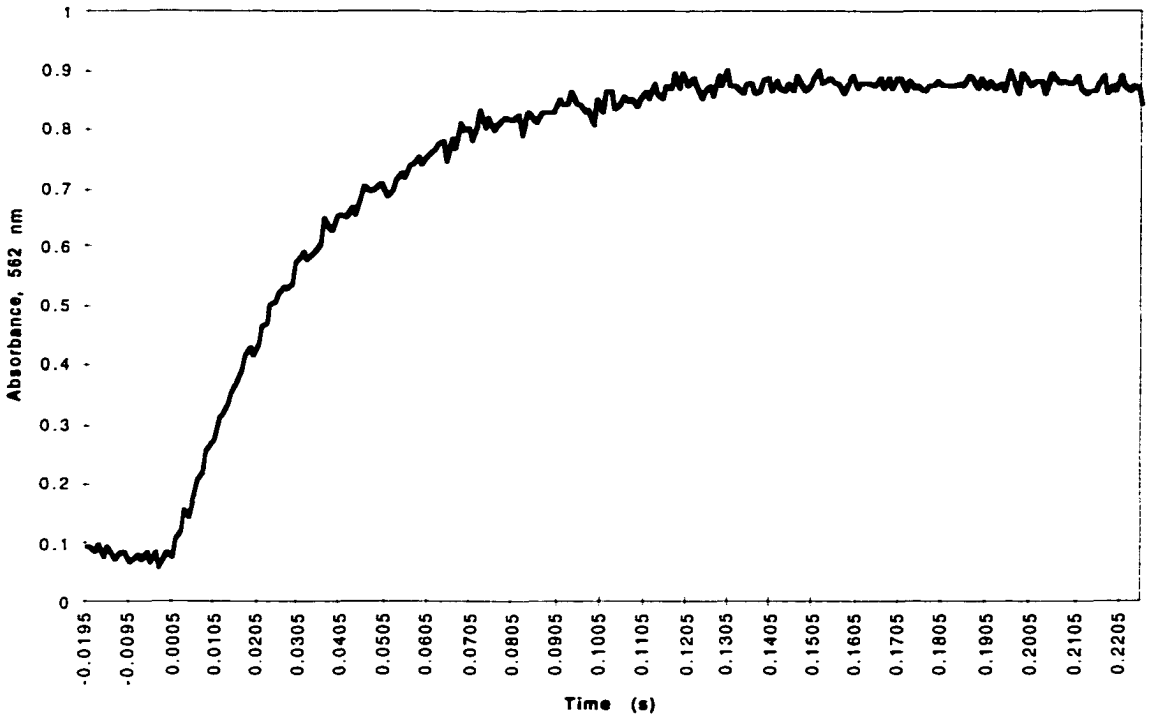

Figure 4.2. Stopped–flow kinetic trace of the ferrozine reaction with iron(II) in the presence of BSA. This is a slice at 562 nm of the individual spectra in Figure 4.1. For this particular reaction (post–mixing conditions), [Fz] = 1.319 mM, [Fe] = 31.95 μM, [BSA] = 126.94 μM, I = 0.1 M, in 50 mM HEPES buffer (pH 7.6 at 5.0 °C).

MacKinetics and fit to a kinetic scheme of the form shown in Eqs 42–43.

$$Fe^{II} \xrightarrow{k_{Fz}} FeX \qquad \textbf{Eq 42}$$

$$FeX + 3Fz \xrightarrow{1x10^{20}} FeFz_3 \qquad \textbf{Eq 43}$$

MacKinetics is a kinetic program which takes a set of chemical equations, starting concentrations of the reactants, time-dependent data, any known rate constants, and initial guesses for the unknown rate constants, all provided by the user, and iteratively optimizes those rate constants and calculates the concentrations of any or all species in

the system during the course of the reaction for the system in question. One can also simulate reactions simply by integrating the model with a rate constant and initial concentrations in order to decide on an initial guess for optimization, or to plan benchtop experiments in such a manner that they have a higher probability of working.

Equation 39 denotes the fact that we are treating the disappearance of iron(II) from solution into ferrozine complex as a first-order process. In transforming Fe^{II} into "FeX", (an artificial species comprised of the equilibrium mixture of Fe, FeFz, $FeFz_2$ and $FeFz_3$) we acknowledge the complexity of the situation and yet retain the ability to write an overall first-order rate constant for sequestering iron in such a way that, once on this pathway, it is destined to become $FeFz_3$. (This issue becomes more important when apo R2 is also in the reaction mixture and there are two possible fates for iron; for consistency between control and competition experiments, therefore, this method is used for both the control and competition reactions.) The second step consumes ferrozine at the correct ratio, and at a fast enough artificial rate that it doesn't otherwise affect the value of the rate constants preceding it.

A typical MacKinetics scriptfile for the reaction of ferrozine with iron(II) is shown below. The pound sign (#) denotes a programming comment, much like "C" in FORTRAN, or "REM" in BASIC. Iterspecies are species for which the program is to calculate concentrations over the course of the reaction. Inittemplate is the list of initial concentrations at time zero; subtemplate (generally one set of observed real data plus asterisks serving as place-holders for all others of interest) provides the format for all following lines of data. In the example, the initial guess for k_{Fz} was set at 40 s^{-1}, and the

program returned a value of 31.6712 s^{-1}. Provided the estimate is reasonably good, the program will find the correct answer. Seldom does MacKinetics not return an answer that isn't clearly valid or not, as it will either converge to a reasonable number, return nonsensical numbers (such as negative rate constants), or simply crash while generating line after line of error messages. The various commands following the data set various parameters within the program such as the fitting tolerances and what results are to be displayed at the end of the run.

```
reset
# Standard rxn for the Iron Uptake by ApoR2 by Competition with Uptake by
# Ferrozine
#       VISCOSITY CORRECTED BY BSA to same mg/mL as competitions
# (same mg/mL BSA = 126.94 uM BSA = 97.3 uM apo; std expt. to match
# 3xapo025)

reactions
        Fe ->FeX, kFz=40
        FeX + 3*Fz -> FeFz3, 1e20
end

set debug 1

iterspecies FeFz3 Fe Fz FeX
inittemplate FeFz3 Fe Fz FeX
subtemplate FeFz3 Fe Fz FeX

dataset STDFZ152    278.2
0       1e-6    30.95e-6        1.319e-3        0.0
0.001   2.74E-06        *       *       *
0.002   3.88E-06        *       *       *
0.003   4.35E-06        *       *       *
0.004   5.73E-06        *       *       *
0.005   5.15E-06        *       *       *
0.006   6.02E-06        *       *       *
0.007   7.36E-06        *       *       *
```

```
0.008  7.94E-06     *      *      *
0.009  9.09E-06     *      *      *
0.01   9.65E-06     *      *      *
:
:
:
:
:
:
0.141  3.10E-05     *      *      *
0.142  3.17E-05     *      *      *
0.143  3.12E-05     *      *      *
0.144  3.12E-05     *      *      *
0.145  3.16E-05     *      *      *
0.146  3.11E-05     *      *      *
0.147  3.21E-05     *      *      *
0.148  3.14E-05     *      *      *
0.149  3.12E-05     *      *      *
0.15   3.13E-05     *      *      *
end

guicmd show output
guicmd show error
set simpsize 1.1
set itol 1e-5
set rtol 1e-5
set atol 1e-6
set nstep 75
set itermax 100
set tfinal 5

iterate 4999

list variables
list iterspecies
list inittemplate
list subtemplate
show
dataplot STDFZ152 Fe FeX FeFz3

list reactions
```

Once MacKinetics has finished, it returns the results in both numerical and graphical form (Figures 4.3–4.4). The k_{Fz}s so determined for the ferrozine–iron reaction (with BSA) are then used within the MacKinetics model of a ferrozine–apo R2 competition reaction to solve for the rate constant for iron(II) uptake into the protein, k_{apo}.

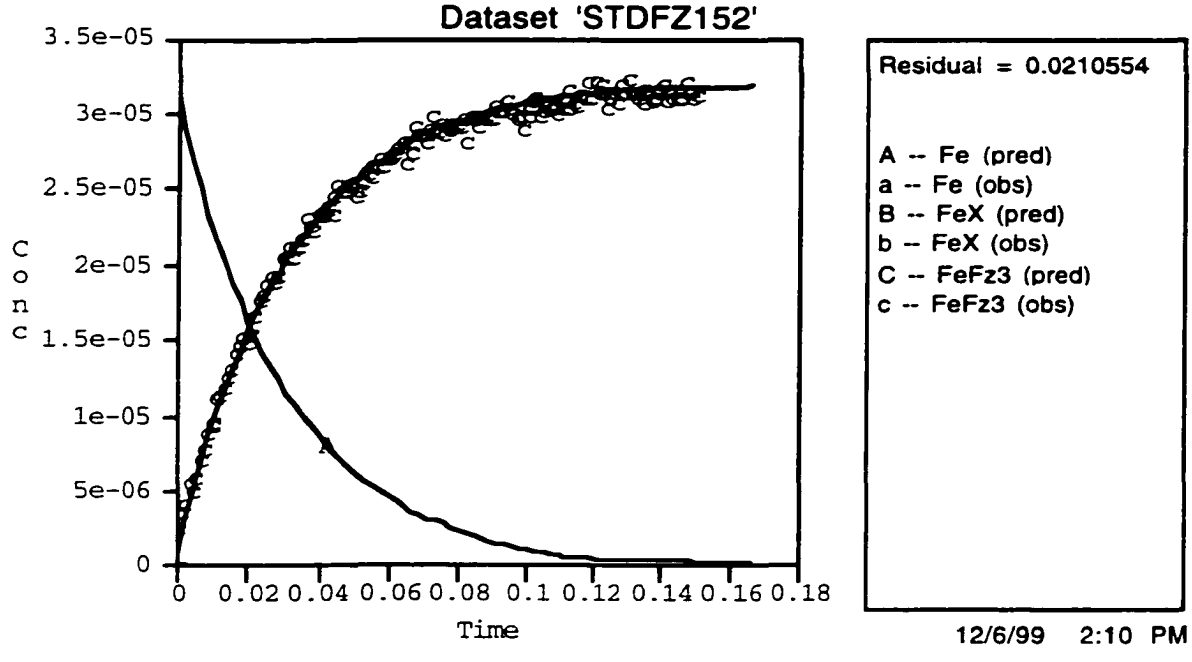

Figure 4.3. Graphical output from a MacKinetics calculation. Time is in seconds, concentration in molarity. Capital letters label the calculated curves (solid lines), while lower-case letters label the actual stopped–flow data points provided to the program (the concentration of $FeFz_3$ is "c" and there is no "a" or "b"). The concentration of FeX ("B") never leaves the baseline, so is not evident in the figure.

```
Final residual = 0.0210554
  (after 31 objective function evaluations)

 Variable          Value
 ========          =====
 kFz               31.6712

Template for iteration species:
  FeFz3
  Fe
  Fz
  FeX

Template for initial concentration:
  FeFz3
  Fe
  Fz
  FeX

Template for subsequent concentrations:
  FeFz3
  Fe
  Fz
  FeX

Global parameters:
  tinit     = 0
  tfinal    = 5
  nstep     = 75
  itermax   = 100
  maxistep  = 0
  gradient  = 1
  temp      = 0
  toff      = 0
  rtol      = 1e-05
  atol      = 1e-06
  itol      = 1e-05
  simpsize  = 1.1
  thresh    = 0.05
  debug     = 1
  heading   =
  itermethod = simplex

Reaction equations:
  Fe -> FeX, 31.6712
  FeX + 3*Fz[3] -> FeFz3, 1e+20
```

Figure 4.4. Output file from a MacKinetics calculation. It includes a listing of all the program parameters as well as the desired rate constant and fit residual.

C. Determination of iron uptake rate constants using MacKinetics.

Initial MacKinetics fit of k_{apo}. The MacKinetics model used to initially fit the competition reactions has one more step than the control reactions, the uptake of iron into the first binding site of apo R2. The rate constant k_{apo} is allowed to float during the run of the model (Eqs 44–46); k_{Fz} is set, using the value determined in the MacKinetics fit of the model (Eqs 42–43) of the corresponding control reaction.

$$\text{apo} + \text{Fe} \xrightarrow{k_{apo}} \text{apoFe} \qquad \textbf{Eq 44}$$

$$\text{Fe}^{II} \xrightarrow{k_{Fz}} \text{FeX} \qquad \textbf{Eq 45}$$

$$\text{FeX} + 3\text{Fz} \xrightarrow{1\text{x}10^{20}} \text{FeFz}_3 \qquad \textbf{Eq 46}$$

Equations 42 and 45 are not mechanistically necessary for MacKinetics to model the removal of iron from solution by ferrozine, but does allow us to account for the decrease of free ferrozine ligand during the reaction concurrently and stoichiometrically with iron. The "rate constant" of 10^{20} was chosen to be high enough not to affect the kinetics. The practical result of this algorithm is a vanishingly small steady-state concentration of FeX, because once it is formed at the rate of k_{Fz} (s^{-1}) it is immediately converted to the product, $FeFz_3$.

Table 4. Summary of preliminary MacKinetics calculations of k_{apo}. Odd–numbered entries are control reactions (Fz + Fe in presence of BSA) and precede the competition reaction to which they are relevant. Even numbered entries are (apo vs. Fz for Fe) competitions. Filename denotes the stopped–flow trace which was imported to MacKinetics for analysis. "%Fe = $FeFz_3$" is the percentage of $[Fe]_0$ which has been trapped by ferrozine.

Entry	Rxn Type	filename	protein, μM	Fz, mM	k_{Fz}, s^{-1}	k_{apo}, $M^{-1}s^{-1}$	%Fe as $FeFz_3$
1	Standard	stdfz081	31.1 (BSA)	1.833	55.4539	—	99.0
2	Compet.	2xapo182	24.4 (apo)	1.833	55.4539	3374430	38.0
3	Standard	stdfz091	38.1 (BSA)	2.0103	42.0312	—	89.0
4	Compet.	2xapo217	29.275 (apo)	2.0103	42.0312	2117450	37.1
5	Standard	stdfz022	190.96 (BSA)	1.23	5.26573	—	102.9
6	Compet.	2xapo039	146.4 (apo)	1.23	5.26573	727902	8.3
7	Standard	stdfz032	127.30 (BSA)	2.07	34.6816	—	99.5
8	Compet.	2xapo070	97.6 (apo)	2.07	34.6816	2550780	16.3
9	Standard	stdfz046	127.30 (BSA)	2.53	34.518	—	94.9
10	Compet.	2xapo098	97.6 (apo)	2.53	34.518	1577830	17.7
11	Standard	stdfz049	127.30 (BSA)	3.80	78.5725	—	90.2
12	Compet.	2xapo124	97.6 (apo)	3.80	78.5725	1713390	37.6
13	Standard	stdfz124	214.79 (BSA)	1.833	38.7403	—	94.2
14	Compet.	3xapo005	164.7 (apo)	1.833	38.7403	769194	18.7
15	Standard	stdfz140	257.0 (BSA)	2.0103	38.9992	—	92.6
16	Compet.	3xapo014	197.6 (apo)	2.0103	38.9992	758467	19.6
17	Standard	stdfz152	126.94 (BSA)	1.319	31.6712	—	98.0
18	Compet.	3xapo025	97.3 (apo)	1.319	31.6712	1141350	17.5
19	Standard	stdfz158	126.94 (BSA)	1.979	58.2061	—	98.0
20	Compet.	3xapo040	97.3 (apo)	1.979	58.2061	1138530	24.6

Second round of MacKinetics on the competition data: k_{apo} and k_{Fz} set; k_{apoFe} varied. Once good fits for k_{apo} were obtained using the initial model of Eqs 44–46, the values of k_{apo} and k_{Fz} from each model were inserted back into the respective MacKinetics script files with another step added to the model: the uptake of the second iron(II) into the active site (Eqs 47–50). The same data sets were fit again, with k_{Fz} and k_{apo} both held fixed at the values determined in previous MacKinetics experiments (the models of Eqs 42–43, and 44–46, respectively). (The 0.77 equivalents of Ydot reflect the experimentally–observed ratio of active R2 formed from apo R2.)

$$\text{apo} + \text{Fe} \longrightarrow \text{apoFe},\ k_{apo} \qquad \textbf{Eq 47}$$

$$\text{apoFe} + \text{Fe} \longrightarrow 0.77^{*}\text{Ydot},\ k_{apoFe} \qquad \textbf{Eq 48}$$

$$\text{Fe} \longrightarrow \text{FeX},\ k_{Fz} \qquad \textbf{Eq 49}$$

$$\text{FeX} + 3\ \text{Fz} \longrightarrow \text{FeFz}_3,\ 1\times10^{20} \qquad \textbf{Eq 50}$$

This model is nearly the same as the model of Eqs 44–46, except k_{Fz} *and* k_{apo} are both set at fixed values and used to determine k_{apoFe}. It uses the same data previously treated in the simpler model. Because of the small amounts of iron available in solution, not all calculations were able to converge to good answers. One didn't converge at all to a positive number, and several others returned values which were positive but several orders of magnitude away from the rest of the data's fits. The results are summarized in Table 5.

Table 5. Results of preliminary MacKinetics fits of k_{apoFe}. Column 5 (k_{Fz}) are from MK fits of the control reactions; column 6 (k_{apo}) are from MK fits where k_{apoFe} wasn't included at all. Column 7 (k_{apoFe}) are from models with k_{apo} and k_{Fz} fixed while k_{apoFe} was iterated. Column 7 is from simultaneously iterating on both k_{apo} and k_{apoFe}, starting from values found in previous runs. Avg's (averages) I are the arithmetic means of the respective columns. Avg's II were determined using the logs of the respective values, calculating the arithmetic means thereof, then converting back. Errors in parentheses are the standard deviations (σ_n) of the mean of each group, determined from Eq 51, and determined from Eq 52 when using the log procedure.

Entry	filename	[apo], μM	[Fz], mM	k_{Fz}, s^{-1} from previous fit	k_{apo}, $M^{-1}s^{-1}$ from previous fit	k_{apoFe}, $M^{-1}s^{-1}$ only k_{apoFe} floated
1	2xapo182	24.4	1.833	55.4539	2994030	128293
2	2xapo217	29.275	2.0103	42.0312	1864800	316199
3	2xapo039	146.4	1.23	5.26573	790081	[–236.802] (no convergence)
4	2xapo070	97.6	2.07	34.6816	2302320	440000.
5	2xapo098	97.6	2.53	34.518	1458600	941084
6	2xapo124	97.6	3.80	78.5725	1485480	204520
7	3xapo005	164.7	1.833	38.7403	769194	338685
8	3xapo014	197.6	2.0103	38.9992	758467	106743
9	3xapo025	97.3	1.319	31.6712	1141350	441390
10	3xapo040	97.3	1.979	58.2061	1138530	298511
Avg's I					**$1.5(7) \times 10^6$**	**$3.6(2.4) \times 10^5$**
Avg's II					**$1.3(3) \times 10^6$**	**$2.9(8) \times 10^5$**

$$\sigma_n = \frac{\sum_{i=1}^{n} (x_i - \bar{x})^2}{n} \qquad \textbf{Eq 51}$$

As previously presented in Table 4, and resummarized in Table 5, the value of k_{apo}, calculating the mean and population standard deviation in the usual manner, = 1.5(7) $\times 10^6$ $M^{-1}s^{-1}$. If one converts the k_{apo} values to log (k_{apo}), averages these and uses the relationship of Eq 52 to solve for the quantity $\sigma(x)$, $k_{apo} = 1.3(3) \times 10^6$ $M^{-1}s^{-1}$.

$$\sigma(\log\ x) = \frac{1}{x}\sigma(x) \qquad \textbf{Eq 52}$$

MacKinetics models: simultaneous fitting of k_{apo} and k_{apoFe}. Both k_{apo} and k_{apoFe} were simultaneously fit by the program. The same model (Eqs 46–49) was used, after removal of the constraint on k_{apo}, so both rate constants related to protein uptake of iron (k_{apo} and k_{apoFe}) are simultaneously varied and fit by MacKinetics. The value of k_{Fz} was once again held constant at the value determined for each specific set of conditions in the model of Eqs 41–42. Initial guesses for k_{apo} and k_{apoFe} were taken as the values returned in the initial rounds when they were fit separately. Again, because of the limited amount of iron available to the apoFe → $apoFe_2$ (→ Ydot) step (Eq 47), we do not consider the solution of k_{apoFe} generated to be more than a rough estimate (Table 6).

Table 6. MacKinetics results for simultaneous fit of k_{apo} and k_{apoFe}. Column 7 is from simultaneously iterating on both k_{apo} and k_{apoFe}, starting from values found in previous runs. Avg's I and II were determined as before.

Entry	[apo], μM	[Fz], mM	k_{Fz}, s^{-1} (previous)	k_{apo}, $M^{-1}s^{-1}$ (preliminary)	k_{apoFe}, $M^{-1}s^{-1}$ (preliminary)	k_{apo} & k_{apoFe} simultaneous
1	24.4	1.833	55.4539	2994030	128293	2756130 763350
2	29.275	2.0103	42.0312	1864800	316199	1639490 1204520
3	146.4	1.23	5.26573	790081	[–236.802] (no convergence)	760453 509375
4	97.6	2.07	34.6816	2302320	440000.	2265450 822656
5	97.6	2.53	34.518	1458600	941084	1497890 522497
6	97.6	3.80	78.5725	1485480	204520	1485480 204520
7	164.7	1.833	38.7403	769194	338685	751175 353347
8	197.6	2.0103	38.9992	758467	106743	761623 35311.8
9	97.3	1.319	31.6712	1141350	441390	1143130 8393.75
10	97.3	1.979	58.2061	1138530	298511	1047110 537232
Avg's I				**$1.5(7) \times 10^6$**	**$4(2) \times 10^5$**	**$1.4(6) \times 10^6$** **$5.0(3.5) \times 10^5$**
Avg's II				**$1.3(3) \times 10^6$**	**$2.9(8) \times 10^5$**	**$1.3(2) \times 10^6$** **$2.7(1.8) \times 10^5$**

Because inclusion of the apoFe → ($apoFe_2$ →) Ydot step (Eq 47) does not significantly affect k_{apo}, it is apparent that the second iron uptake step of apo R2 reconstitution is not a factor in the mechanism under conditions employed in our experiments. This is probably because k_{apoFe} is only a fraction of k_{apo}, and cannot compete with the first iron uptake or the ferrozine reaction, and thus doesn't account for

any meaningful amount of ferrous ion. With the small amount of iron in the second site, therefore, we don't have enough information for a quantitative fit of the rate constant k_{apoFe}. We have great confidence in our ability to extract k_{apo} from the data, however. The results of MacKinetics fits of k_{apo} from Table 6 are summarized in Figure 4.5; the average value of k_{apo} is $1.3(2) \times 10^6$ M^{-1} s^{-1}.

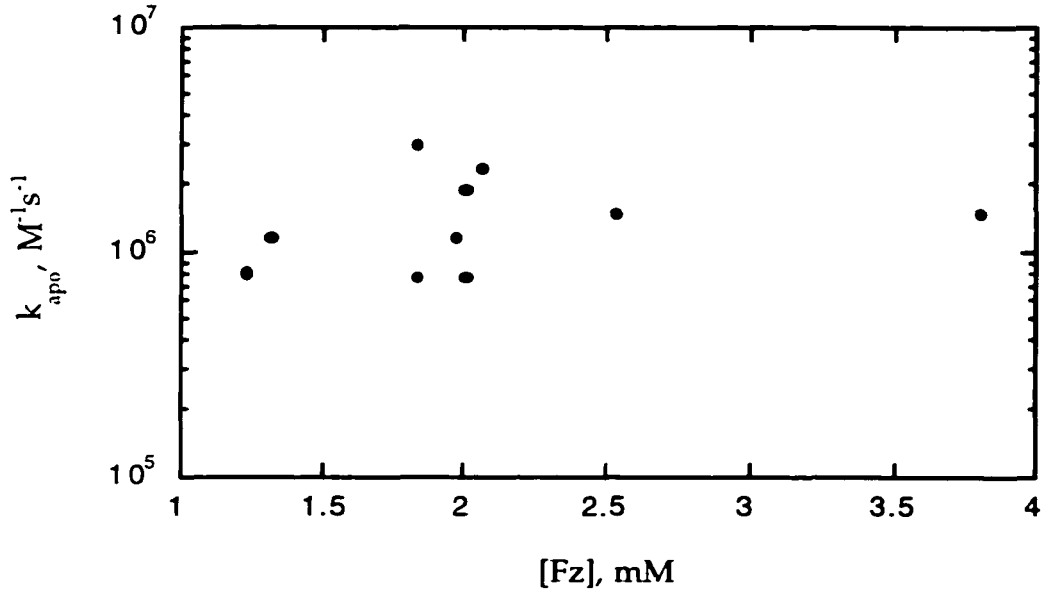

Figure 4.5. The k_{apo} values calculated by the final MacKinetics models. Concentrations and k_{Fz}'s from BSA–ferrozine control experiments are in Table 4. Concentration values are post–mixing.

MacKinetics models: fitting of k_{apo} when a conformational change is added to the model. The value of k_{apo} was fit by MacKinetics. A similar model as before (Eqs

43–45) was used, which featured iron removal routes with rate constants of k_{apo} and k_{Fz}, determined as before. Also included in the scheme (Eqs 52–55) was a protein conformational change, proposed[45] to be the experimentally–observed iron–independent step that proceeds at 10 s^{-1}. The value of k_{Fz} was once again held constant at the value determined for each specific set of conditions in the model of Eqs 41–42. Initial guesses for k_{apo} were taken as the values returned for k_{apo} when they were fit without the k_{conf} or k_{apoFe} steps (Eqs 43–45) included.

$$\text{apo} + \text{Fe} \longrightarrow \text{apoFe},\ k_{apo} \qquad \textbf{Eq 52}$$

$$\text{apoFe} \longrightarrow \text{apoFeconf},\ k_{conf} \qquad \textbf{Eq 53}$$

$$\text{Fe} \longrightarrow \text{FeX},\ k_{Fz} \qquad \textbf{Eq 54}$$

$$\text{FeX} + 3\ \text{Fz} \longrightarrow \text{FeFz}_3,\ 1\times10^{20} \qquad \textbf{Eq 55}$$

Final MacKinetics models: fitting of k_{apo} and k_{apoFe} when a conformational change is included the scheme. Finally, all possible routes for iron removal were included in the model (Eqs 56–60), along with the conformational change as discussed above. The values for k_{Fz} and the initial settings for k_{apo} and k_{apoFe} were as determined and used previously, while k_{conf} was held at 10 s^{-1}.

$$\text{apo} + \text{Fe} \longrightarrow \text{apoFe},\ k_{apo} \qquad \textbf{Eq 56}$$

$$\text{apoFe} \longrightarrow \text{apoFeconf},\ k_{conf} \qquad \textbf{Eq 57}$$

$$\text{apoFe} + \text{Fe} \longrightarrow 0.77^{*}\text{Ydot},\ k_{\text{apoFe}} \qquad \textbf{Eq 58}$$

$$\text{Fe} \longrightarrow \text{FeX},\ k_{\text{Fz}} \qquad \textbf{Eq 59}$$

$$\text{FeX} + 3\ \text{Fz} \longrightarrow \text{FeFz}_3,\ 1\times10^{20} \qquad \textbf{Eq 60}$$

The results of fitting the data with the additional step did not significantly differ from those of the models lacking the conformational change, as shown in Table 7.

Comparison of the results in Tables 6 and 7 illustrated how little difference the additional step made. As expected, large effects due to changing the model from those previously used (Eqs 43–45 and 46–49) were not observed, as most of the available iron was removed from solution prior to the conformational change, which in our model is the rate–determining–step.

Table 7. Final MacKinetics results. Fits of k_{apo} alone (Column 5) and simultaneously with k_{apoFe} (Column 6), with a conformational change added to the models. Avg's I and II were determined as before.

Entry	[apo], μM	[Fz], mM	k_{Fz}, s^{-1} from previous fit	k_{apo}, $M^{-1}s^{-1}$ floated only; (no k_{apoFe} step; k_{conf} step added)	k_{apo}, $M^{-1}s^{-1}$ & k_{apoFe}, $M^{-1}s^{-1}$ both floated; (k_{conf} added)
1	24.4	1.833	55.4539	2989960	2987010 128443
2	29.275	2.0103	42.0312	1971090	1733750 30471750
3	146.4	1.23	5.26573	789987	785143 514062
4	97.6	2.07	34.6816	2346320	2269890 784292
5	97.6	2.53	34.518	1548850	1499880 533609
6	97.6	3.80	78.5725	1501290	1499410 203561
7	164.7	1.833	38.7403	769194	769194 338685
8	197.6	2.0103	38.9992	762929	762763 93097.8
9	97.3	1.319	31.6712	1144400	1141350 8000
10	97.3	1.979	58.2061	1096050	1095840 289183
Avg's I				**$1.5(7) \times 10^6$**	**$1.5(7) \times 10^6$** **$3(9) \times 10^6$**
Avg's II				**$1.3(3) \times 10^6$**	**$1.3(3) \times 10^6$** **$3(3) \times 10^5$**

CHAPTER V. ATTEMPTS TO MEASURE IRON UPTAKE RATES BY OTHER METHODS.

A. Measurement of the rate of iron loss from reduced R2.

As the rate of iron uptake by the R2 apoprotein could in principle be calculated from the binding constants and the rates of iron loss from the reduced protein (the back reaction of uptake, after all, is iron loss), we attempted to determine the rate of iron loss from reduced R2. Bollinger, Huynh, and co-workers[151] have used anaerobically (stoichiometrically) preloaded protein and reported a rate constant of Fe^{2+} departure for bulk solution of 0.05 s^{-1}, with no differentiation between the two binding sites. However, in the same paper they reported labelling studies (^{56}Fe and ^{57}Fe) that distinguished two iron binding sites with different affinities: the one with the higher affinity they called Fe_B and the one with the lower affinity they called Fe_A, with apoFe_B being the preferred monoferrous form by a factor of at least 4:1 (the observed isotopic distribution). Fe_B was identified as the site which has Fe(IV) character in Intermediate **X**. Subsequent

[151] Bollinger, J. M., Jr.; Chen, S.; Parkin, S. E.; Mangravite, L. M.; Ley, B. A.; Edmondson, D. E.; Huynh, B. H. Differential Iron(II) Affinity of the Sites of the Diiron Cluster in Protein R2 of *Escherichia coli* Ribonucleotide Reductase: Tracking the Individual Sites through the O_2 Activation Sequence. *J. Am. Chem. Soc.* **1997**, *119*, 5976–5977.

experiments by the Bollinger group have found separate rates of Fe^{2+} loss of 0.02 and 0.06 $M^{-1}s^{-1}$.[152]

The differential affinities of the two binding sites for iron(II) in R2 are anecdotally confirmed by studies using the mutant F208Y.[41] Fe_A remains relatively fixed as the Fe(II)-containing mutant protein is reconstituted, while Fe_B moves significantly; the Fe_A ligand Asp84 is less flexible and in a more congested area of the matrix than Glu204, an Fe_B ligand which is in a less dense environment (water molecules). The F208Y "apo" has 20% occupancy at Fe_B and none at Fe_A; diferrous F208Y has full occupancy at Fe_B and 50% at Fe_A.

The Fe^{2+} loss rate published by Bollinger and Huynh[151] is an order of magnitude faster than what we observed (Figure 5.1) when we examined the long–term behavior of the effluent from the apoprotein/ferrozine stopped-flow Fe^{2+} competition experiments in Chapter 4. (We emptied the stopping syringe of the stopped–flow into a cuvette.) As we had used a sub–stoichiometric concentration of Fe^{2+} in the stopped-flow experiments, the subsequent color development should be due to the trapping of Fe(II) that has been lost from the metal center of apoFe (*monoferrous* R2), Fe_B. A sample trace is shown in Figure 5.1. At low ferrozine concentrations (i.e., less than 1 mM in Figure 5.1) the reaction was not yet complete at the end of observation; at higher concentrations of ferrozine the yield of $FeFz_3$ was nearly quantitative.

[152] Chaudhuri, D.; Bollinger, J. M., Jr. Personal communication.

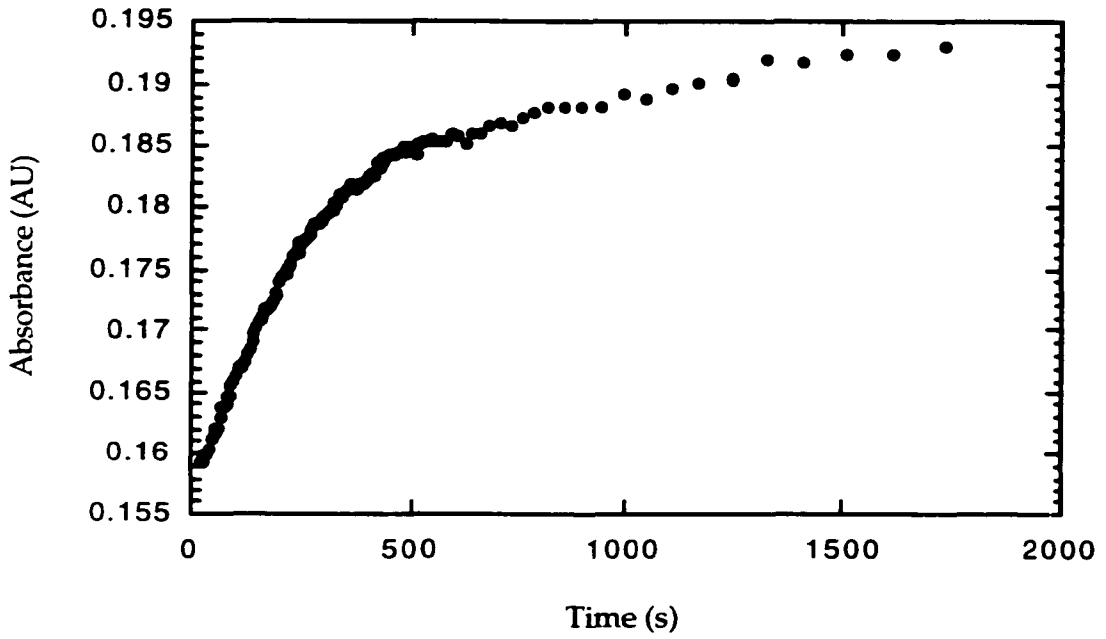

Figure 5.1. Long–term behavior of stopped–flow effluent following competition experiments. A sample trace of excess ferrozine scavenging iron(II) (which has been released from apoFe). Several stopped–flow "shots" are pooled in the UV-vis cuvette.

The apparent rate constants were independent of protein concentration (Figure 5.2), but increased with ferrozine concentration (Figure 5.3) in a fashion consistent with the saturation behavior expected (quantitative trapping of lost Fe^{2+} only at higher ferrozine concentrations).

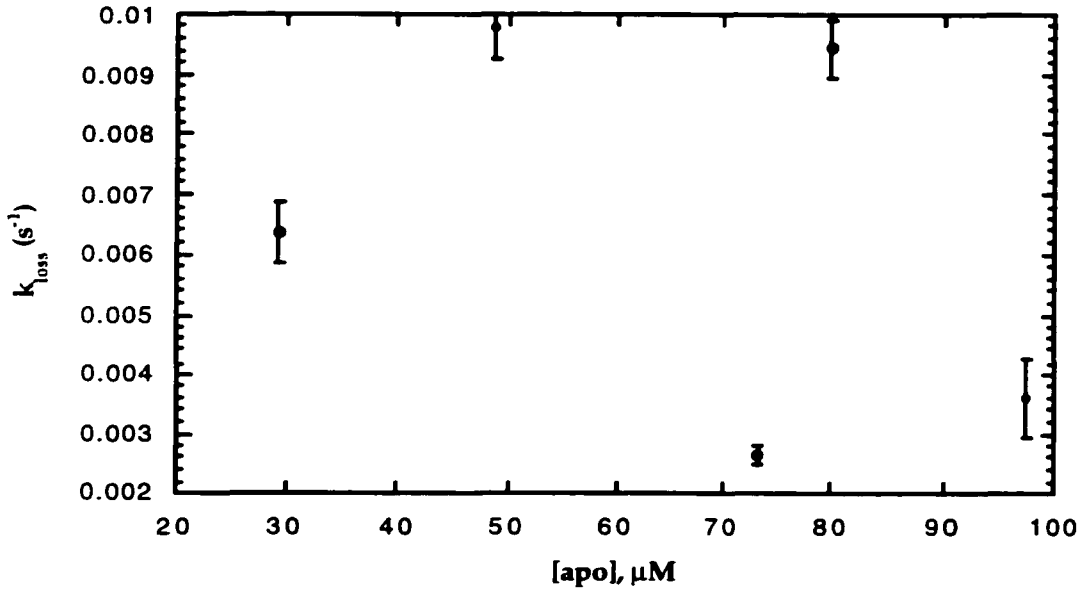

Figure 5.2. Long–term behavior of stopped–flow effluent is independent of protein concentration. The average $k_{loss} = 6.4 \times 10^{-3}$ s^{-1}. Concentration values are post–mixing.

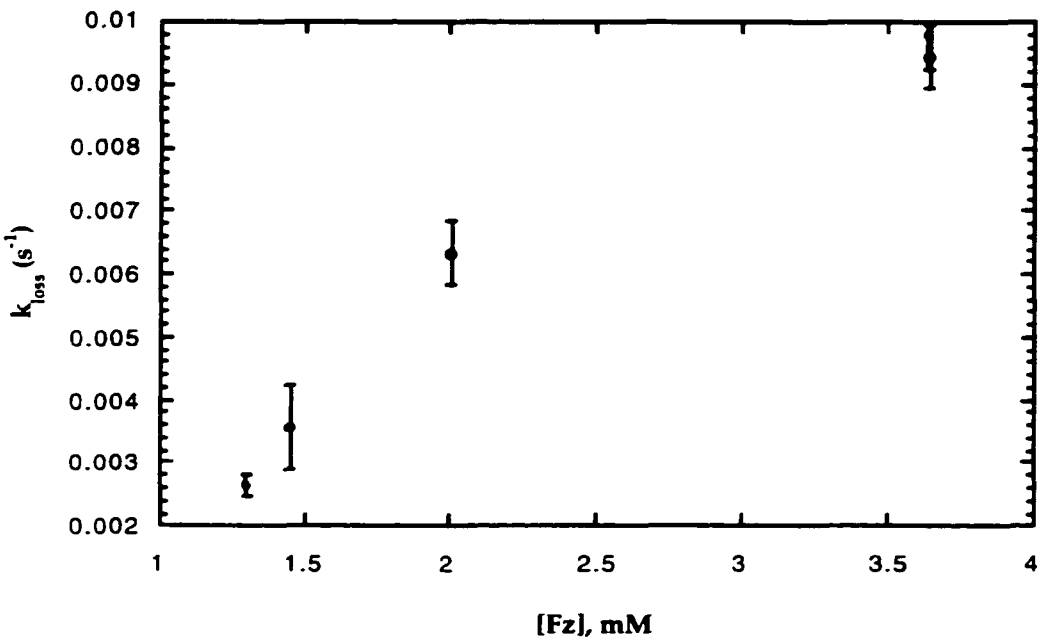

Figure 5.3. Ferrozine dependence of k_{loss} during long–term observation of stopped–flow effluent. Concentrations are post–mixing.

B. Reduction of active R2 by methyl viologen radical, and trapping of freed iron by ferrozine.

We also tried to measure (using stopped–flow techniques) the rate of Fe^{2+} loss from R2 that had been freshly reduced by dithionite, with methyl viologen radical ($\bullet MV^{+}$) as catalyst. Reaction of active R2 with $\bullet MV^{+}$ reduces both the tyrosyl radical and the μ–oxo diiron cluster at the active site.[65] Methyl viologen (Figure 5.4) is widely used as an artificial electron carrier in the study of enzymic systems, but it has an intense absorbance (ε_{600} = 1.18-1.19×10^4 $M^{-1}cm^{-1}$)[129] quite close to that of $FeFz_3$ (λ_{max} = 562 nm) and

interferes with analysis if present at too high a concentration. The catalyst ("mediator") was necessary as dithionite in solution with *E. coli* R2 and ferrozine will not cause any iron to be released and trapped. (This is in contrast to the mouse enzyme, which *can* be reduced by dithionite alone.[153]) Addition of ferrozine allowed measurement of the amount of iron released[89,90,91] and potentially of the rate of that process. As monitored by UV–visible spectroscopy (Figure 5.5), ferrous iron did indeed become complexed by ferrozine when a solution of methyl viologen/dithionite was mixed with a solution containing R2 and ferrozine. (Ferrozine does not remove any iron from oxidized, active R2.)

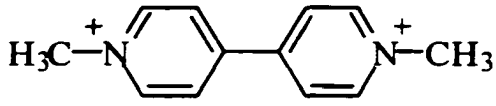

Figure 5.4. Methyl viologen. When reduced it is an effective electron delivery system for reducing R2.

[153] Davydov, A.; Schmidt, P. P.; Gräslund, A. Reversible Red–Ox Reactions of the Diiron Site in the Mouse Ribonucleotide Reductase R2 Protein. *Biochem. Biophys. Res. Commun.* **1996,** *219,* 213–218.

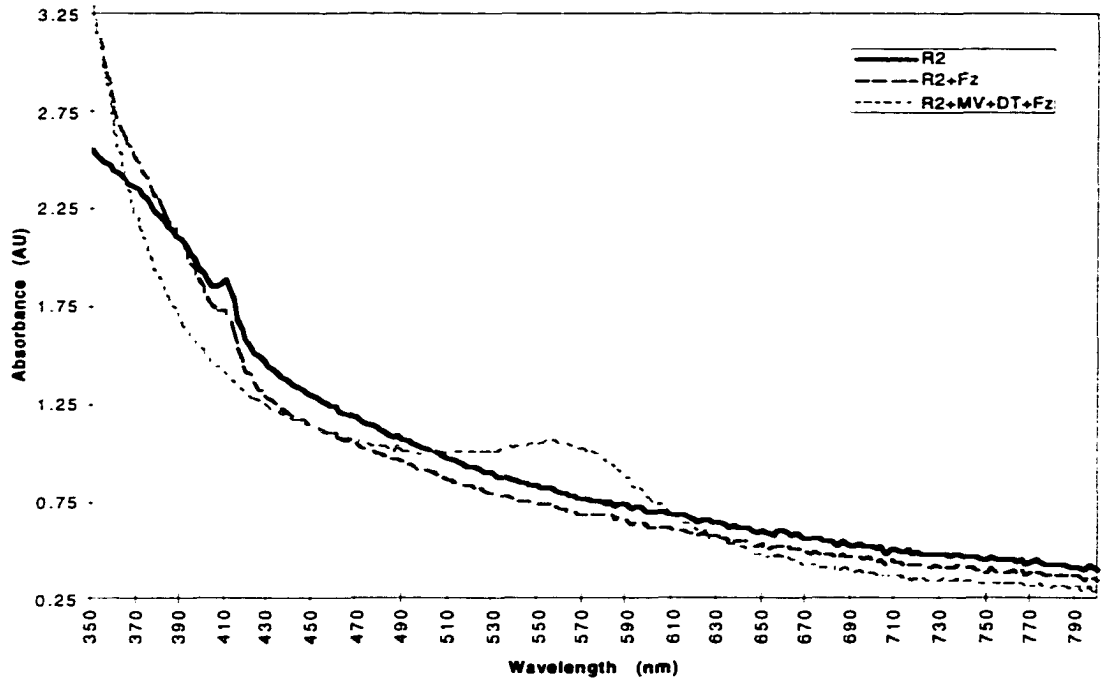

Figure 5.5. Reduction of R2 by $\bullet MV^{+}$ and dithionite, and trapping of released iron. Ferrozine alone cannot chelate iron from the protein's active site, but the addition of methyl viologen to deliver reducing equivalents to both the tyrosyl radical and the oxo bridge causes the iron to be released. The observed loss of intensity in the "R2 + Fe" UV-vis spectrum is simply from dilution of the sample when ferrozine was added.

Reduction and trapping: stopped–flow experiments. The signature peak (562 nm) of the tris(ferrozine) complex of iron(II) was observed to grow after mixing, but the single–wavelength trace at 562 (Figure 5.6) demonstrated that this was *not* a simple first–order reaction; there may be *three* exponentials contributing to this curve.

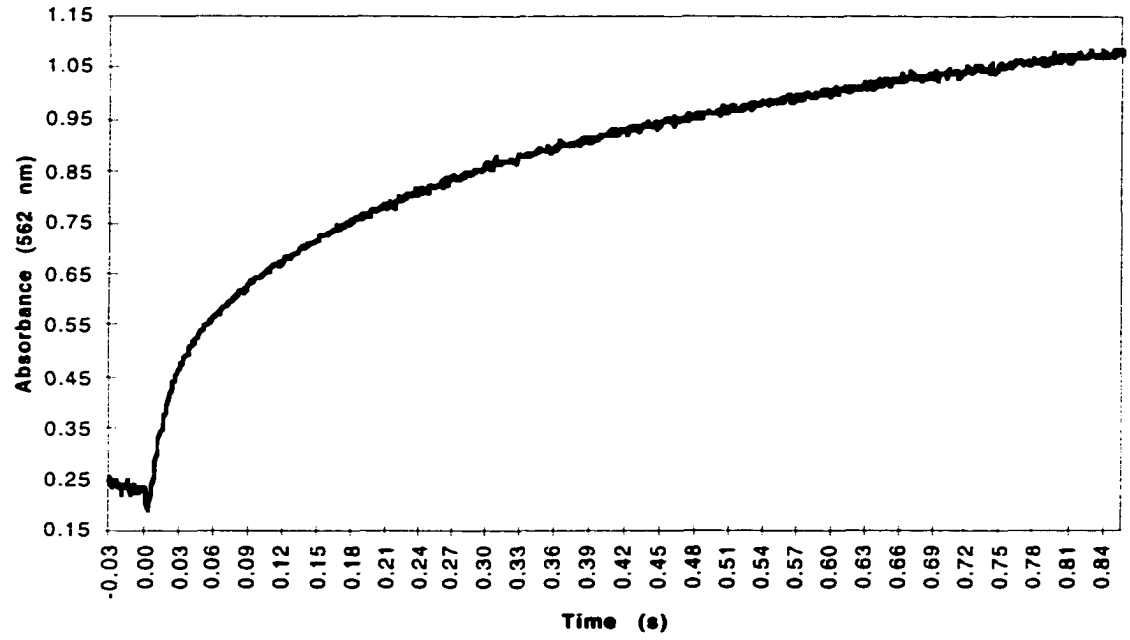

Figure 5.6. Trapping of iron(II) released by reduced R2 (single–wavelength trace). Iron is released following treatment by $\bullet MV^{+}$ (as followed at the λ_{max} of $FeFz_3$). There are multiple processes combining to create this curve.

There were potentially three different types of iron present in the reaction mixture: free iron that had escaped from the protein during the several–minute interval between reduction in the Schlenk tube and the reaction with ferrozine in the stopped–flow; iron released from Site A, the low affinity binding site; and iron released from Site B, the high affinity binding site implicated as the preferred monoferrous form.

Added iron(II) in solution. Similar experiments were undertaken with extra ferrous ion added to the protein solution. The concentrations of added iron ranged from zero to 35.6% with respect to the iron in the protein already (twice the protein concentration). In all three–exponential fits the observed rate constants were independent

of the concentration of added iron (Figure 5.7). While the largest of the three rate constants, 76(4) s^{-1}, is consistent with the uptake of free iron (II) by ferrozine, the others, 1.59(2) s^{-1} and 12(2) s^{-1}, are much larger than the Fe^{2+} loss rate constants measured (see previous section) by Chaudhuri and Bollinger directly from preloaded apoprotein;[151] plainly these two rate constants are associated with other processes.

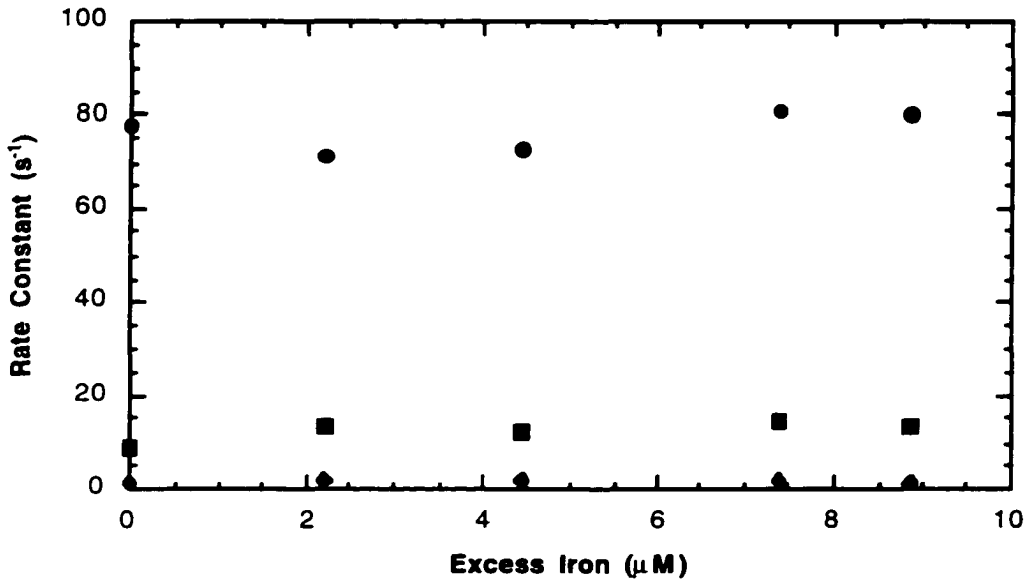

Figure 5.7. Rate constants observed in the reduction and trapping experiments. The largest of the three rate constants in each experiment (circles) are consistent with the ferrozine reaction. The two smaller ones (squares, diamonds) must therefore represent the two iron binding sites of R2.

Time interval between the two mixing steps. When the interval between reduction by methyl viologen/dithionite and the reaction with ferrozine was increased, all three rate constants remained unchanged (Figure 5.8).

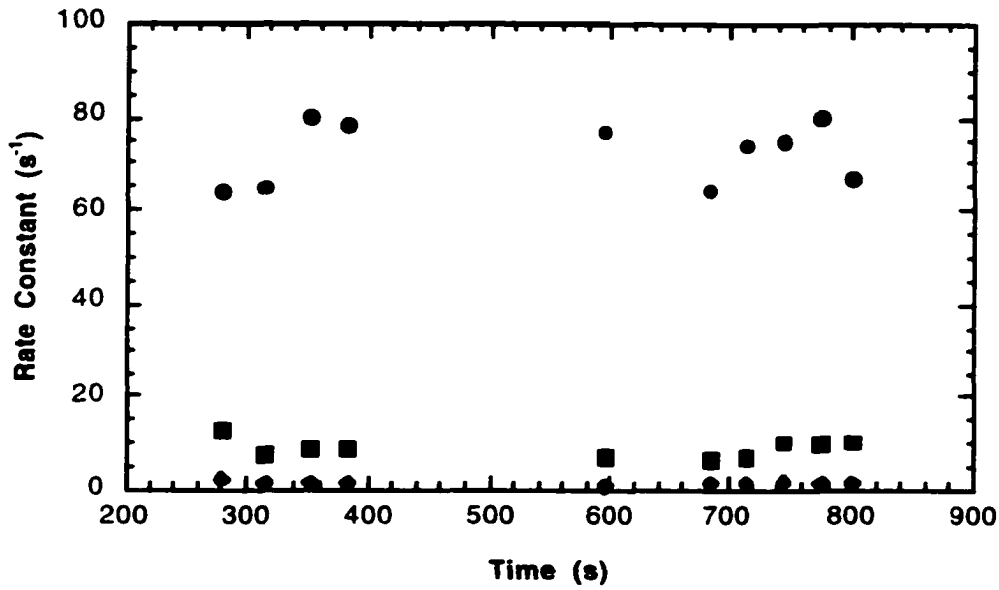

Figure 5.8. Rate constants from reduction and trapping experiments are time–independent. The time interval is that between the addition of $\bullet MV^{+}$ to active R2, and the reduced R2's reaction with ferrozine in the stopped–flow. The largest of the three rate constants (circles) is believed to be the ferrozine–free iron reaction, while the smaller two (squares, diamonds) are believed to be the protein–freed iron.

The amount of free iron in solution, however, increased with the interval between the two events (Figure 5.9).

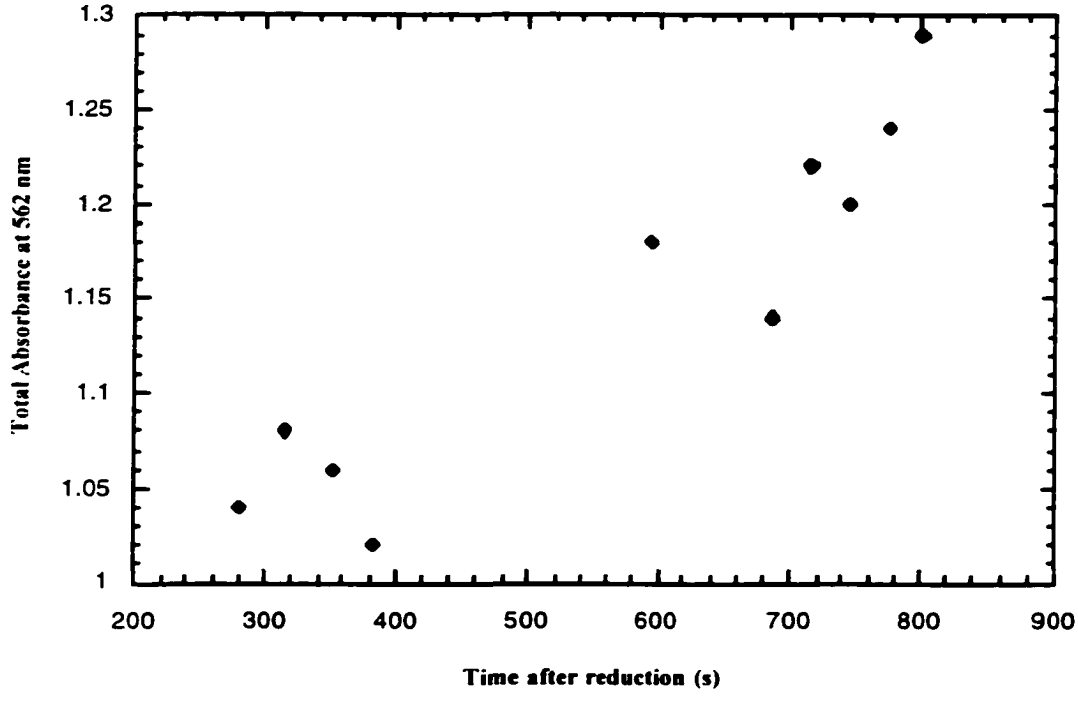

Figure 5.9. The amount of available iron as a function of time between reduction and trapping. All points are from the same reaction mixture; the stopped–flow reagent syringes required refilling during the experiment.

CHAPTER VI. CONCLUSIONS.

A. Summary of results.

The kinetic order in ferrozine of its complexation of iron(II), said to be three by earlier workers (at concentrations ≤ 800 μM), proved to decrease at higher ferrozine concentrations.

Ferrozine will compete effectively with apo R2 for Fe^{2+} in solution. Reactions can be successfully modeled and fit by MacKinetics, using Eqs 61–65. The rate of iron binding by ferrozine (k_{Fz}) proved to be dramatically affected by viscosity. We modeled this effect by measuring a k_{Fz} for each specific combination of ferrozine and protein concentrations with BSA, similar in molecular weight to R2, as a viscogen.

$$\text{apo} + \text{Fe} \longrightarrow \text{apoFe},\ k_{apo} \qquad \textbf{Eq 61}$$

$$\text{apoFe} \longrightarrow \text{apoFeconf},\ k_{conf} \qquad \textbf{Eq 62}$$

$$\text{apoFeconf} + \text{Fe} \longrightarrow 0.77*\text{Ydot},\ k_{apoFe} \qquad \textbf{Eq 63}$$

$$\text{Fe} \longrightarrow \text{FeX},\ k_{Fz} \qquad \textbf{Eq 64}$$

$$\text{FeX} + 3\ \text{Fz} \longrightarrow \text{FeFz}_3,\ 1\times10^{20} \qquad \textbf{Eq 65}$$

The rate constant of the first step in iron uptake by apo R2, k_{apo}, is 1.3(2) × 10^6 $M^{-1}s^{-1}$ (Figure 6.1). According to our models, k_{apoFe} is smaller than k_{apo}; uptake of the second Fe^{2+} is clearly slower than the first, and plausibly explained as occurring after a conformational change triggered by the uptake of the first Fe^{2+}.

Our evidence supports the sequence of steps as iron uptake (presumably into site B), conformational change, iron uptake (presumably into site A), and oxygen uptake.

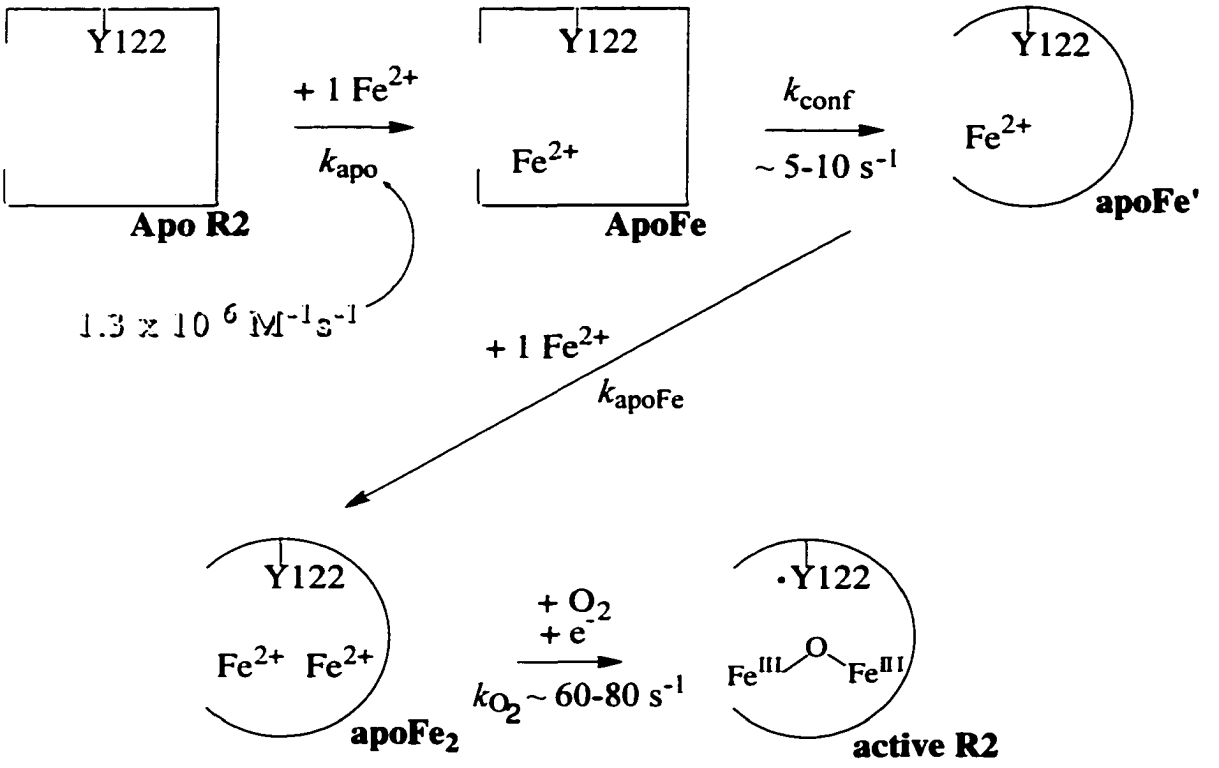

Figure 6.1. Proposed expanded scheme for the iron uptake steps of the reconstitution of *E. coli* ribonucleotide reductase R2. The intermediates between apoFe′ and active R2 (i.e., •W48H$^+$ and **X**) are omitted for the purposes of clarity only.

B. Suggested future work.

It should be possible to examine more closely the uptake of the second Fe^{2+}. The use of a double–mixing stopped–flow (Figure 6.2), which was not available for this work, would help. (Double–mixing stopped–flows enable two sequential reactions to be monitored, with variable reaction times between the two steps.) Premixing of apoFe and ferrozine (a combination that cannot be left together for long because the first iron will come out and be trapped by the ferrozine) would enable them to compete for Fe^{2+}.

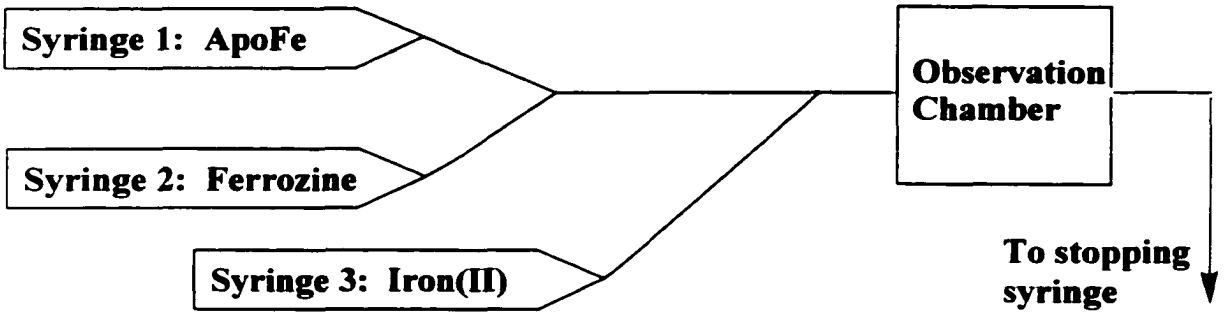

Figure 6.2. The layout of a double–mixing stopped–flow.

Ultimately, the viscosities of BSA and R2 solutions should be measured, both as a test of whether our approximations were valid, and to generate a standard baseline from which the community could work. While a significant quantity of R2 would be required to make the measurements, viscosimetry is a non–destructive technique, so the protein could be easily recovered.

The supreme viscogen to use would be a non–iron–binding R2 mutant. A good candidate would be E115A.[57] (Glutamate 115 bridges the two metals in reduced wild-

type R2; and, along with oxygen, bridges the metal site in active R2.) Kinetics experiments could be performed with a constant total concentration of R2, but with a varying ratio of wild–type apoprotein to mutant apoprotein.

APPENDIX. NON-LINEAR LEAST–SQUARES FITTING (USING MATHCAD) OF FERROZINE REACTION ORDER TO EQUATION 40.

:=

C:\..\Ferrozine

i := 0..8

Fz := Ferrozine<0>

kobs := Ferrozine<1>

$$diff(kcalc, kobs) := \sum_{i=0}^{8} (kcalc_i - kobs_i)^2$$

K1 := 3175

K2 := 1600

k3 := 70000

$$kcalc_i := K1 \cdot K2 \cdot k3 \cdot \frac{(Fz_i)^3}{1 + K1 \cdot Fz_i + K1 \cdot K2 \cdot (Fz_i)^2}$$

i := 0.. 8

diff(kcalc, kobs) = 443.799

Given

K1·K2 = 132000

diff(kcalc, kobs) = 0